Belz, M. (1998). Pollutant monitoring with fibre optics in the deep ultraviolet. (Unpublished Doctoral thesis, City University London)

CITY UNIVERSITY LONDON
EST 1894

[City Research Online](#)

POLLUTANT MONITORING WITH FIBRE OPTICS IN THE DEEP ULTRAVIOLET

by

Mathias Belz

A thesis submitted to City University for the Degree of

Doctor of Philosophy

City University

Measurement and Instrumentation Centre

Department of Electrical, Electronic and Information Engineering

Northampton Square, London EC1V 0HB

December 1998

List of Headings

List of Tables and Figures

Figures

Acknowledgements

Declaration

I grant powers of discretion to the University Librarian to allow this thesis to be copied in whole or in part without further reference to the author. This permission covers only single copies made for study purposes, subject to normal conditions of acknowledgements.

Abstract

This thesis reports on work carried out in the development of ultraviolet fibre-optic based absorption sensor systems, including those with the newly available ultraviolet improved silica fibres having low attenuation in the 200 nm to 250 nm wavelength region. Several approaches to optimize the optical design of such sensor systems, their sensitivity and stability are discussed. These fibre-optic sensor systems may be used for remote on-line and real-time analysis of process and water quality, enabling a separation of monitoring equipment from the sensor cell, which thus may be situated in a potentially hazardous environment.

The effect of temperature variations on wavelength stability and dark output of inexpensive spectrometer modules, potentially useful for field applications, and the subsequent effect on the accuracy of absorption measurements, as well as the sensitivity of such spectrometer modules at wavelength below 250 nm, is investigated. Further, the performance of a remote fibre-optic sensor system, based on a reflectance cell with an optical pathlength of 1 cm, to measure nitrate concentrations in the wavelength region between 200 nm and 250 nm, is reported.

Finally, to improve the sensitivity of such ultraviolet sensor systems, the performance of two fibre-coupled sensor cells with increased optical pathlengths has been investigated. The first sensor cell, based on an aluminium coated fused silica capillary cell, having an optical pathlength of 43 cm, is demonstrated in the construction of a residual chlorine sensor. The second sensor cell, a capillary cell with an inner coating of Teflon AF, uses the low refractive index and the high transparency of Teflon AF in the ultraviolet to form a liquid-core waveguide (LCW). This sensor cell has an optical pathlength of 203 mm, extending the use of long pathlength cells to the 200 nm to 250 nm wavelength region. Its performance is illustrated when applied to monitoring low concentrations of nitrates, chlorine and acetylsalicylic acid.

List of Symbols

B_{Power}	power budget [dB]
P_{source}	light power emitted from a light source [W]
$P_{Detector}$	light power reaching a detector [W]
λ	wavelength [nm]
G	geometric extent
S	area of light emitting source [mm^2]
NA	numerical aperture
$Loss$	power loss [dB]
I_λ	light intensity measured with a spectrometer [a.u.]
$I_{\lambda,Sam}$	sample intensity measured with a spectrometer [a.u.]
$I_{\lambda,Ref}$	reference intensity measured with a spectrometer [a.u.]
$I_{\lambda,Stray}$	stray light intensity measured with a spectrometer [a.u.]
$I_{\lambda,Drk}$	dark intensity measured with a spectrometer [a.u.]
c	molar concentration [mol l^{-1}]
l	optical pathlength [cm]
k	proportionality coefficient [l mol^{-1} cm^{-1}]
ε_λ	molar absorption coefficient [l mol^{-1} cm^{-1}]
$a.u.$	arbitrary units
AU	absorbance units
A_λ	true absorbance [AU]
A_λ^*	measured absorbance, influenced by stray light [AU]
T_λ	transmittance [%]
ln	logarithm to base e (Napierian)
lg	logarithm to base 10
SNR	signal to noise ratio [dB]
α	stray light transmittance [%]
S	fractional stray light [%]

FOS	fibre optic spectrometer
v	sample volume [l]
c	concentration [mg l^{-1}]
c_{Limit}	limit of detection [mg l^{-1}]
n	refractive index
t_{UV}	time fibres are exposed to UV light
$P(\lambda, t_{UV})$	spectral output power measured at fibre endface
$\Delta a_L(\lambda)$	UV-induced loss in a silica fibre
z	distance [m]
$a_{L,tot}(\lambda, t_{UV})$	total light loss in a fibre
UVI	ultraviolet improved
$t_{3\,dB}$	lifetime of hydrogen treated fibre [month]
SF_T	scaling factor - temperature dependence of diffusion process
SF_D	scaling factor - influence of fibre diameter
d_{core}	core diameter [μm]
$d_{cladding}$	cladding diameter [μm]
	coupling efficiency
	emission peak of mercury calibration lamp [a.u.]
	intercept of I_{Hg} [a.u.]
p	pixel number
p_c	pixel position at peak maximum
w	standard deviation of peak maximum [pixel]
A	area covered by Gaussian-shaped peak
$FWHM$	full width half maximum
Δp_{FWHM}	linewidth of spectrometer [pixel]
$\Delta \lambda_{FWHM}$	linewidth of spectrometer [nm]
$\Delta \lambda_p$	pixel dispersion [nm pixel^{-1}]
Δp_c	relative pixel accuracy [pixel]
$\delta \lambda$	relative wavelength accuracy [nm]

$A, B_1, B_2, ...$	coefficients for polynomial least square fit
SEE	standard error of estimate
$\lambda(p_c)$	calculated calibration wavelength at p_c [nm]
λ_c	true calibration wavelength [nm]
n_c	number of calibration wavelengths
n_p	number of polynomial coefficients
$a(\lambda)$	attenuation of water
jk	complex part of refractive index, n
$P(\lambda, z)$	light power at distance, z, from light source
$P(\lambda, 0)$	light power at light source
L_w	light loss in water
ID	inner diameter [mm]
OD	outer diameter [mm]
DL	deuterium lamp
LS	lens system
FI	input fibre
FO	output fibre
CE	capillary based absorption cell
MS	mode scrambler
Cl_2	dissolved chlorine
OCl^-	hypochlorite ion
$HOCl$	hypochlorous acid
NO_3^-	nitrate ion
$C_9H_8O_4$	acetylsalicylic acid (aspirin)
A, B	parameters of linear regression
SD	standard deviation
R	correlation factor
Δc	concentration error [mg l^{-1}]
c_{Limit}	detection limit [mg l^{-1}]

Θ	temperature [°C]
LCW	liquid core waveguide
Z_{LCW}	optical pathlength in the LCW

1. Introduction and Background

A major concern in the scientific and industrial world has always been to determine the composition of bulk matter in either its aqueous, solid or gaseous form. This has resulted in a expanding effort to develop a variety of analysis techniques, enforced by an increasing concern about environmental quality and cost-effectiveness in recent years. The development of sensors, which are capable of continuously and reversibly recording of either physical parameters or the concentration of chemical or biochemical species was a logical consequence. Existing analytical methods rely on the transducing effect generated when a parameter is subject to a physical, chemical or electrical disturbance and can be grouped into four major categories. These categories comprise electrochemical methods, chromatography, optical, spectroscopic methods and miscellaneous methods. Typical applications of such sensors can be found, for example, in the food or pharmaceutical industry, for monitoring the quality and possible toxicity of their products. In the biomedical field, the concentration of a number of substances, such as carbon dioxide, oxygen and pH in blood or urine are monitored during surgical operations to observe a patient's health. Another most important field for sensor application is the Water Industry, which has to comply with the recent increase in legislation from the EC for tighter control of water-borne pollution [1]. A set of standards concerning acceptable concentration limits of pollutants, such as nitrate (NO_3), ammonia (NH_3), and total organic carbon (TOC), which can be used to predetermine the level of pollution in sources waters and effluents from sewage treatment plants, has been issued and created a need for simple and robust sensor systems in this area.

The development and application of optical sensor schemes and especially fibre-optic sensor schemes has been described widely in the scientific literature [3, 4, 5, 6]. Some of their important characteristics and advantages are for example their immunity to electromagnetic interference, having a non-electrical method of operation, small size and weight, low power consumption and in many cases comparatively low cost. The rapid advancement

found in this field owes much to the development and usage of optical fibres and associated optoelectronic devices for the telecommunication industry.

Spectroscopic analysis, on which this work is based, relies on the interaction of electromagnetic waves with matter. The interaction is seen through an exchange of energy between the two systems, i.e. molecules or atoms and the surrounding media. Quantitative information related to the species observed can be obtained through the analysis of returned energy, as in the case of light absorption and emission. This results from rules, established in quantum mechanics, which predict that molecules and atoms interact with the wave by exchanging fixed amounts of energy. Different types of molecules or structures can be determined with absorption or emission spectroscopy, depending on the wavelength of the interacting wave. Whereas in the ultraviolet and visible part of the light spectrum, valence electrons are involved, an interaction in the infrared part of the light spectrum depends on vibrational and rotational energies [2].

A number of optically-based sensors have been designed in the past to measure the concentration levels of different species. Using ultraviolet (UV) absorption techniques, in the wavelength region below 300 nm, for example, chlorine in the form of hypochlorite ions, nitrate and nitrite ions can be determined. Although the absorbance of these species is significant in water-cells, the usage of such sensor system has largely been restricted, in the past, to laboratory analysis. The advantages of incorporating optical fibres with small diameters (< 1 mm), introducing high levels of flexibility into such sensor systems were often nullified by a number of reasons, such as solarization effects in the fibre, caused by the exposure to UV-light during light transportation through the fibre core, the unavailability of suitable light sources and wavelength resolving detectors, as well as sample cells, featuring an acceptable light loss and efficiency in the deep ultraviolet. However, such a sensor arrangement would only require small sample volumes due to the small dimensions of the fibre and additionally result in the separation of the sample cell, placed in a potentially hazardous environment, and the monitoring equipment.

1.1 Aims and Objectives

The research described in this work discusses the development of a fibre-optic-based polychromatic chemical sensor system for use in the ultraviolet part of the light spectrum at wavelengths below 250 nm and investigates a range of design aspects of such a sensor system which ultimately may have field use.

The principle aims and objectives of the thesis are to describe and discuss:

- the development of a fibre-optic based polychromatic chemical sensor system.
- an investigation of the underpinning physics of the sensor systems considered.
- the characterization of novel UV transmitting fibres in a sensor system.
- the characterization of a series of spectrometer systems in terms of their performance at varying temperatures representing the extremes of field use.
- the development and characterization of a reflectance cell, an aluminium coated capillary cell and a novel flow cell optical waveguide using a Teflon AF coating with a lower refractive index than water at the inner wall of the sample cell.
- a range of measurements with the sensor systems on a number of chemicals to determine their applicability.
- several conclusions of the research and suggestions for future work.

1.2 Structure of the Thesis

A brief introduction to fibre-optic sensing schemes is given in Chapter 1, mainly citing relevant literature offering a review of the relevant aspects in the area of fibre-optic sensing. Following that, a simple model, describing the flow of light power and the wavelength-dependent losses in the individual components of a fibre-optic based sensor scheme, is presented. Then, the measurement principle of the Bouger-Lambert-Beer Law, its range and possible deviations are described and related to the subsequent work.

In Chapter 2, the effect of UV-radiation on hydrogen treated optical fibres with a fused silica core and a fluorine doped cladding is investigated and its improved stability in the

wavelength region of interest shown. A simple UV-lens coupling system consisting of a deuterium lamp and two fused silica lenses is introduced. The advantage of this arrangement is to use the chromatic aberration of the lenses to compensate for increasing losses in the wavelength region of interest in the remaining optical components of the sensor system.

Novel research on the effect of temperature variation on the optical and electronic stability of inexpensive spectrophotometer modules, potentially useful in field sensor systems, is discussed in Chapter 3. This is followed by a comparative discussion on the relative optical sensitivity of two inexpensive spectrophotometer modules used in a sensor arrangement optimized for the most interesting wavelength region below 250 nm.

Based on the forgoing, a simple nitrate sensor, relying on a fibre-optic based reflectance cell is described in Chapter 4, proving the applicability of the proposed deep UV sensor system in a laboratory based environment.

However, only short optical pathlengths and therefore only low sensitivities are possible with such a sensor cell. To increase the optical pathlength and therefore the sensitivity of the sensor arrangement, the usage of a aluminium coated capillary cells, working as a light guide, is presented in Chapter 5, to determine low concentrations of chlorine in aqueous solutions. Finally, the design and application of a liquid core waveguide, confining the optical energy in its core to form a ultra sensitive sample cell containing the sample solution, is described.

Conclusions and suggestions for future work are included, as is a detailed reference list.

1.3 Review of fibre-optic sensor schemes in chemical monitoring

The progress achieved in fibre-optic sensing technology has been extensively reviewed by many authors [3, 4, 5, 6]. Thus, the scope of this sub-section is only to guide the interested

reader to the different sensing techniques possible with fibre-optics by giving a brief overview. There are several ways in which fibre-optic sensors can be classified. A first possibility may be to distinguish between extrinsic and intrinsic sensors. In the case of extrinsic sensors, optical fibres are only used as a guide to transport light to and from the sensor cell, while in case of intrinsic sensors the measurand directly modulates some physical property of the optical fibre. These systems could then be subdivided by their transduction mechanisms in intensity or interferometric based sensors. Typical measurands that can be addressed with fibre-optics by intensity are particle size, turbidity and pH, by intensity or phase are pressure, displacement, position, magnetic field, temperature, gas, chemical concentration, vibration and level and most frequently by phase are laser velocimetry, vibrometry and holography.

However, in the field of optical fibre-based chemical sensors and biosensors, which this work is focused on, commonly used transducing effects are absorbance, fluorescence, fluorescence decay, infrared spectroscopy, Raman spectroscopy, as well as reflectrometry, refractometry, evanescent wave spectroscopy and several miscellaneous methods. Absorbance spectroscopy can be configured in various forms, probably the most popular method in conventional analytical chemistry is based on the absorbance of light by the analyte or an indicator. The linear relationship between absorbance and concentration, described by the Beer-Lambert Law and extensively discussed in Section 1.6, can be used to determine the concentration of an analyte. Fluorescence, on the other hand, is light emitted by a molecule in its first excited singlet state and was, for example, used to measure pH with the dye fluoresceinamine [7] or fluorescence quenching of oxygen [8]. Infrared spectroscopy is an absorption technique covering the near infrared (NIR) and infrared (IR) of the light spectrum and is mainly used in the NIR to detect C-H, O-H and N-H bonds that absorb in that region. Another emission technique involving inelastic scatter of absorbed (laser) light is Raman spectroscopy, with Raman bands arising from changes in polarizability in a molecule during vibration, while infrared bands reflect a change in polarization during such a vibration. Raman techniques are the method of choice when highly polarizable bonds of a sample, such as C=C, C≡C, C≡N, or S-S are observed,

---

Introduction and Background ...

5

which are often invisible in the infrared, but produce strong Raman bands. Reflectance spectroscopy is based on the reflection of a light beam at the surface between two media. Useful information may be extracted from diffuse light reflected from the second (observed) medium, as for example is realized in the development of a heart beat monitor based on the variation of light reflected from a jugular vein caused by blood flow [9]. Since the feasibility of transporting light in an optical fibre is based on total internal reflection between the fibre core and cladding, a change of the cladding refractive index by chemical means is a direct way to transduce a chemical parameter. This technique is called refractometry and has, for example, been exploited to measure the refractive index of liquids [10]. Another experimental approach is to attach a chemically sensitive cladding to the core of a waveguide and use the evanescent field at the core/cladding interface to detect the presence of an analyte. However, the evanescent wave decays exponentially with distance from the interface with a characteristic $1\,e^{-1}$ decay distance of 50 - 100 nm and therefore this restricts the spatial volume probed. This is the principle of evanescence wave spectroscopy and has, for example, been used to develop a reversible optical waveguide sensor for ammonia vapours [11]. Additionally to the techniques described, a number of miscellaneous methods have been developed, such as opto-acoustic techniques, where the sample absorbs and re-emits the energy as heat; interferometric techniques, relying, for example, on physical change of the fibre length, and ellipsometry where the polarisation state of the reflected light from a thin layer surface is monitored.

Although fibre-optic sensors developed to date are not easily summarized in one representative system, they commonly consist of a light source, optical fibres, wavelength-selection system, light detection system and readout device. Low-cost tungsten halogen lamps and most recently, ultra-bright light emitting diodes are often used in the visible part of the light spectrum, with xenon and deuterium lamps in the ultraviolet (UV), to perform reflectance and absorbance measurements. To obtain high intensity light for fluorescence sensors, xenon or low pressure mercury lamps, as well as helium-neon, helium-cadmium or argon lasers have been used. A variety of optical fibres have been developed for the communications industry and have been widely utilized for sensor applications.

Measurements in the UV are currently performed with fused silica fibres, whereas quartz, glass or polymethylmethacrylate optical fibres are used in the visible region. To extend remote measurements to the infrared part of the light spectrum, fibres containing special fused silica, zirconium fluoride, or chalcogenide glasses have been developed. Two types of wavelength selective detector systems are used to observe the desired wavelengths. These are cut-off or interference filters for inexpensive and broad band detectors and prism or grating monochromators.

A variety of fibre-optic based sensor cells has been developed for chemical analysis and these may be classified into three main categories, being single strand, double strand and bifurcated probes, as shown schematically in Fig. 1-1. In probes based on an industrial single strand fibre, a single fibre is used to transport light to a chemically sensitized part of the fibre system, which may either be an uncladded part of the fibre or the fibre tip. Changes in colour or refractive index of this coating caused by varying analyte concentrations can then be detected by monitoring transmission losses of radiation passing through the sensitive zone. In this case, excitation light and sensor response light are guided in the same optical fibre, and they should either be of different wavelengths, or the light should be modulated or phase shifted to ensure optical separation and avoid interference between both. Optical sensors based on a double strand arrangement avoid this problem. Incident radiation is guided to the sensor tip and the emerging radiation is collected by an adjacent optical fibre. To perform absorbance measurements, either a mirror can be placed at a certain distance from the fibre tips, or the two single optical fibres can be positioned face-to-face in an optical cell.

A bifurcated optical sensor is based on using a fibre bundle divided into two equal parts to guide light to a probe and collect the returning radiation respectively. Such sensors either using a sensitive layer, a mirror or without any sensitive device in the tip have been described for fluorescence, absorbance and reflectance measurements.

Single Strand

straight   U-shaped   coiled   sensitive tip

Double Strand

sensitive tip   mirror   analyte chambe

Bifurcated

sensitive tip   mirro
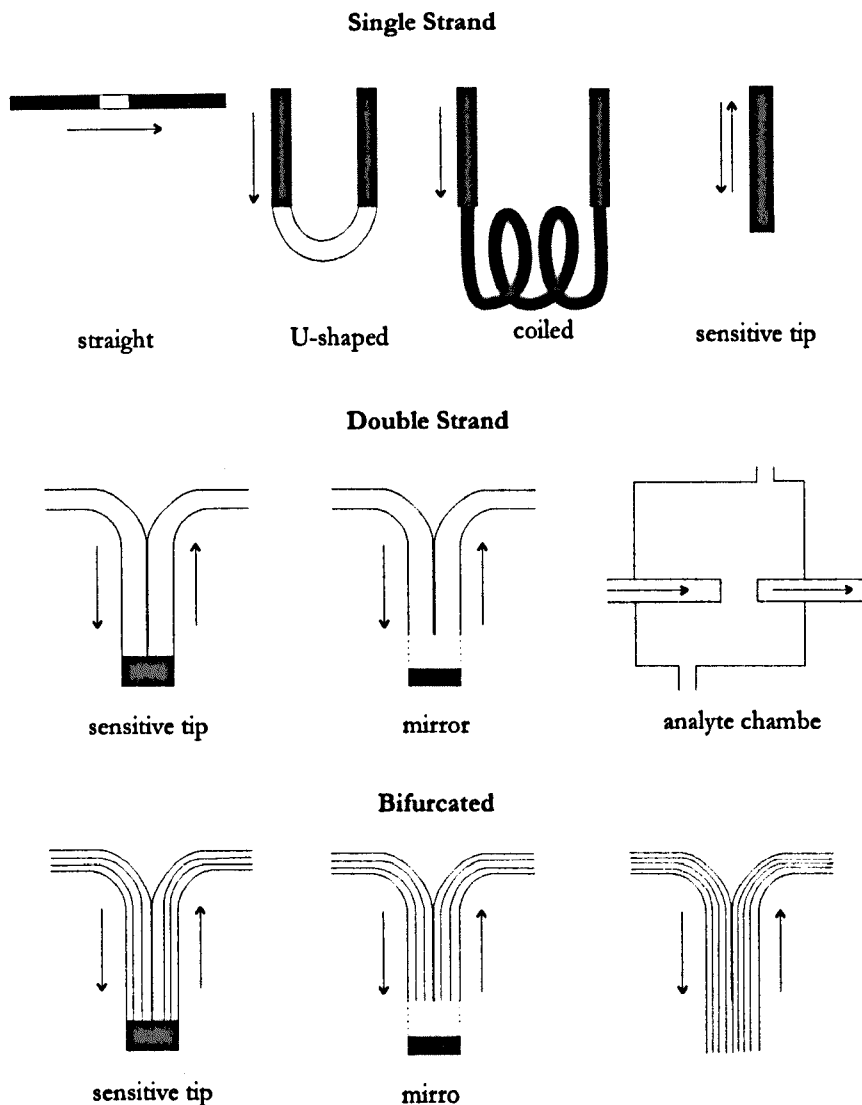
Fig. 1-1: Different types of fibre-optic based sensor cells.

1.4 Advantages and disadvantages of fibre-optic sensors

The essential advantage of fibre-optic sensors is the optical nature of the transduction process. The fibre is usually made from silica based glass, and less frequently from an organic polymer (e.g. polymethylmethacrylate). Depending on the field of application, a fibre-optic sensor can offer a number of advantages over other sensor types, such as:

- Possibility of remote *in-situ* observations, enabling a separation between the sample cell and the measurement equipment, which has for example been demonstrated in the measurement of radioactive species [12].

- Non-destructive analytical method (except for some reservoir optrodes).

- No effect such as electrical interference caused by static electricity, strong magnetic fields or surface potentials on the sensor head.

- Complete electrical isolation between the electrical and the liquid part of the sensor e.g. detector, power supply, signal processing unit and pumps.

- Miniaturization of fibre-optic systems can exceed that of electro-chemical based techniques, making them potentially attractive for medical use.

- Multi-parameter sensor systems can be developed due to wavelength multiplexing and large information capabilities of fibres.

- Most fibre sensors can be employed over a wider temperature range than electrodes and some have even a smaller temperature dependence.

- In many cases the sensor head does not consume the analyte in a measurable rate, which is particularly useful when dealing with small sample volumes.

However, fibre-optic sensors do exhibit some severe limitations which have to be taken into account when designing a fibre-optic based sensor system, such as:

- Ambient light may interfere with the optical signal of interest.

- Limited dynamic range of most reagent based sensors. This can be observed for example in fibre-optic based colorimetric techniques used to determine pH of water.

- Large diameter fibres cannot be bent easily to a narrow radius without creating micro-cracks reducing light transmission but barley visible to the naked human eye.

- Long sensor response time caused by mass transport to and in the reagent phase.

- Limited lifetime of immobilised reagents in optrodes and membrane technology.

1.5 Light power flow in a fibre-optic-based sensor system

In fibre-optic sensor schemes based on multimode fibres, intensity is the most convenient property available for sample modulation. The approach of this Section is to establish some performance criteria and formalize a general system description of a fibre-optic sensor scheme. The optical elements of a fibre-optic-based sensor system are shown in Fig. 1-2, comprising a light source, a fibre coupler, input and output fibres, a sensor cell and a detector. The performance of such a measurement arrangement is dependent on a number of factors, such as sensitivity, noise, signal-to-noise ratio, resolution, range, accuracy, temperature, stability, range and response time. Additionally, the effect of transient responses, either caused by the measurand or the sensor system, have to be considered.

| Light Source | Coupling Optics | Input Fibre | Sensor Cell | Output Fibre | Detector |
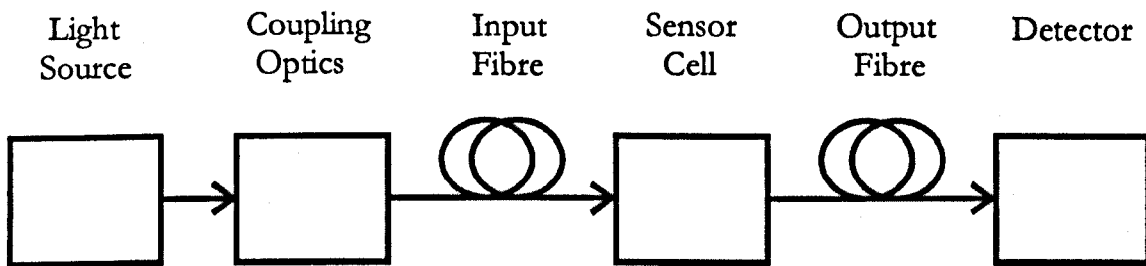
Fig. 1-2: Optical set-up of typical optical fibre-based sensor.

The key factor in designing a polychromatic sensor system, as envisaged in this work, is the wavelength - dependent power budget, $B_{Power}(\lambda)$, which may be defined as

$$\blacksquare \tag{1-1}$$

where $P_{Source}(\lambda)$ is the light power emitted from the source and $P_{Detector}(\lambda)$ the light power reaching the detector at a particular wavelength, λ. Thus, the goal in designing a polychromatic sensor system is to match the spectral dependence or sensitivity of the individual optical components, to obtain an acceptable signal to noise ratio over the desired wavelength range. However, the transfer and conservation of light power depends on a number of factors, including the efficiency of light coupling from one optical component

to the next. This most important factor, the coupling of light between the optical components, is characterized by what is termed the geometric extent (G), which describes the ability of each optical component to accept light. This is defined by

$$\blacksquare\blacksquare\blacksquare \qquad\qquad (1\text{-}2)$$

where S_i is the area of the emitting source and NA_i is a generalized value of the numerical aperture of the optical components i.e.

$$\blacksquare\blacksquare\blacksquare\blacksquare\blacksquare\blacksquare\blacksquare\blacksquare\blacksquare\blacksquare$$

where $S_{Detector}$ is the input area of the polychromatic detector, $NA_{Detector}$ is the numerical aperture, more generally termed the NA, of the detector, S_{Fibre} is the area of the input and output fibre (assumed the same here), NA_{Fibre} their numerical aperture, $S_{Sensor\ Cell}$ is the optically active area of the sensor cell and $NA_{Sensor\ cell}$ is its value of NA.

The other aspects of the loss function depend on a range of intrinsic aspects of the optical components. These can be described by the equation given below for the resultant intensity at the polychromatic detector as a function of wavelength, λ, source size, S, numerical aperture, NA, ambient temperature of the sensor system, T, and time, t, taking the lifetime of the light source and the degradation of the optical components by the UV radiation present, into account.

The light power collected by the polychromatic detector, $P_{Detector,dBm}(\lambda)$, is given by a function comprising several factors and their dependencies can be seen in the following equation

$$P_{Detector,dBm}\left(\lambda, S_{Detector}, NA_{Detector}, t, T\right) = P_{Source,dBm}\left(\lambda, S_{Source}, NA_{Source}, t, T\right)$$
$$- Loss_{Coupling}\left(\lambda, S_{in,out}, NA_{in,out}\right)$$
$$- Loss_{Input\,Fibre}\left(\lambda, S_{Input\,Fibre}, NA_{Input\,Fibre}, t, T\right)$$
$$- Loss_{Sensor\,Cell}\left(\lambda, S_{Sensor\,Cell}, NA_{Sensor\,Cell}, t, T\right)$$
$$- Loss_{Output\,Fibre}\left(\lambda, S_{Output\,Fibre}, NA_{Output\,Fibre}, t, T\right)$$

$$(1-4)$$

where $P_{Source,\,dBm}$ is the spectral power of the light source, $Loss_{Coupling}$ is the coupling loss from the light source to the fibre input, $Loss_{Input\,Fibre}$ and $Loss_{Output\,Fibre}$ are the absorption losses inside the input and output fibres respectively and $Loss_{Sensor\,Cell}$ is the optical loss inside the sensor cell, caused by sample modulation and guiding losses. With knowledge of the above, the power budget, can be optimized in the choice of the components used.

The optical configuration mainly used and investigated in this work comprises a deuterium lamp as a light source, two fused silica lenses used to couple light from the spark of the deuterium lamp to the input fibre (Chapter 2), solarization resistant input and output fibres (Chapter 2), an inexpensive spectrophotometer (Chapter 3) and one of three sensor cells (Chapters 4 and 5). Their performance will be described in the subsequent chapters.

1.6 Measurement principles: The Bouguer-Lambert-Beer Law

A mathematical-physical basis of light-absorption measurements to determine the molar concentration of certain substances in gases and liquids if defined by the Bouguer-Lambert-Beer (BLB) law in the ultraviolet, visible and infrared part of the light spectrum. The reduction of intensity, dI_λ, at a wavelength λ, that occurs when light of a monochromatic incident intensity I_λ, passes through a sample of thickness dl, containing an absorbing species with a molar concentration c, can be expressed by

█████████████

$$(1-5)$$

which when integrated over the pathlength, l, gives

$$\int_{I_{\lambda,Ref}}^{I_{\lambda,Sam}} \frac{1}{I} dI = k_\lambda \int_0^l c \, dl \tag{1-6}$$

where $I_{\lambda,Ref}$ is the initial, or so-called reference intensity, $I_{\lambda,Sam}$ is the intensity transmitted through the sample, the so-called sample intensity, and k_λ as a proportionality coefficient. Assuming that the concentration, c, is uniform and independent of l, this will result in

$$\ln \frac{I_{\lambda, Ref}}{I_{\lambda, Sam}} = k_\lambda c l \tag{1-7}$$

and

$$I_{\lambda,Sam} = I_{\lambda,Ref} e^{-k_\lambda c l} \tag{1-8}$$

indicating that the intensity decreases exponentially with the sample thickness and concentration. However, the BLB law is often expressed as

$$I_{\lambda,Sam} = I_{\lambda,Ref} 10^{-\varepsilon_\lambda c l} \tag{1-9}$$

where

$$k_\lambda = \varepsilon_\lambda \quad \ln 10 = 2.303 \varepsilon_\lambda \tag{1-10}$$

with ε_λ as the molar absorption coefficient of the absorbing species observed. Then, the absorbance, A_λ, and the transmittance, T_λ, can be defined as

$$A_\lambda = \lg \left(\frac{I_{\lambda,Ref}}{I_{\lambda,Sam}} \right) = \varepsilon_\lambda c l \tag{1-11}$$

and

$$T_\lambda = 100 \frac{I_{\lambda,Sam}}{I_{\lambda,Ref}}$$

<div align="right">(1-12)</div>

respectively, with the dimensions for A_λ in absorbance units, AU, for T_λ in %, for $I_{\lambda\,Ref}$ and $I_{\lambda\,Sam}$ in arbitrary units, a.u., for ε_λ in l mol^{-1} cm^{-1}, for c in mol l^{-1} and for l in cm. Thus, the concentration, c, of the species observed can be calculated as

$$c = \frac{A_\lambda}{\varepsilon_\lambda l}$$

<div align="right">(1-13)</div>

The BLB law is usually valid for dilute analyte solutions, for strongly monochromatic, parallel and coherent radiation and in optically homogeneous (isotropic) media. There should be no luminescence or scattering in the solution observed and the optical pathlength should be strictly defined. Its validity is demonstrated by strictly linear plots of A_λ versus cell pathlength, l, or concentration, c, of the absorbing analyte in solution. The sensitivity of the measurement can be elevated by increasing the pathlength in case of species with low molar absorption coefficients, such as, for example, the hypochlorite ion. A more detailed description may be found in several texts, e.g. [13, 14, 15].

1.7 Range and detection limit in absorbance spectroscopy

The problem of defining the range and the detection limit of a measurement procedure in optical spectroscopy has been investigated by many authors [14, 21, 16, 17, 18]. The approach of this Section is to define the terms "range" and "detection limit", by a signal to noise (SNR) approach, based on statistical observations, taking the effects of stray light and dark output (Chapter 3), both found in the detector array-based spectrometers used, into account.

1.7.1 Mean and standard deviation of an intensity measurement

To investigate the accuracy of an intensity measurement, a number of n individual samples are taken from each detector element. The mean intensity value, $\bar{I}_\lambda$, and its standard deviation, ΔI_λ, may be calculated from these samples by using the following equations

$$\blacksquare \qquad (1\text{-}14)$$

$$\blacksquare \sqrt{\frac{\overset{i=1}{\blacksquare}}{n-1}} \qquad (1\text{-}15)$$

The magnitude and accuracy of such a measurement could then by defined as

$$\blacksquare \qquad (1\text{-}16)$$

Throughout the experiments performed in this work a number of $n=10$ samples were used to increase the accuracy of the measurements.

1.7.2 Signal to noise ratio (SNR) of an intensity measurement

In the absence of an optical signal nearly any detectors exhibit a small residual output. This output is known as the dark output, $I_{\lambda,Drk}$, and has to be subtracted from the measured intensity, $I_{\lambda,Sam}$, to obtain the true intensity signal collected from a sample, $I_\lambda = I_{\lambda,Sam} - I_{\lambda,Drk}$. Thus, in the absence of stray light, the signal to noise ratio, SNR, of an dark output corrected intensity measurement may be estimated by

$$SNR = 10 \lg \left[\frac{\bar{I}_\lambda}{\Delta I_\lambda} \right] = 10 \lg \left[\frac{\bar{I}_{\lambda,Sam} - \bar{I}_{\lambda,Drk}}{\Delta I_{\lambda,Sam}} \right] \qquad (1\text{-}17)$$

where $\bar{I}_\lambda$ and ΔI_λ are the mean of the true intensity and its standard deviation, $\bar{I}_{\lambda,Sam}$ and $\bar{I}_{\lambda,Drk}$ mean of the sample and dark intensity respectively and $\Delta I_{\lambda,Sam}$ the standard deviation of the sample intensity [17, 18].

1.7.3 Error analysis of the BLB-Law

The BLB-Law relies on a logarithmic relationship between the concentration of an analyte observed and the light transmittance of the sample at a particular wavelength. This is the reason why the concentration error, caused the individual parameters to calculate the concentration, is not linear, but varies with its transmittance (or absorbance) value. However, as described in Section 1.6, the absorbance, A_λ, of an analyte can be calculated using

$$A_\lambda = \lg\left(\frac{\bar{I}_{\lambda,Ref} - \bar{I}_{\lambda,Drk}}{\bar{I}_{\lambda,Sam} - \bar{I}_{\lambda,Drk}}\right) \tag{1-18}$$

where $\bar{I}_{\lambda,Ref}$, $\bar{I}_{\lambda,Sam}$ and $\bar{I}_{\lambda,Drk}$ are the mean reference, sample and dark intensity values obtained from the detector element in three separate and independent measurements respectively. To estimate the error of the absorbance, ΔA_λ, equation (1.5-5) is differentiated with respect to the reference, sample and dark intensity to determine individually their effect on the accuracy of the measurement. The combined absorbance error, ΔA_λ, may then be derived by their variances to be

$$\tag{1-19}$$

resulting in

$$\Delta A_\lambda = \frac{1}{\ln 10} \blacksquare$$

<div align="right">(1-20)</div>

where additionally $\Delta I_{\lambda, Ref}$, $\Delta I_{\lambda, Sam}$ and $\Delta I_{\lambda, Drk}$ are the standard deviations of the variables shown above. Thus, the performance of the instrument can be evaluated by calculating the relative concentration error using equation (1.3-9)

$$\frac{\Delta c}{c} 100\% = \frac{\Delta A_\lambda}{A_\lambda} 100\%$$

<div align="right">(1-21)</div>

with c and Δc as the concentration and the concentration error, and A_λ, and ΔA_λ as the absorbance and the absorbance errors respectively.

A plot of the relative absorbance error as a function of absorbance, which could be expected using an inexpensive fibre-optic-based spectrometer, having a 12 bit analogue to digital converter and a detector dominated noise level of 1 a.u. for the mean, sample and dark intensity, estimated by their standard deviations, is shown in Fig. 1-3. It can be observed that, with a decreasing reference signal and therefore a decreasing signal to noise ratio, that the relative error of absorption increases. Furthermore, accepting a relative error of absorbance of 25 % with a measurement, a range with a lower limit of detection of 0.0007 AU, 0.0013 AU, 0.0024 AU, 0.0049 AU, 0.0098 AU, 0.020 AU, 0.0416 AU and a higher limit of 3.79 AU, 3.45 AU, 3.10 AU, 2.75 AU, 2.39 AU, 2.01 AU and 1.62 AU could be expected for the intensity values described above, varying between 4000 a.u. and 62 a.u.

0.0   0.5   1.0   1.5   2.0   2.5   3.0   3.5   4.0   4.5   5.0
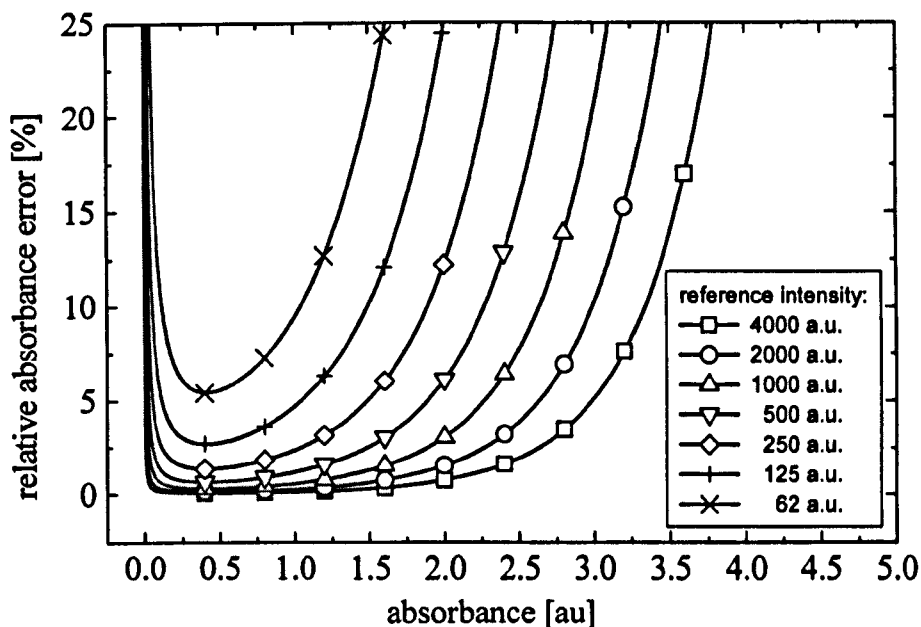
absorbance [au]

Fig. 1-3: Relative absorbance error as a function of absorbance, simulated for reference intensity values ranging from 62 a.u. and 4000 a.u. with a background dominated noise level of 1 a.u., typically expected with inexpensive fibre-optic based spectrometers.

1.8 Deviations from the Bouguer-Lambert-Beer Law

The BLB law cannot be applied in a number of situations to describe a linear relationship between the transmitted light and the concentration of the analyte observed, due to several interfering effects discussed below.

1.8.1 Stray light

A monochromator or polychromator is designed to observe a wavelength-resolved optical spectrum. This means that in the case of a polychromator equipped with an array detector only light of a particular, selected wavelength should reach a particular detector element. However, in practice a polychromator is not a perfect device, resulting in the fact that a small flux of light different from the selected wavelength reaches the detector element.

This "unwanted" component of light flux outside the selected spectral bandwidth of the detector element is known as stray light and can cause serious measurement errors in emission and especially absorption spectroscopy. Stray light can, for example, be caused by surface imperfections of the optical components, overfilling of the spectrometer's numerical aperture and less often by light leaks into the instrument [19, 20].

Because the light transmitted by most samples varies with wavelength, the proportion of stray light transmitted by a sample may not be equal to the sample transmittance, T_λ, at the analytical wavelength observed. Thus, assuming the incident light intensity as $I_{\lambda,Ref}$ and the stray light intensity as $I_{\lambda,Stray}$, then the total light flux observed by the detector would be $I_{\lambda,Ref} + I_{\lambda,Stray}$ without the sample present. If the sample would reduce the light flux within the spectral bandwidth observed from $I_{\lambda,Ref}$ to the sample intensity $I_{\lambda,Sam}$ and reduce the amount of stray light $I_{\lambda,Stray}$ from outside this spectral bandwidth by a proportion α_λ, which may be called the stray light transmittance, then the total light flux measured by the detector with the sample present would be $I_{\lambda,Sam} + \alpha_\lambda I_{\lambda Stray}$. The effect of the interfering stray light can be seen through the BLB-law which relies on the ratio of the initial to the transmitted lights to determine the concentration of the observed species, by calculating the measured absorbance, A_λ^*, as

$$A_\lambda^* = \lg\left(\frac{I_{\lambda,Ref} + I_{\lambda,Stray}}{I_{\lambda,Sam} + \alpha_\lambda I_{\lambda,Stray}}\right) \qquad (1\text{-}22)$$

where $I_{\lambda,Ref}$, $I_{\lambda,Stray}$ and $I_{\lambda,Sam}$ are the reference, stray light and sample intensity respectively. Defining the fractional stray light, S_λ, as

$$S_\lambda = \frac{I_{\lambda,Stray}}{I_{\lambda,Ref} + I_{\lambda,Stray}} \qquad (1\text{-}23)$$

and using equation (1.3-8), the measured absorbance, A_λ^*, can be expressed as

$$\blacksquare$$ (1-24)

It is thus clear that the existence of stray light will influence the absorbance measurement and therefore may cause errors during the determination of an analyte's concentration. Some particular cases will be examined to illustrate the practical effects of stray light.

Most commonly is that $\alpha_\lambda > T_\lambda$, resulting in the case that most of the stray light is transmitted through the sample, but the measured absorbance will be decreased at higher absorbencies, depending on the fractional stray light.
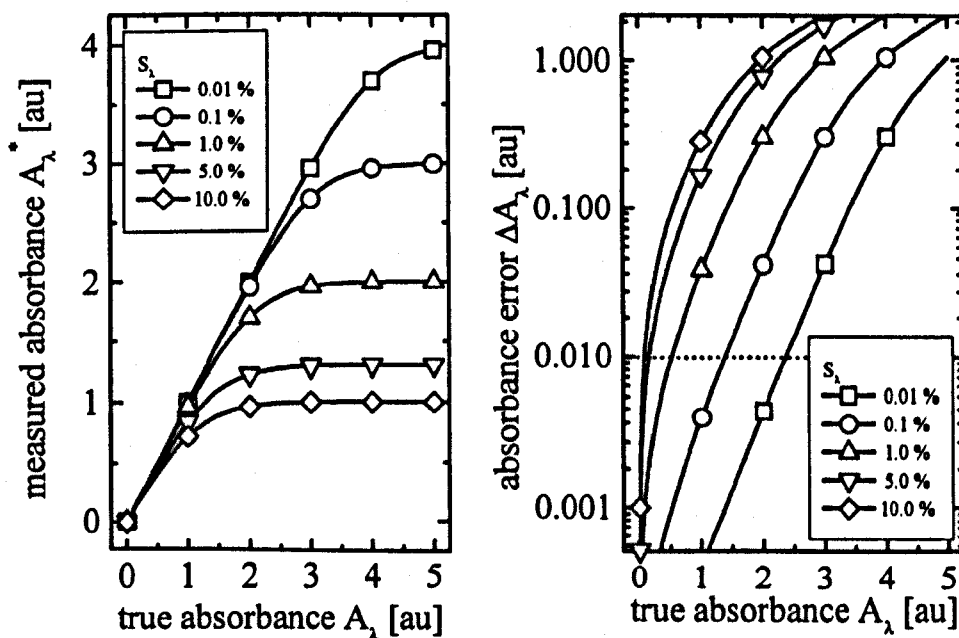
Fig. 1-4: Measured absorbance, A_λ^*, and absorbance error, ΔA_λ, as a function of true absorbance, A_λ, shown for several stray light levels, S_λ.

Fig. 1-4 shows the measured absorbance, A_λ^*, and the absorbance error, ΔA_λ, as a function of the true absorbance, A_λ, assuming the ideal case when $\alpha_\lambda = 0$, and all the stray light is transmitted through the sample. The concentration of a sample would be proportional to the measured absorbance in the absence of stray light (BLB-law), however with an instrument having an accuracy in absorbance measurements of 0.01 AU, deviation caused by stray light could be expected at absorbance values starting from 2.37 AU, 1.38 AU, 0.52 AU and as low as 0.17 AU and 0.09 AU for fractional stray light levels of 0.01 %, 0.1%, 1 %, 5 % and 10 % respectively, decreasing the instruments sensitivity and limiting its range. A polynomial regression fit could be used to increase the range at high stray light levels. However, the stray light would still limit the maximum absorbance to a lower value, independent of its capabilities given by the signal to noise ratio of the instrument.

A positive deviation from the true absorbance is created, if $\alpha_\lambda < T_\lambda$. This happens when most of the stray light is absorbed by the sample while the analytical wavelength remains almost unaffected. A practical but rare example is the spectrum of benzene (C_6H_6) vapour at about 250 nm wavelength, sometimes used for spectral calibration or wavelength resolution tests [19, 21]. In this case, stray light can cause absorbance minima of the benzene absorption peaks to be partially "filled" by the positive absorbance error, apparently degrading the spectral resolution.

Finally, the effect of stray light is eliminated, when the same amount of stray light and light at the analytical wavelength are absorbed by the sample, with $\alpha_\lambda = T_\lambda$, resulting in the fact that no absorbance errors occur. This however means that the sample has a flat response over the observed spectral range, only seen with, for example, calibrated neutral glass filters used to check the accuracy of the instrument without being affected by stray light.

Thus, it may be concluded that the effect of stray light in absorbance measurements can in some cases limit the linear response of an instrument, decreasing its range below the capabilities defined by its signal to noise ratio.

1.8.2 Lack of monochromasy

The relationship between absorbance and analyte concentration is defined by the BLB-law for monochromatic light. Therefore, the spectral resolution of a spectrometer should be less than the halfwidth of the absorption peak observed, otherwise the linear relationship between absorbance and concentration may be deformed [14].

1.8.3 Radiation scattering

Especially in the ultraviolet part of the spectrum, the effect of light scattering may be found, when large colloidal suspended particles are present in a sample. The observed molar absorption coefficient may be found to decrease with increasing concentration of the colloid analyte, caused by an increase of the transmitted radiation due to scattering into the direction of the radiation transfer. Thus, the total incident light collected by the spectrometer will consist of an absorption term and a scattering term, expanding equation (1-5) to

$$\blacksquare \tag{1-25}$$

where dI_λ is the reduction of intensity at the wavelength λ, that occurs when light of a monochromatic incident intensity I_λ, passes through a sample of thickness dl, containing an absorbing species with a molar concentration c, with a proportionality coefficient k_λ in a sample of the volume, v, with a number of scattering particles, n, [14].

1.8.4 Effect of fluorescence

The transmittance of a sample may be increased if an absorbing analyte solution simultaneously exhibits a fluorescence signal close to or at the wavelength used for the absorbance measurement. As a result, a lower concentration value may be obtained. However, this problem can be solved by selecting the spectrometer wavelength resolution and the analytical wavelength observed, ensuring in such a way that the signal obtained does not contain the fluorescent light emitted [14].

1.8.5 Changes in the refractive index

The molar absorption coefficient, ε_λ, is found to increase with increasing values of a solution refractive index [14]. However, this applies only to very high concentrations exceeding 10^{-3} molar, such as, for example, found for a 0.07 mol l^{-1} solution of eosin causing an error in ε_λ of 1.8 %. The relation between the refractive index and the molar absorption coefficient can be described by

$$\blacksquare \qquad\qquad\qquad\qquad\qquad (1\text{-}26)$$

where n is the refractive index of the aqueous solution. Calibration curves can be employed to measure high concentration values in a sample. However care should be taken when dealing with a larger range of concentrations.

1.8.6 Changes is the chemical equilibrium

The wavelength position and magnitude of a molar absorption coefficient may vary if the chemical equilibrium of a sample is changed due to, for example, dissociation, association or polymerisation [14]. This can, for example, be observed with the pH-dependent chemical reaction of chlorine with water to form dissolved chlorine (Cl_2) at a pH lower than 3,

hypochlorous acid (HOCl) at pH values ranging between 3 and 9, and hypochlorite ions (OCl⁻) at pH values greater than 9, with corresponding absorption peaks centered around 229 nm, 233 nm and 290 nm respectively, as described in Chapter 5.

1.8.7 Instrumental Deviations

These deviations may be found with the use of unstable light sources, causing power and temperature dependent intensity drifts and noise levels, wavelength drifts in the spectrometer itself, as discussed in Chapter 3, repeated reflection of radiation in the sample cell, effectively increasing its optical pathlength and various kinds of instrumental reflections. In general it may be found that the lower part of the absorbance versus concentration relationship of the BLB-law, and therefore the concentration limit, is circumscribed by noise and fluctuations in the electro-optical system, but at larger absorbance by stray light effects.

1.9 Summary

The interaction of light with matter can be used to determine the concentration of certain chemical species, for example nitrate, nitrite or ammonia in aqueous solution, as described by the Bouger-Lambert-Beer Law. Although a number of instrumental and other factors, such as monochromaticity, stray light, and changes of the refractive index can cause deviations, the Bouger-Lambert-Beer law can be used as an appropriate and simple method to provide adequate accuracy and stability for measuring certain chemical species within a limited conentration range.

However, to design a polychromatic sensor system based on fibre-optics, particular care has to be taken to match the wavelength-dependent sensitivity of the detector to the sensor arrangement. This will be a crucial factor, as the signal to noise ratio (SNR) defines the detection limit, and the amount of stray light the measurement range of such an optical sensor system.

In the following Chapter, the application of hydrogen treated silica fibres which transmit light at wavelengths below 250 nm will be investigated.

1.10 References

1 EC Directives (80/778/EEC) obtainable from HMSO High Holborn London, U.K.

2 P. W. Atkins, "Physical chemistry", Oxford University Press, UK, forth edition, (1993).

3 K. T. V. Grattan, B. T. Meggitt (Editors), "Optical Fiber Sensor Technology Vol. 1 (Optical and Quantum Electronics Series)", Chapman & Hall, London, UK, (1995).

4 O. S. Wolfbeis (Editor), "Fiber Optic Chemical Sensors and Biosensors", Vol. I & II, CRC Press, Boca Raton, Florida, USA, (1991).

5 E. Wagner, R. Dändliker, K. Spenner (Volume Editors), "Optical sensors: A comprehensive survey. - (Sensors), W. Goepel, J. Hesse, J. N. Zemel (Series Editors), VCH Verlagsgesellschaft mbH, Weinheim, Germany, (1992).

6 D. L. Wise, L. B. Wingard, Jr. (Editors), "Biosensors with Fiberoptics", Humana Press, Clifton, New Jersey, USA, (1991).

7 L. A. Saari, W. R. Seitz, "pH Sensor Based on Immobilized Fluoresceinamine", Anal. Chem., Vol. 54, No. 4, 821-823.

8 D. Meadows, T. S. Shultz, "Fiber-Optic Biosensors Based on Fluorescence Energy Transfer", Talanta, (1988), Vol. 35, No. 2, 145-150.

9 Y. Shah, R. A. Valsler, A. W. Palmer, "Optical Fibre Plethysmograph", J. Biomed. Eng., Vol. 7, (1985), 326-328.

10 T. Takao, H. Hattori, "Fluid observation with an optical fiber refractometer", Jpn. J. Appl. Phus., (1982), Vol. 21, 1509.

11 J. F. Giuliani, H. Wohltjen, N. L. Jarvis, "Reversible optical wavguide sensor for ammonia vapours", Optics Lett., (1983), Vol. 8, 54.

12 C. Moulin, S. Rougeault, B. Dureault, P. Mauchien, "Uranium Remote Sensing by Laser-Induced Fluorescence", in Proceedings of the 1st conference presented in Graz, April, (1992), p-81.

13 H.-H. Perkampus, "UV-VIS spectroscopy and its applications", Springer-Verlag Berlin Heidelberg New York, (1992), 3-9.

14 L. Sommer, "Analytical absorption spectrophotometry in the visible and ultraviolet: the principles", Elsevier Science Publishers, Amsterdam, the Netherlands, and Akadémiai Kiadó, Budapest, Hungary, (1989), 13-44.

15 P. W. Atkins, "Physical chemistry", Oxford University Press, UK, forth edition, (1993), 500-530.

16 P.W.J.M Boumas, "Atomic emission detection limits: more than incidental analytical figures of merit! - A tutorial discussion of the differences and links between two

complementary approaches -", Spectrochimica Acta, (1991), Vol. 46B, No. 6/7, 917-939.

17 International Union of Pure and Applied Chemistry, "Nomenclature, Symbols, Units and their usage in Spectrochemical Analysis-II, Data Interpretation", Pure & Appl. Chem., Pergamon Press, (1976), Vol. 45, 100-103.

18 S. Ebel, U. Steffens, "Error and Error Propagation in Quantitative UV-Spectroscopy" (in German), Fresenius Z. Anal. Chem., (1980), Vol. 301, 389-401.

19 M. R. Sharpe, "Stray light in UV-VIS Spectrophotometers", Analytical Chemistry, (1984), Vol. 56, No. 2, 339A-356A.

20 S. Thomaßen, "Miniaturisierte Spektrometer", Photonik, AT-Fachverlag GmbH, (1998), Vol. 1, 20-22.

21 American Society for Testing and Materials, "Standard Practice for Describing and Measuring Performance of Ultraviolet, Visible, and Near-Infrared Spectrophotometers", Annual Book of ASTM Standards, (1997), Vol. 03.06, E 275-93, 708-717.

2. Characterization of UV-Improved optical fibres for sensor applications

2.1 Abstract

A major problem when developing a fibre-optic-based sensor system for ultraviolet spectroscopic applications has been solarization effects in silica fibres with a fused silica core and a fluorine-doped cladding. These solarization effects have made the transmission of ultraviolet light of wavelengths below 230 nm practically impossible. However, ultraviolet improved fibres (UVI-fibres), showing a significantly reduced UV-absorption, have been developed. This improvement has been realized due to a passivation of the UV-defects by hydrogen gas doping. This Chapter compares the performance of standard silica fibres with these new, improved, UVI-fibres, investigates the long term and short term behaviour of UVI-fibres, introduces the concept of a wavelength selective fibre coupler and discusses the applicability of UVI-fibres for UV-sensor applications.

2.2 Introduction

Two major events in the 1960s provided significant impetus for the introduction of new technology for sensing systems, these being the invention of the laser and the optical fibre by Kao *et al.* [1]. Although originally designed for telecommunications, optical fibres were increasingly used for sensor applications. An optical fibre is a particular type of dielectric waveguide which allows the propagation of electromagnetic waves in the frequency range, from 10^{12} to 10^{15} Hz. The energy coupled into an optical fibre is confined in its core and guided by a mechanism of multiple reflection at the core/cladding boundary along the fibre. A typical optical fibre consists of a cylindrical core made, for example, of fused silica, having a higher refractive index than its surrounding cladding layer composed of a similar material. The two concentric cylinders are protected by a plastic jacket, giving the fibre its mechanical strength and protecting it from environmental effects. A more detailed de-

scription of optical fibres and their application can be found elsewhere [2, 3]. The attenuation of light travelling inside optical fibres can be attributed to three major sources, these being absorption, scattering and mechanical losses. These have been conveniently summarized in the literature [3]. Absorption results from the interaction of light as an electromagnetic wave with the constituents of the fibre material and its associated impurities. Such losses can be classified by their source of origin as intrinsic, extrinsic and defects originated losses. Scattering is the second cause of attenuation with Rayleigh scattering being the most common source of attenuation, followed by bulk and wavelength imperfections generated during the fabrication process and Raman and Brillouin scattering. Finally, light attenuation can be induced into optical fibres mechanically by bending and coupling losses.

However, one of the most serious limitations in many spectroscopic applications arises from the restricted spectral transmission of commercially available low-cost fibres. In the spectral region between approximately 250 nm and 1.6 μm, silica is the most widely used material for the fabrication of light-guiding fibres because of its low attenuation [4]. Unfortunately, the light transmission is not stable under certain conditions which are often encountered in existing sensor systems, where, for example, the light source is a pulsed high-power laser [5,6], a UV-laser [6,7] or a deuterium lamp [8]. In the latter case, the wide potential spectroscopic applications are restricted to the wavelength region at above about 230 nm, because standard fibres may be damaged by UV-light below 230 nm so quickly that a stable and acceptable transmission in any practical device is impossible. The reasons for this effect is the generation of UV-induced colour centres with absorption bands in the spectral regions where transmission is thus reduced [4, 8 , 9]. In addition, ionizing radiation can generate the same transient or stable fibre defects described above which significantly disturb the transmission.

In this Chapter, the applicability of new optical fibres having a nearly constant UV-transmission in the 200 nm to 250 nm wavelength region for sensor applications is investigated. Due to the improved UV-properties when compared to those commercially avail-

able, these new fibres are tested as a potential transmission medium for the broadband-spectrum of a deuterium lamp. In addition, a fibre coupling system with a wavelength-selective coupling efficiency, comprising a deuterium light source, two fused silica lenses and an input fibre is described.

2.3 Basic and UV-induced attenuation in silica fibres in the ultraviolet

Intrinsic losses and Rayleigh-scattering mainly determine the basic attenuation at wavelengths below 300 nm in fused silica fibres with an undoped core and a fluorine doped cladding. It is known that Rayleigh scattering varies as $1\ \lambda_0^{-4}$, where λ_0 is the wavelength of interest [10]. Fabian *et al.* have measured a basic attenuation of 1.1 dB m^{-1} at a wavelength of 200 nm, which appeared to define the minimum loss in that wavelength region [11]. Another common source of attenuation is related to the hydroxyl ion (OH$^-$), but can be neglected for applications described in this work because of its absorption peaks in the near infrared. However, ultraviolet light below 230 nm, coupled into silica fibres, can damage the transmission properties of such a fibre by the generation of UV induced colour centres (E'-centres) [12, 13, 14], using, for example, deuterium lamps [15] or excimer-lasers [16]. Thus, when describing the total light loss, $\alpha_{L,tot}$, of a fibre of a total length, L, the wavelength-dependent basic attenuation, $\alpha_B(\lambda)$, and UV-induced attenuation, $\Delta\alpha(\lambda)$, have to be taken into account. Further, due to the fact that the fibre behaves as a long-pass filter, the extent of defect generation decreases along the fibre length, z. Therefore, the induced loss, $\Delta a(\lambda)$, does not increase linearly with fibre length and may be described as

$$\Delta a_L(\lambda) = \int_0^L \Delta\alpha(\lambda,z)\,dz \qquad (2.3\text{-}1)$$

In addition, the damage is time-dependent, leading to the following equation for the total light loss, $\alpha_{L,tot}(\lambda,\,t_{UV})$, where t_{UV} is the UV-exposure time

In the following section, a mechanism is described to reduce the generation of E'-centres and therefore the UV-induced attenuation.

2.3.1 Improvement of UV-transmission in silica fibres by gas doping

The mechanism of improvement, presented here in a summarized form, has been published by Klein *et al.* [17]. This work emphasised that the treatment of synthetic silica bulk or fibres in a hydrogen atmosphere [18, 19, 20] results in an improved resistance to UV-induced defects which are similar to UV-defects generated by ionizing radiation like X-ray or gamma ray [9, 21, 22]. The proposed mechanism is transferable to UV-damage. As discussed above, E'-centres are generated in fibres or bulk material during UV-light irradiation arising from a number of reasons, such as breaking weak bonds between silicon, Si, and oxygen, O, [21, 23], or impurities like metals [8, 9, 22], or chlorine, Cl, [24], as for example shown in the following chemical reactions caused by UV-light, $h\nu$ exposure

$$\equiv\text{Si-O-Si}\equiv \ + \ h\nu \quad \Rightarrow \quad \equiv\text{Si}\bullet \ + \ \bullet\text{O-Si}\equiv \qquad (2.3\text{-}3)$$

$$\equiv\text{Si-Cl} \quad + \ h\nu \quad \Rightarrow \quad \equiv\text{Si}\bullet \ + \ \bullet\text{Cl}° \qquad (2.3\text{-}4)$$

However, in the presence of molecular hydrogen, a hydrogen atom, H, is able to passivate the E'-centre

$$\equiv\text{Si}\bullet \quad + \ H_2 \quad \Rightarrow \quad \equiv\text{Si-H} \ + \ H° \qquad (2.3\text{-}5)$$
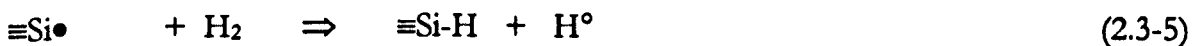
Thus, the E'-centre is removed and the absorbing UV-defect is no longer is present. Such hydrogen treatment has, for example, been performed with the amorphous silicon found in high-efficient solar cells [25]. A key factor in optimizing the technique was to find a

method of ensuring a homogeneous distribution of hydrogen in the fibre. This was achieved by optimizing the parameters of the diffusion process. Fused silica fibres with a high OH-content in the core were "loaded" with hydrogen in a pressure chamber until a hydrogen concentration of approximately $5 \cdot 10^{19}$ molecules cm^{-3} was reached. These ultra-violet improved fibres (UVI-fibres) showed a significant improvement in the transmission of light at wavelength below 230 nm. However, after the hydrogen treatment, the molecular hydrogen diffuses out of the fibre again, decreasing the capability of the fibre to passivate the generation of E'-centres. This process, which is dependent on the hydrogen diffusion coefficient in silica, ambient temperature, fibre diameter and time starts at the outer surface of the fibre and leads to time-dependent hydrogen profiles in the fibre [17]. It was found that the lifetime of the hydrogen treated fibres, $t_{3\,dB}$, which was defined as the time a fibre of 1 m length would transmit UV-light at a wavelength of 214 nm with a light loss of less than 3 dB caused by UV-radiation, could be estimated at a fixed temperature with scaling function

$$t_{3\,dB} = 0.5 \text{ month} * SF_T * SF_D \tag{2.3-6}$$

with SF_T being a scaling factor describing the temperature dependence of the diffusion process and SF_D being a scaling factor describing the influence of the fibre diameter on the diffusion process. The scaling factors SF_T and SF_D are shown in Fig. 2-1. As a result, both the reduction of fibre temperature and the increase of fibre diameter increase the lifetime of the fibre. Using a fibre with a core diameter of 500 µm or 600 µm, as commonly used in sensor applications, in a laboratory having a temperature of 21 °C, a lifetime of approximately 15 month and 21 month could be expected respectively, rendering them well suited to the UV-sensor applications envisaged in this work.
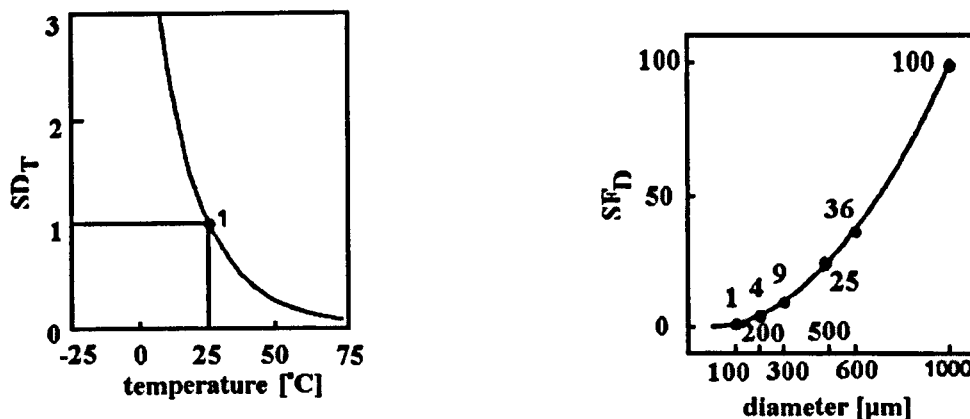
Fig. 2-1: Scaling factors SF$_T$ and SF$_D$ for life time prediction of UVI-fibres

As shown in Fig. 2-1, reducing the ambient fibre temperature would greatly reduce its lifetime. However, when using such fibres, temperature-dependent transient defect generation can be observed, limiting their usage, as discussed in the following sections. Nevertheless, the UVI-fibres should be stored in a cool place to minimize the out-diffusion of the hydrogen gas, if the fibres are not used.

2.3.2 Experimental determination of UV-induced losses in standard and UVI-fibres

The experimental arrangement shown in Fig. 2-2 was used to measure the UV-induced losses, $\Delta a(\lambda, t_{UV})$, as a function of the wavelength, λ, and time, t_{UV}. The broadband spectrum emitted from a D$_2$-lamp, type DO 904/05 [26], was coupled into the test-fibre which had the following geometrical data: core diameter 200 μm, cladding diameter 220 μm, coating diameter approximately 350 μm, with fibre lengths from 1 m up to 10 m being used. At the output, the fibre end-face was imaged with the lens-system shown onto the slit of a monochromator. However, due to the wavelength-dependence of the refractive index of fused silica and therefore the focal length of the lens, the lens coupling system used is only valid for one particular wavelength. Thus, the distance between the fibre and the monochromator must be varied during the spectral testing procedure, to accommodate a variety of wavelengths. The light power was detected with a photomultiplier, and

Characterization of ultraviolet improved optical fibres ...

32

the other components in the system shown are essentially used for signal processing and noise-reduction.

ELECTRICAL SYSTEM

PC
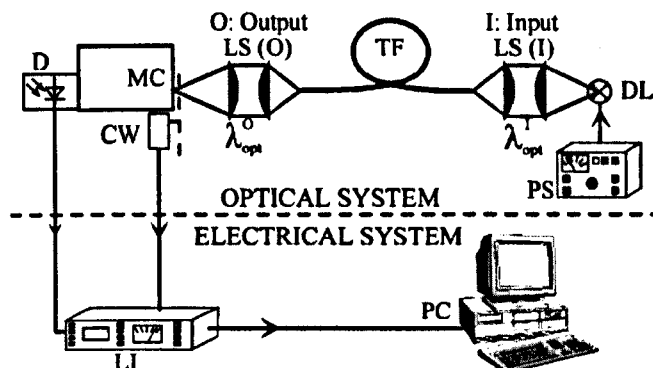
Fig. 2-2: Experimental arrangement of the measurement system, comprising a deuterium lamp (DL), lens coupling systems (LS(0), LS(I)), a test fibre (TF), a monochromator (MC), a chopper wheel (CW), a photo-multiplier (D), a lock-in amplifier (LI), and a power supply (PS).

In the determination of the UV-induced losses, $\Delta a_L(\lambda, t_{UV})$, the spectral photocurrent which is related to the spectral output, $P(\lambda, t_{UV})$ was measured at the fibre end-face, after different exposure-times, t_{UV}, as

$$\Delta a_L\left(\lambda, t_{UV}\right) = 10 \log\left\{\frac{P\left(\lambda, t_{UV} = 0\right)}{P\left(\lambda, t_{UV}\right)}\right\} \qquad (2.3\text{-}1)$$

In order to obtain results on the characteristics of this fibre, which may be more meaningfully compared with those other fibres, essentially the same spectral output power was used at the beginning ($t_{UV} = 0$) with therefore the same spectral input power coupled into the fibres. It was assumed that the basic attenuation, $\alpha_B(\lambda)$, remains the same. Using the D2-lamp described as a source, the characteristics obtained from a fibre of 1 m length are given in Tab. 2-1. As will be shown later, the output power is essentially stable in the new fibre, where the exposure data reported were taken during one day of experimentation to avoid errors due to any possible longer term system changes.

wavelength [nm]	193	214	240
spectral power [nW nm⁻¹]	125	50	37
spectral intensity [µW (nm mm⁻²)⁻¹]	4	1.6	1.2

Tab. 2-1: Output power at the fibre end-face with a fibre length of 1 m.

As a reference, a commercially available step-index multimode fibre with undoped high-OH core and fluorine-doped cladding drawn from a Fluosil-preform (type SSU) was used. Fig. 2-3 shows the wavelength-dependent photo current at the beginning (dashed line) and after a typical period of UV-irradiation (solid line): an 11 hour exposure to UV-light through the light-guiding core was used. After exposure, the output power detected in the region below ~250 nm was found to be significantly decreased.
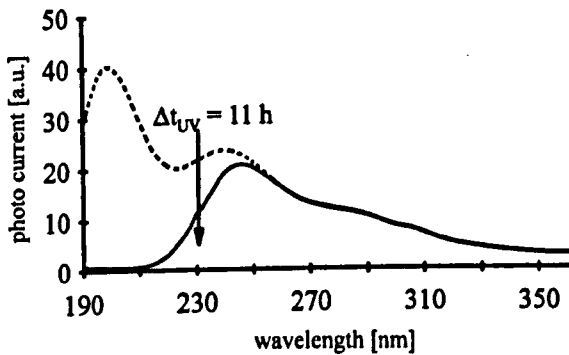
Fig. 2-3: Spectral output power of a reference fibre before (dashed line) and after (solid line) 11 h of UV-light irradiation.
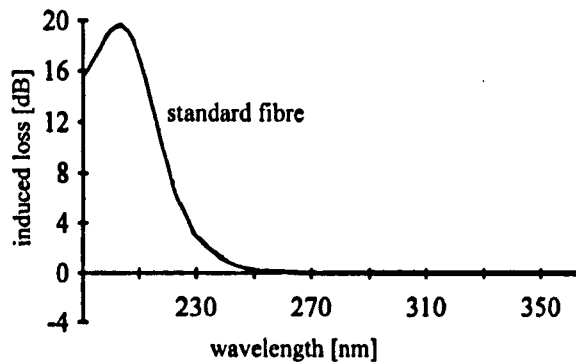
Fig. 2-4: Spectral induced losses of a standard fibre after 11 h of UV-light irradiation.

Measuring the induced losses described above, the nature of the defects causing the UV-losses during UV-irradiation of wavelengths below 230 nm becomes obvious: this is due to the presence of E'-centres and exemplified by the evidence of a UV-absorption band around 210 nm [9]. The maximum values of the induced losses were determined by coupling UV-light into short fibre samples of 1 m length. Thus, losses of 15 - 20 dB could be determined at 210 nm after an exposure time of 11 hours with a fibre having a core diameter of 200 µm, as shown in Fig. 2-4. These losses are significantly higher when com-

pared to the basic (non-exposed) loss of 1 dB (basic attenuation $\alpha_B(210 \text{ nm}) \approx 1 \text{ dB m}^{-1}$). The variations are mainly due to modifications in the fibre material itself due to the irradiation. Looking at the time-dependence of the process, the induced losses shows a trend of being nearly linear with exposure time at the beginning. However, a saturation level is reached after approximately 10 hours, when the generation and recombination of the defects are in equilibrium. In addition, it was found that following this, the induced losses are seen to decrease slightly, after the UV-irradiation ends.

A significant difference has been found when using UVI-fibres for the transmission UV-C light. Fig. 2-5 illustrates the improvement of the new fibre samples to the problem of UV-damage, these fibre samples having the same geometrical data as the previously tested reference fibres.
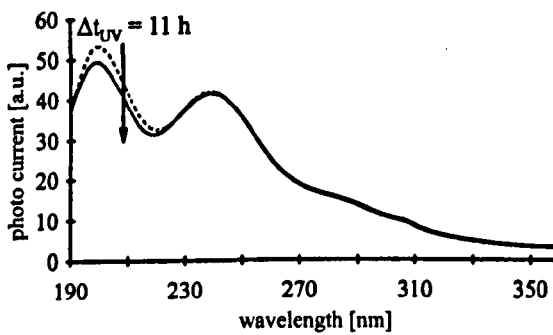
Fig. 2-5: Spectral output power of a UV-improved fibre before (dashed line) and after (solid line) 11 h of UV-light irradiation.
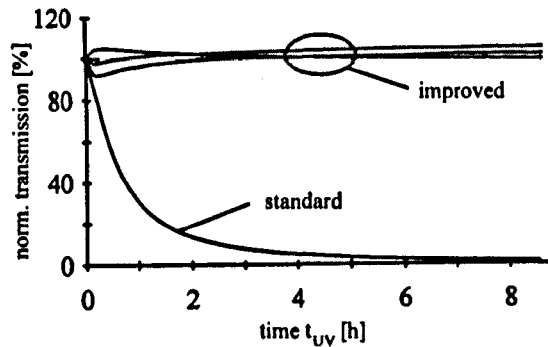
Fig. 2-6: Normalised transmission at 210 nm wavelength for three UV-improved fibre samples (upper curves) and one reference fibre (lower curve).

Using the same exposure conditions, the difference between the spectral output power at the beginning ($t_{UV} = 0$ h) and after the total exposure in this test ($t_{UV} = 11$ h) is not obvious. The absorption maximum around 214 nm (due to the E'-centres) is less than 0.3 dB. The same value can be determined from Fig. 2-6 showing the time-dependent normalised transmission, with the variations seen to be less than 8% in total.

2.3.3 Transient light losses in UV-improved fibres

UVI-fibres have been tested with several different and important UV sources, such as deuterium lamps [15, 27], excimer-lasers [28, 16], a tunable UV-laser [29], and a frequency-doubled Ar^+-laser. Both their short-term and the long-term behaviour is of importance for sensor applications. With the monochromator set-up described in section 2.3.2, the time resolution of the experimental arrangement was limited by the scanning speed of the monochromator. Using a fibre-optic based spectrometer (Chapter 3), the presence of a low concentration of E'-centres could be observed during illumination of the UVI-fibres.
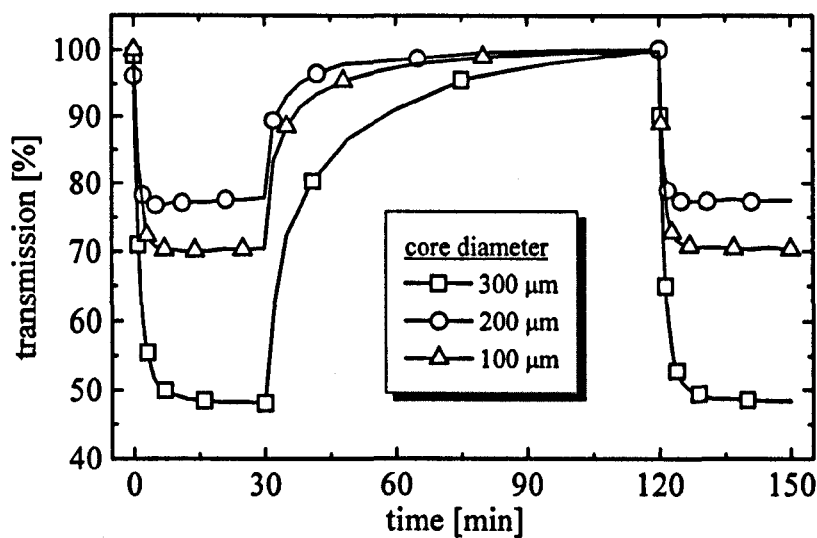
Fig. 2-7: Temporal fibre transmission behaviour of 2 m long UV- improved silica fibres for three different fibre core diameters; the illumination of the fibre starts at t = 0 min, is switched off at t = 30 min and starts again at t = 120 min

The transmission of UV light as a function of time, normalized to the start of the measurement cycle, is shown in Fig. 2-7 for fibres with core diameters of 100 μm, 200 μm and 300 μm. It is obvious that the normalized transmission decreases with time during the period of UV-illumination, because of UV damage due to the generation of E'-centres. However, a plateau value is reached after approx. 10 minutes which is different for the different core diameters of the fibres used. On the other hand, the transmission is seen to

increase during the period of darkness (zero illumination starting at t= 30 min), due to defect annealing, rising nearly to the starting value. In order to produce a consistent series of results for the system during this period, the fibres were illuminated only during the time of measurement for approx. 5 seconds. Three points are important in relation to this. The first is that, in a similar way to radiation induced losses, the UV damage increases with decreasing fibre diameter [see Fig. 2-7 and the work of Greenwell *et al.*[30]]; secondly, the fibre recovery to the starting value takes place during a period of zero illumination within less than one hour; and thirdly, a time period of approx. 10 min is needed until the fibre transmission, or output power, is stable over the full range of wavelengths starting from λ= 185 nm and including the region of E'-centre absorption. This time is comparable to the "warm-up" period of the deuterium lamp itself.

While a constant recovery behaviour could be observed within the measurement errors of the experiment, the creation of E'-centres is influenced by several parameters. First of all, the power density below 225 nm was found to influence the plateau magnitude, because a stable output will be reached, when defect generation and recombination reach equilibrium, thus increasing the power density results in a lower plateau value, i.e., an increased loss. Secondly, the recombination process will increase with higher temperatures [21]. This was investigated for fibre having a core diameter of 100 µm and resulted in a relative transmission shift of 1 % K^{-1}. Further information on these aspects of these fibres can be found in the work of Klein *et al.* [17]. However, for the sensor applications envisaged in this work, UVI-fibres with core diameters of 500 µm and 600 µm may be used, where the generation of E'-centres was found to be far lower, Additionally, the transient effects described above have been obtained with comparatively high UV light powers (such as for example a UV-irradiation of approximately 270 nW nm^{-1} at 214 nm, the absorption maximum of the E'-centre) coupled into a fibre with a core diameter of 300 µm. However, the transient effects shown above are decreased significantly due to the increased core diameter of the fibres envisaged for sensor use, rendering them suitable for use in UV sensor applications.

2.4 Coupling of ultraviolet light into optical fibres

A critical part of any fibre-optic spectrometer system is the light source. To take full advantage of the capabilities of the fibre-coupled miniature UV/VIS spectrometers used in this work, the source used should have, as far as possible, a continuous and even spectral distribution across the required wavelength range, a high and stable radiant flux output combined with an emitting source area well suited to the optical coupling conditions.

2.4.1 Commonly used light sources for ultraviolet spectroscopy

Broad-band light sources like the deuterium lamp or pulsed xenon-discharge lamps are commonly used to provide ultraviolet and visible (VIS) light of a continuous and more or less even spectral distribution for optical spectrometers. Deuterium discharge lamps have been used in this work to provide a continuous spectrum between 190 nm and 350 nm wavelengths. Their construction is described in several texts [31, 32]. A tungsten coil is fitted as the anode on the axis of a cylindrical, thin-walled, quartz discharge tube filled with deuterium. An activated tungsten double coil, mounted laterally, is generally used as a cathode. Depending on the lamp type, a heating voltage of 2 V, 2.5 V or 10 V is applied. The lamp is started with an ignition voltage between 200 V and 400 V and then runs with a voltage of about 85 V and an anode current of 400 mA. In order to produce the highest possible radiation intensities, it is necessary to restrict the discharge between the cathode and the anode by means of an aperture of small cross-section, commonly of a diameter of 0.3 mm, 0.5 mm or 1 mm, formed from a high melting point metal, for example molybdenum [31, 26]. A gradual decrease in power, with the age of the light source [15], has been reported but this is usually not a problem, as replacement is easy. Usually, a lifetime of approximately 1000 hours can be expected.

2.4.2 Design of a fibre coupler with wavelength-selective coupling efficiency

The envelope of the deuterium light source has a diameter of ≈ 30 mm [26]. A simple coupling arrangement would suggest the input fibre of the sensor system be placed ≈ 15 mm away from the emitting area of the source, but even then only a fraction of the

light flux emitted by the deuterium lamp would be coupled into the fibre. To increase the light flux entering and thus propagating within the fibre, a suitable imaging system has to be designed and employed to image the emission area of the source on the fibre tip. As it was simpler and cheaper to use lenses rather than mirrors or UV-achromats, two plano-convex fused silica lenses with a focal length of 40 mm at λ=589 nm and a lens diameter of 25.4 mm were employed to construct a simple 1:1 imaging system, as shown in Fig. 2-8. UV light is coupled from a 208/05R deuterium lamp discharge lamp (DL) [33] with a light aperture of $\approx$ 0.5 mm, and a NA $\approx$ 0.34 into a fibre with a core diameter, d $\approx$ 400 µm, and a NA $\approx$ 0.2 via a lens coupling system, made from two fused silica lenses.
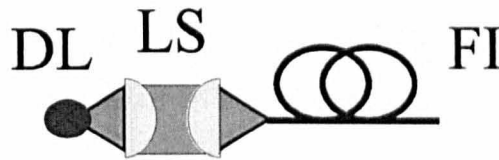
Fig. 2-8: Simple 1:1 imaging system comprising a deuterium lamp (DL), a lens system (LS) and an input fibre (FI).

However due to the strong increase of refractive index of fused silica in the deep UV, the focal length of the lens system decreases in this arrangement significantly from 41 mm at λ =730 nm to 34 mm at λ=200 nm wavelength [34]. The variation of the refractive index of fused silica and the resulting variation of the focal length of the fused silica lenses used in the lens system are shown in Fig. 2-9. Therefore, the fibre front face can only be accurately located in relation to the lens system for one optimized wavelength at the focal point of such an imaging system. Because of the small diameter of the fibre core and the large shift of the focal point, only a part of the incoming light is coupled into the fibre at higher or lower wavelength with respect to the optimized value. This chromatic aberration of the lenses can be used to tailor the spectral distribution of the source, through the optical system, to match the spectral sensitivity of the fibre-optic spectrometers used. The effect of using this wavelength-dependent coupling efficiency of the lens system, optimized for 225 nm, 272 nm and 443 nm and compared to positioning the fibre in front of the deuterium lamp, is shown in Fig. 2-10 and Fig. 2-11.
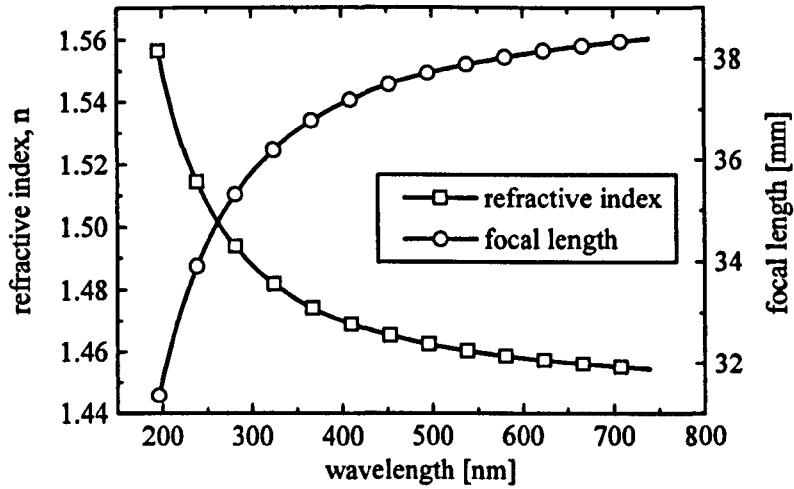
Fig. 2-9: Variation of the refractive index, *n*, of fused silica and the resulting focal length variation of the fused silica lens used in the imaging system (LS) as a function of wavelength.
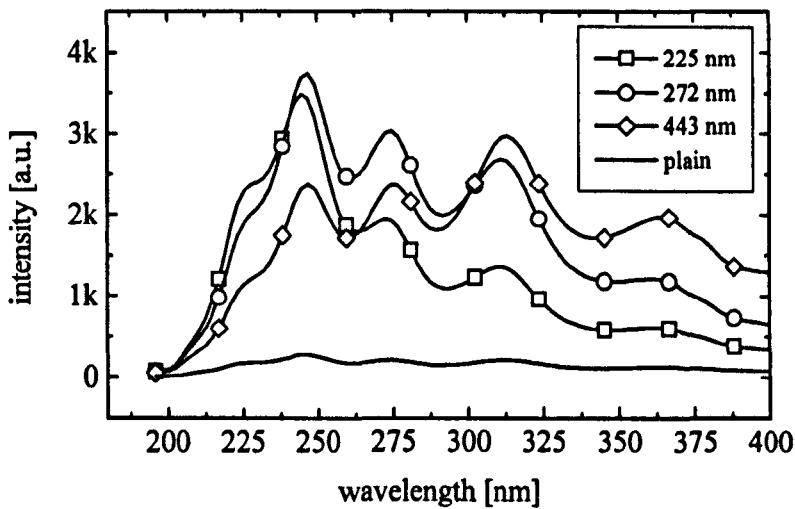
Fig. 2-10: Relative intensity output at the fibre end-face with a lens system, optimized for 225, 272, and 443 nm. The sample "plain" is the reference, showing the intensity coupled into the fibre without a lens system.

This illustrates the tailored intensity output at the fibre output in Fig. 2-10 and the relative gain and wavelength dependence of the imaging system compared to direct coupling, by placing the fibre in front of the light source, as shown in Fig. 2-11.
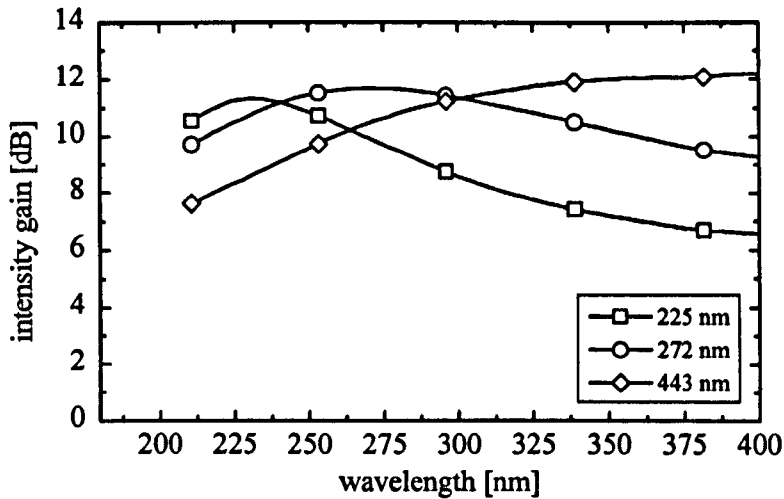
Fig. 2-11: Relative gain which can be achieved with a simple lens system compared to direct coupling, by placing the fibre in front of the deuterium lamp.

The intensity spectrum optimized for 225 nm offers two advantages, compared to the spectrum optimized for 443 nm, in its use for deep UV-applications. First, the intensity is increased at lower wavelengths, resulting in an improved signal to noise ratio and secondly, the effect of stray light is significantly reduced due to the increased intensity at the wavelength of interest and the decrease in intensity at the non-optimized wavelengths, mainly causing the stray light (Chapter 1). However, for light intensities coupled in the fibre under non-optimized wavelength conditions, the spectral power and the corresponding far field-distribution at the fibre output changes, as for example shown in Fig. 2-12. In this experiment, the lens system was optimized for the 200 nm wavelength region. It can be observed that the higher modes of the fibre in the non-optimized, higher wavelength region are not excited, leading to a suppression of higher farfield angles.
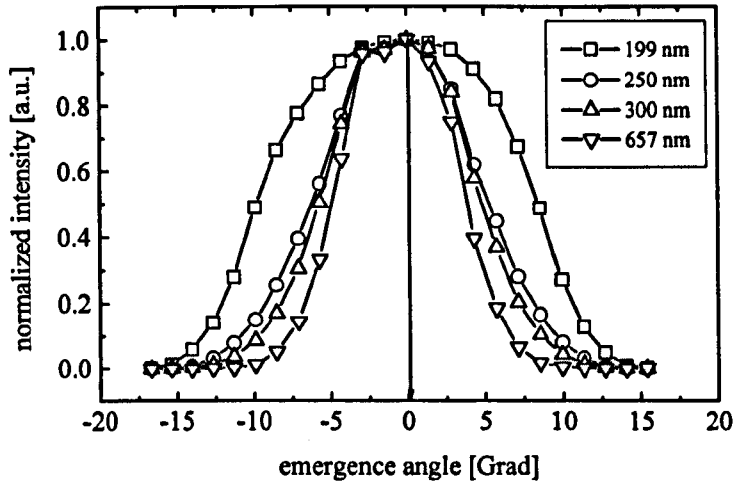
Fig. 2-12: Normalized far field distribution of a lamp-fibre system, optimized for 200 nm wavelength at the output of fibre with a core diameter 600 μm fibre, typically used in the subsequent sensor systems.

With such an arrangement, frequently used in the following experiments, light power levels in the range of 177 nW nm⁻¹, 69 nW nm⁻¹ and 28 nW nm⁻¹ were coupled into a UVI-fibre with a core diameter of 600 μm at 214 nm, 260 nm and 300 nm respectively.

2.5 Summary

Fibre samples with an improved UV performance at wavelengths below 250 nm have been introduced and their applicability for sensor use investigated. The more stable UV-transmission was mainly achieved by a reduction of defect generation during UV-light exposure. The induced attenuation of the main UV-absorption band around 214 nm is less than 0.4 dB m⁻¹ and therefore is nearly two orders of magnitude smaller, under the same test-conditions, when compared to the use of standard fibres. Lifetimes of approximately 15 month and 21 month for UVI-fibres with a core diameter of 500 μm or 600 μm respectively could be expected at room temperature, rendering these fibres suitable for UV-sensor applications envisaged in this work. UVI fibres will be used in the following chapters as a basis to design fibre-optic remote UV sensors for the wavelength region between

200 nm and 300 nm.

2.6 References

1 C. Kao, G. Hockham, "Dielectric fibre surface waveguides at optical frequencies", Proc. IEE, Vol. 113, 1158-1163.

2 K. T. V. Grattan, B. T. Meggitt (Editors), "Optical Fiber Sensor Technology Vol. 1 (Optical and Quantum Electronics Series)", Chapman & Hall, London, UK, 1995.

3 S. R. Nagel, "Optical Fiber: The Expanding Medium", IEEE Circuit Design Magazine, (1989), 36-49.

4 K. -F. Klein and A. Mühlich, Quarzglas für unterschiedliche Anwendungen im Bereich von 0.2 μm bis 2.4 μm, VDI-Bericht, Karlsruhe, (1988), 673, 147-177.

5 R. H. Stolen, Non-linear properties of optical fibres, in Optical Fiber Communications, Acad. Press, New York (1979), pp 125.

6 M. Dressle, W. Neu and H. Gerhardt, Quarzglasfasern für die Übertragung von Excimerlaserpulsen hoher Leistung, Laser und Optoelektronik, (1990), 22, 76.

7 P. Karlitschek, G. Hillrichs and K.-F. Klein, Photodegradation and nonlinear effects in optical fibres introduced by pulsed UV-laser radiation, Opt. Comm., (1995), 116, 219.

8 H. Fabian, U. Grzesik, K.H. Worner and K.-F. Klein, Optical fibre for UV-applications Proc. SPIE 1513.

9 E. J. Frieble and D. L. Griscom, Radiation effects in glass, in Treatise on material science and technology, Acad. Press, New York (1979), 257.

10 W. Heitman, Attenuation analysis of silica-based single-mode fibres, J. Opt. Comun. 11, (1990), 122.

11 H.Fabian, U.Grzesik,G.Hillrichs, W.Neu, Optical fibers with enhanced performance for excimer laser power transmission". Proc. SPIE 1693 (1993), 24.

12 E.J. Frieble and D.L. Griscom, Radiation effects in glass, in Treatise on material science and technology, Acad. Press, New York (1979), 257.

13 R. A. Weeks, "The many varieties of E'-centers: a review", J. Non-Cryst. Solids, (1994), Vol. 179, 1-9.

14 R. A. Weeks, R. H. Magruder, P. W. Wange, "Some effects of 5 eV photons on defects in SIO2", J. Non-Cryst. Solids, (1992), Vol. 149, 122-136.

15 K.-F. Klein, P. Schließmann, E. Smolka, G. Hillrichs, M. Belz, W.J.O. Boyle, K.T.V. Grattan: "UV-stabilized silica based fiber for applications around 200 nm wavelength", Paper presented at Europt(r)ode III, Zürich, (April 1996), Book of Abstracts ,160, published in Sensors and Actuators B, (1997), Vol. 39-123, 305-309.

16 K.-F. Klein, G. Hillrichs, P. Karlitschek, K. Mann, "Possibilities and limits of optical fibers for the transmission of excimer laser radiation", (Boulder 1996), SPIE Proc. Vol. 2966, 564-573.

17 K. F. Klein, S. Hüttel, R. Kaminski, J. Kirchhoff, S. Grimm, G. Nelson, "Stability and life-time improvements of UV-fibers for new applications", Conference on Surgical-Assist Systems, SAN JOSE, CA, (1998), SPIE, VO- 3262, CH- 37, 150-160.

18 J. E. Shelby, "Reaction of hydrogen with hydroxyl-free vitreous silica", J. Appl. Phys. (1980), Vol. 51, 2589, and Reaction of hydrogen with optical defects in glasses", J. Am. Ceram Soc., (1984), Vol. 64, C-93.

19 B. D. Evans, "The role of hydrogen as a radiation protection agent at low temperature in a low-OH pure silica optical fiber", IEEE Transactions on Nuclear Science, (1988), Vol. 35, 1215.

20 K.-F. Klein, A. Mühlich, K.-W. Wörner, H. Henchel, O. Köhn, H.-U. Schmidt, "Influence of Hydrogen-treatment and water-content on the recovery characteristics of undoped core fibers after pulsed and continuous irradiation", SPIE Proc., Vol. 867, pp. 17.

21 D. L. Griscom, "Defect structures of glass", J. Non-Cryst. Solids, (1985), Vol. 73, 51-78.

22 H. Fabian, U. Grzesik, K.-F. Klein, "Producing radiation hard all silica fibres - state of the art and future aspects -", Proc. of "Large Hadron Collider Workshop", CERN 90-10/ECFA 90-133 (Aachen, Oct. 1990), 736-742.

23 G. H. Sigel Jr., "UV spectra of silicate glasses", J. Non-Cryst solids, (1973/74), Vol. 13, 372-398.

24 D. L. Griscom, E. J. Friebele, "Fundamental radiation induced defect centres in synthetic fused silica: atomic chlorine, delocalized E'-centers, and triple state", Phys. Review B, (1986), Vol. 34, pp. 7524.

25 R. J. VanOverstraten, R. P. Mertens, "Physics, technology, and use of photovoltaic", Adam Hilger Ltd., Bristol, (1996).

26 Fa. Heraeus Noblelight GmbH, Hanau, "Manufacturers' Data on D2-lamps", (1997).

27 M. Belz, W.J.O. Boyle, K.-F. Klein and K.T.V. Grattan: "Water Quality Measurement using fibre optics at wavelength below 250 nm", in: J. Halttunen (ed.), *Proceedings of the XIV IMEKO World Congress* (Tampere 1-6. June 1997), Finnish Automation Support, Helsinki, (1997), paper 352, Vol. XA, 151 - 155.

28 K.-F. Klein, G. Hillrichs, P. Karlitschek, U. Grzesik: "Improved optical fibers for excimer laser applications" Proc. LASERmed 95, Munich, (June 1995), paper 107b.

29 K.-F. Klein, L.S. Greek, H.G. Schulze, M.W. Blades, C.A. Haynes, R.F.B. Turner: "Fiber-guided tunable UV-laserlight system around 215 nm" Proc. BiOS 97, (1997), paper 2977-14.

30 R.A. Greenwell, C.E. Barnes, G.W. Nelson: "The effects of ionizing radiation on various core/cladding ration step index pure silica fibers" Proc. SPIE Vol. 867, (1988), 10-16.

31 H.-H. Perkampus, "UV-VIS spectroscopy and its applications", Springer-Verlag Berlin Heidelberg New York, 1992, 22-23.

32 J. Kiefer (Ed), "Ultraviolette Strahlen", (1977), Walter de Gruyter, Berlin, 96.

33 Heraus Noblelight GmbH, "Brochure on D2 lamps", Hanau, 1996.

34 L. H. Malitson, Interspecimen Comparison of the Refractive Index of Fused Silica, J. Opt. Soc. Am., (1965), Vol. 55, 1205-1209.

3. Experimental Characterization of Fibre-optic-based Spectrometers for UV applications

3.1 Abstract

It is particularly important in fibre-optic spectrometer-based systems that the characteristics of the major components be investigated in terms of their stability and performance. A cross comparison of two inexpensive fibre-optic-based spectrometer modules, such as would be used in the systems, has been performed. The optical arrangement and the detectors are described and the temperature dependence of the dark output and the detector noise levels are determined. Following this, the wavelength stability of the spectrometer as a function of temperature is investigated and a correction algorithm for wavelength drifts in such spectrometers is proposed. Finally, the sensitivity of the two spectrometers in the important 200 nm to 300 nm wavelength region is investigated with the spectrometers incorporated in an optimized UV sensor arrangement.

3.2 Introduction

There is a long history of absorption-based sensing methods which were among the first types of chemical sensors to have been developed that included fibre optics. Several reviews of the subject are available for the interested reader [1, 2, 3], showing the diversity of designs which have been reported. The advantages of incorporating optical fibres with small diameters (<1 mm), introducing high levels of flexibility into such sensors systems, were often nullified by the problems of the use of conventional spectrometers, which were originally developed as laboratory instruments. These types of grating- or prism-based systems did not fulfil well the needs of industry for the use of absorption-based sensors in the field, even where the coupling via the fibres often removed some of the problems of window fouling seen with conventional systems.

Direct spectroscopic measurements, especially of absorption (but to a lesser extent fluorescence), require in most cases a detailed knowledge of the spectral properties of the analyte observed. In such a way the concentration of the absorbing species can be measured, with the spectral data correlated closely to the absorbing (and thus polluting) species present. Early work to overcome some of these problems involved an *a priori* assumption of the spectral nature of a particular feature (usually through a simplification of the chemical system to minimize the variety of significant species present), and with that an obviation of the need for an exact measurement of the wavelength of absorption. An other approach was found in the use of the chemical manipulation of the sample to ensure that particular species change their absorption features, for ease of identification. This principle was, for example, used Mouaziz *et al.* [4] who developed a residual chlorine monitor, where the absorption feature at 290 nm due to the presence of OCl^- ions was destroyed in a comparative measurement made by the addition of a suitable reagent. For ease of measurement, the usage of a fixed wavelength spectral filter, centred around the wavelength associated with this feature, was found to be sufficient.

Recent advances in the technology of optical fibre sensors have included the development of novel sensor cells [5,6], ultraviolet transmission improved fibres [7, 8, 9], light sources and detectors. Additionally, the advances of spatially distributed detectors, such as charge coupled devices (CCDs) or photodiode arrays (PDAs) and their improving sensitivity in the ultraviolet has opened up the possibilities of further miniaturization in the field of wavelength selective fibre-optic sensor systems for the ultraviolet [10, 11, 12]. This is through imaging the dispersed absorption spectrum onto these devices, to achieve a simple wavelength calibration of the transmitted signal, while keeping the overall system small and compact for field use. Thus, a range of multichannel spectrometers [13, 14, 15] and other wavelength-selective techniques, such as for example integrated acousto-optic tuneable filters as tuneable monochromatic wavelength selective elements [16], has been developed for process and pollution monitoring.

Recently, several fibre-optic based-miniature spectrometers have been manufactured and marketed both in the EU and USA, with optimistic reports from the manufacturers on the performance of these systems. However, a number of criteria have to be fulfilled, when selecting such miniature spectrometers for fibre-optic sensor systems, designed for laboratory or field applications. For example, a robust and efficient coupling to the other optical components of the fibre-optic sensor systems has to be possible. Further, their performance should not degrade by the sort of problems that regularly arise in the field, such as elevated temperatures, optical and mechanical instabilities, solarization effects etc.

In this Chapter, a cross-comparison is made of two miniature fibre-optic-based spectrometer systems (FOS), especially taking temperature effects into consideration. The optical arrangement inside the spectrometer modules is described and their influence of temperature on the dark output and the wavelength stability discussed. Additionally, their sensitivity in the deep ultraviolet in the 200 nm to 300 nm wavelength region has been investigated by comparing their performance when configured into a fibre-optical nitrate monitor (described in Chapters 5 and 6), reflecting one of the most relevant pollution monitoring issues in the water industry [17, 18]. In this way, the essential difference in the systems in this comparison study will arise due to the influence of the miniature spectrometer used.

3.3 Optical Configuration

3.3.1 Spectrometer requirements for fibre-optic sensors

Spectrometers employed in optical sensors developed for laboratory and more important for field application are required ideally to be small, robust, thermally stable and feature a high sensitivity in the wavelength region of interest, as well as show a good and repeatable optical coupling to the sensor. For use in the ultraviolet spectral region,

the spectrometer should in particular be resistant to solarization effects. Its optical characteristics should be optimized for fibre use, to be able to accept the light flux transmitted through an input fibre without significant coupling loss. The ability of an optical system to accept the light flux from a conical beam may be described by the so-called geometric extent, G, with its light entrance area, S, and its acceptance angle, Ω, [19] given by

$$\blacksquare \qquad\qquad\qquad\qquad\qquad (5.1)$$

Adapting this formula for fibre use and assuming the input area, S, to be circular it may be expressed in terms of the beam diameter d_{input}, and for small Ω by its numerical aperture, NA_Ω, as

$$\blacksquare \qquad\qquad\qquad\qquad\qquad (5.2)$$

with $NA_\Omega = n_\lambda \sin(\Omega)$, where n_λ is the wavelength-dependent refractive index of the coupling medium. The coupling efficiency, η, between an input fibre, described by its core diameter, d_{core}, and its numerical aperture, NA_{fibre}, and the input of the spectrometer, can then be approximated by

$$\blacksquare \qquad\qquad\qquad\qquad\qquad (5.3)$$

indicating the strong dependence of the core diameter and the numerical aperture of the input fibre on the light power entering the spectrometer [6]. Equation 5.3 shows that the light power entering the spectrometer and (therefore its sensitivity) has a square law dependence, if d_{core} is doubled. However, in some spectrometers, the core diameter of the input fibre represents their input slit width and therefore defines the optical

resolution of the instrument. Thus, increasing the diameter of the input fibre to increase the amount of light flux entering the instrument results in a decrease of the optical resolution if no additional slits are employed at the optical entrance to the spectrometer, which then again, would decrease the light flux entering the optical system. However, equation 5.3 shows as well that the capability of the spectrometer to accept light power at its entrance is squared if its numerical aperture is doubled, indicating that the input slit width, defined by the core diameter of the input fibre and numerical aperture of the spectrometer has to be suitable for fibre use. Typical bench-based monochromators or spectrographs, as, for example, manufactured by ISA [19], have numerical apertures ranging from 0.03 to a maximum of 0.16. The NA of silica fibres with a fused silica core and a fluorine doped cladding, typically used in ultraviolet and visible fibre-optic-based spectroscopy, is around 0.22 in the visible, increasing to 0.25 in the ultraviolet [18]. Thus the numerical aperture of spectrometers designed for fibre optic use has to be more closely matched to avoid "overfilling" the spectrometer, both losing photons and creating stray-light in the system. Additionally, using ancillary optics at the spectrometer entrance is not recommended, since on the one hand, the optical setup of the spectrometer would become more complicated and on the other, the advantage of lowering the numerical aperture would be compensated by the enlarged optical light spot at the spectrometer entrance, resulting in lower wavelength resolution.

3.3.2 The Miniature Spectrometers used

The miniature spectrometers described in this investigation were commercial devices, intended for use in a range of experiments for research and teaching purposes, representing the "state of the art" for inexpensive fibre-based spectrometer systems. Tab. 3-1 summarizes the optical characteristics of these spectrometers used from data given by the manufacturers. Unfortunately the manufacturers did not publish all the relevant parameters, resulting in some gaps in Tab. 3-1. The optical configuration of both spectrometers, labelled FOS-I and FOS-II in this work and used in the experiments is shown in Fig. 3-1.

Spectrometer	FOS-I	FOS-II
Detector	Hamamatsu, S 3904 - 256Q diode array detector with high UV sensitivity.	NEC, linear CCD-array silicon detector, coated with fluorescence dye for UV conversion
Number of pixels	256	1024
Dimension of one pixel	25 μm*2500 μm	12.5 μm*14 μm
Spectral response of detector	200 nm - 1000 nm	200 nm - 1000 nm
Spectral range of FOS specified by manufacturer	220 nm - 730 nm	(220 nm - 575nm) usable range with > 30% efficiency
Maximum spectral range (observed)	≈195 nm - 740 nm	≈180 nm - 738 nm
Pixel dispersion (software resolution) [nm pixel^{-1}]	≈2.1	≈0.55
Optical configuration & grating	Concave holographically blazed flat field grating with 366 lines mm^{-1} (center) and blazed for approx. 220 nm	Cross Czerny-Turner configuration consisting of 2 spherical mirrors and a flat-field plane diffraction grating, ruled with 600 lines mm^{-1} and blazed for approx. 300 nm
Linewidth FWHM (full width half maximum) [nm] / Rayleigh criterion [nm]	≈ 5.6 / 7.0	≈ 2.5 / 3.2 [d$_{core}$=50μm] ≈5 / 6.3 [d$_{core}$=100μm] ≈10 / 12.6 [d$_{core}$=200μm]
Absolute accuracy (nm)	0.3	-
Temperature drift (nm K^{-1})	0.006	-
Sensitivity	10^{12}-10^{13} Counts Ws^{-1} at λ=633 nm	-
Stray light	0.22 % [Xenon lamp] 0.04 % [Deuterium lamp] 0.42 % [Halogen lamp] at λ=230 nm	< 0.05% at λ=600 nm
Optical entrance:	Cross section converter, fiber bundle consisting of 30 fused silica fibers having a core diameter of 70 μm and a numerical aperture, NA=0.2	UV improved single strand multimode fiber, NA = 0.2
Dimensions	70 mm* 60 mm * 40 mm cross-section converter (l=240 mm)	130 mm * 120 mm* 40 mm
Options	Second-order dielectric cutoff filter coated on the diode array detector	Cylindrical fused silica lens fixed on the CCD-array detector for sensitivity improvement.

Tab. 3-1: Manufacturers' data on FOS-I and FOS-II.

Concave diffraction grating

CCD array detector   Mirror

—Mirror

Diode array dete

Plane diffraction grating

Fibre optic i
with fibre bi

Fibre optic inpu
with single fibr
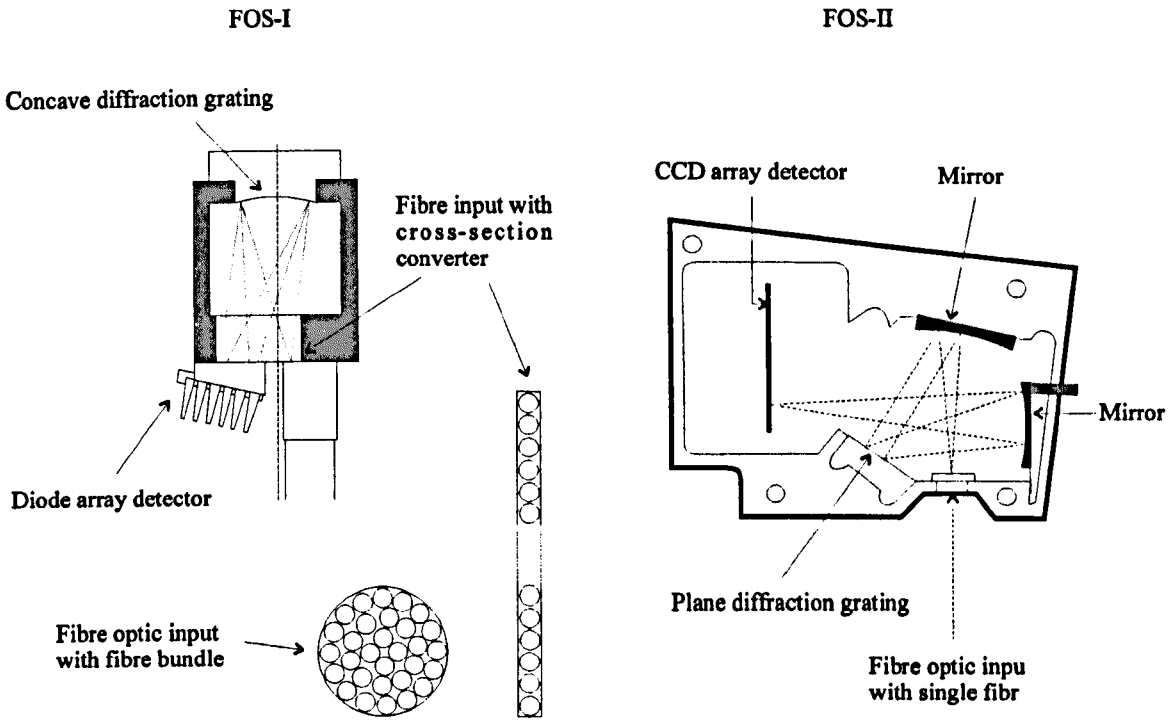
Fig. 3-1: Optical setup of the investigated miniature spectrometers FOS-I and FOS-II.

Both spectrometers tested are polychromators, using a detector array to observe the resolved optical spectra. As a result, light intensities can be recorded at many different wavelengths simultaneously, thus avoiding moving parts in the optical set-up and reducing the time required to complete a spectroscopic experiment, which is a great advantage compared to single element detectors. Assuming such a single element detector and an array detector have the same sensitivity and integration time, the array detector gives a signal-to-noise (SNR) advantage of $\sqrt{N_{pixels}}$, where N_{pixels} is the number of pixels in the array. Within the ultraviolet and visible regions of the optical spectrum, silicon based photodiode arrays (PDAs) or charge coupled device (CCD) arrays [20] are commonly used for detection. These detectors offer a broad spectral responsivity, excellent linearity, high quantum efficiency and a high dynamic range, but have to be cooled to reach the highest sensitivity levels. While PDAs can be used to detect light levels at wavelengths as low as 200 nm, CCD arrays are most often coated with a fluorescent dye to improve their quantum efficiency at lower wavelengths by converting UV light to a longer wavelength emission [20, 21] to which the device is more sensitive.

In the first case investigated, light is coupled into FOS-I via a cross-section converter, consisting of a fibre bundle with 30 individual fused silica fibres having a core diameter of 70 μm and a numerical aperture, NA = 0.2, as illustrated in Fig. 2. At the light input of FOS-I, a fibre bundle was assembled on one side and connected into an SMA connector to form a round fibre-optic input with a diameter of 0.5 mm and a NA≈0.2 and on the other side formed into a cross-section converter by arranging the fibre in one line to form an entrance slit for the spectrometer. This optical arrangement enables light coupling from fibres with core diameters of up to 500 μm into the spectrometer but features, on the other hand, a slit-width of ≈70 μm with a slit height of ≈2500 μm at the spectrometer entrance. However, the disadvantage of this robust, and optically very stable approach is that when connecting input fibres with small core diameters, such as 100 μm or lower, efficient and repeatable light coupling cannot be guaranteed, as parts of the input fibre area may be coupled on the "blind" spots of the cross-section converter between the different active areas of the fibre bundle. A single optical element, being a concave flat field grating is used both to focus and to diffract the incident light from the entrance slit onto a UV-enhanced PDA. With a single photodiode of the array used having a pitch of 25 μm and a height of 2500 μm, the entrance slit is imaged on approximately 3 photodiodes. The PDA and its on-board pre-amplifier convert the diffracted light intensity into a voltage which is sampled by an analogue-to-digital converter (A/D card) and processed with an IBM-compatible personal computer (PC). The rather simple optical arrangement reduces the number of optical components to a minimum, to increase the optical stability and decrease the cost of the instrument. To suppress the second order of the grating, the diode array of FOS-I has been directly coated with a dielectric cut-off filter by the manufacturers.

The optical design of the miniature spectrometer FOS-II is based on a cross Czerny-Turner configuration, as shown Fig. 3-1. This polychromator consists of two concave spherical mirrors and a plane flat-field diffraction grating. Light enters the spectrometer from a single strand fibre via the fibre-optic input and is focused on the grating by the spherical mirror 1. The dispersed light is collected from the ruled grating by the spheri-

cal mirror 2 and imaged on a CCD-array detector. With a single CCD-element having a pitch of 12.5 μm and a height of 14 μm, the fibre is imaged on approximately 8 CCD elements. The grating was blazed for approximately 300 nm to enhance the sensitivity of the spectrometer in the UV. By using the asymmetrical geometry shown in Fig. 3-1, a flattened spectral field is obtained on the CCD-array detector, which converts the wavelength-resolved intensity spectrum with its associated electronics into a voltage. To enhance the sensitivity of the spectrometer a cylindrical lens, made from fused silica, was used to correct the mismatch between the slit height, defined by the core of the input fibre, and the pixel dimensions. With an input fibre having a core diameter of 100 μm, a wavelength resolution (FWHM) approximately equivalent to that of FOS-I can be observed.

Position and width of the entrance slit are defined in this spectrometer by the input fibre. As the position of the entrance slit defines the absolute wavelength accuracy of the instrument and the slit-width its wavelength resolution, it is obvious that the performance of these two parameters is strictly dependent on the quality and repeatability of the SMA fibre connector at the spectrometer entrance. To ensure repeatable results, the input fibre of the spectrometer was not removed or re-positioned during the experiments. The voltage obtained from the preamplifier of the CCD-array is sampled by an A/D converter of the same type used with FOS-I and processed in an IBM-compatible PC.

Both spectrometers are equipped with array-based detectors to measure the wavelength dispersed light spectrum. Although FOS-I uses a self-scanning linear photodiode array (PDA), multiplexing each signal charge to a common video line, and FOS-II a CCD-array, shifting the signal charge sequentially to an output sensing node, both arrays rely on the principle of charge storage (or photon-flux integration). The charge storage element used in such a detector can be a p-n junction diode such as, for example, a PDA or a MOS-induced junction, as in a CCD-array. The charge storage operation is based on the principle that, if such a junction is reverse-biased and then an open circuit is cre-

ated, the charge stored on the depletion-layer capacitance decays at a rate proportional to the incident illumination level [29]. Thus the photon generated current is directly proportional to the illumination level and therefore the amount of charge removed in a given interval of time is directly proportional to the integral of the illumination taken over that interval. The time between two subsequent readings may then be termed the integration time, determining the sensitivity of the array.

3.3.3 Data output and computer interfacing

Both spectrometers used were interfaced to an IBM-compatible PC with a 12 bit A/D converter and supplied by the manufacturer with a simple, unsophisticated, DOS-based spectral acquisition software. On demand, both manufacturers offered DOS-based drivers either in PASCAL (FOS-I) or C (FOS-II). As a part of developing an on-line measurement system, a dynamic link library (DLL) was developed for FOS-I, to simplify the data transfer between the spectrometer hardware and a windows-based analytical software, Microcal Origin™, used to store and analyze the spectral data obtained.

3.4 Effects of temperature variation on the spectrometer dark output

The miniature spectrometers FOS-I and FOS-II described in this work were designed and advertised for usage in bench-top and on-line applications. They are, compared to bench-based spectrometer systems, compact, robust, small and inexpensive and relatively easy to handle. However, not all on-line application are in a laboratory-based environment, with fixed temperature and humidity. A major concern for field applications is to evaluate the performance of the two spectrometers at varying temperatures by observing the effect of temperature on the dark output and the wavelength stability in particular.

3.4.1 Dark output variations as a function of temperature and integration time

In the absence of an optical signal any detector exhibits a small output. In the case of a conventional photodiode, this output signal is known as the dark current, which is chiefly a sum of the diffusion, generation, surface and avalanche currents and is mainly dependent on the temperature and reversed biasing. Having in mind that the spectrometers used are working in the charge-storage mode, the detector dark output may therefore be expressed as the product of the semiconductor dark current and the integration time. However, the dark output of the spectrometers will be the sum of the detector dark output of the intensity offset of the preamplifier.

To investigate the effect of integration time and temperature on the dark output of the spectrometers FOS-I and FOS-II, both were situated in an air conditioned cabinet. The temperature in the cabinet was varied between 0°C and 50°C in steps of approximately 5°C with a precision of ±1°C, as it was assumed that such temperatures are easily reached in a sensor system designed for field use. To observe the absolute temperature and the temperature drifts, semiconductor-based temperature sensors having a precision of 0.1°C were fixed to each spectrometer body, in addition to which the temperature of the air flow in the cabinet was observed with a digital thermometer during the experiments. An appropriate time was chosen to allow the spectrometers to adapt to the temperature of the air flow in the cabinet between the different experiments. The dark output spectra of FOS-I and FOS-II were measured at temperatures ranging from 5 °C to 43 °C with integration times of 13 ms, 50 ms, 99 ms, 204 ms, 409 ms and 585 ms. The mean dark output of FOS-I is shown as a function of temperature and integration time in Fig. 3-1. It could be observed in Fig. 3-1A that the dark output data obtained grows exponentially and doubles if the temperature of the spectrometer is increased by approximately 7 °C. This result shows on the one hand a good agreement with data obtained from the manufacturer and the work of Starks *et al.* [22] for diode arrays and indicates that the dark output of the spectrometer may be modelled relatively simply, if the temperature dependence of the PDA and its electronic configuration are known. On the other hand, Fig. 3-1 shows clearly that the range of FOS-I begins to be

severely limited at temperatures higher than 40°C and integration times greater than 500 ms.
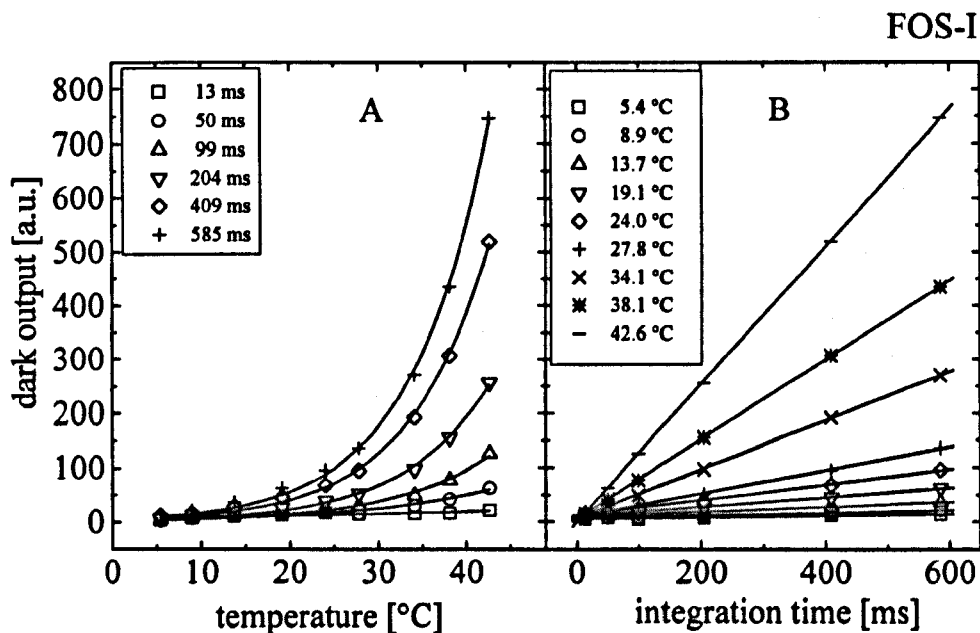
Fig. 3-1: Dark output of FOS-I at 203 nm wavelength as a function of temperature with integration times ranging from 13 ms to 585 ms (A) and as a function of integration time at a temperatures between 5.4 °C and 42.6 °C (B).

However, Fig. 3-1B shows the effect on the mean dark output of FOS-I as a function of the integration time over the given temperature range. As expected from the theory, the increase in integration time would cause a linear increase of the dark output over the whole measurement range. Using the instruments over a total period of 3 years, it was found that dark output of the PDA elements exposed to ultraviolet light radiation below 300 nm wavelength slightly increased. This may be explained by the fact that PDAs tend to deteriorate after continuous exposure to UV radiation [23], shown by an increase of the leakage current in the PDA, resulting a an increased dark output.

Within the same experiment, the dark output of FOS-II was investigated as a function of temperature and integration time over a similar temperature range to produce a di-

rect comparison. However, in contrast to FOS-I, the data output of one measurement cycle of FOS-II can be divided into a signal output and dark output, whereby the dark output can be subdivided into an electrical and an optical dark output. This is realized by shielding the first 24 CCD-elements (pixels) of the detector array from light exposure to measure the dark output of these elements. The following 1024 elements are used measure the sample output in the specified wavelength range. Finally, a number of samples is taken with the preamplifier being connected to a short circuit instead of a CCD detector element to measure the dark output of the electronic read-out circuit. All these data are acquired sequentially during one measurement cycle and could be used for automatic dark output correction. However, for comparison, the dark output of FOS-II, representing the uncorrected dark output at a wavelength of 203 nm, is shown as a function of temperature (A) and integration time (B) in Fig. 3-2. Here, a basically non-linear behaviour was observed, as the dark output was found to decrease at low integration times when the temperature increased. Around integration times of 100 ms, the dark output was found to be approximately stable with changing spectrometer temperatures and was found to increase at higher integration times. This behaviour may be explained as resulting from two competing effects. The dark output of the electronic read-out circuit was found to decrease with increasing temperature at integration times lower than 100 ms and then to increase. Subtracting the so-called electronic dark output from the dark output obtained at the pixel associated with a wavelength of 203 nm resulted in the optical or detector dark output of the CCD detector array at that wavelength, which then followed an exponential law. The optical dark output obtained was found to double each 9 to 10 °C, when fitting the data to an exponential function. The mean dark output as a function of integration time is shown in Fig. 3-2B over the given temperature range. It could be observed that the relationship between dark output and integration time is not linear, and this may be caused by stray capacitance in the readout circuitry. Although UV light is measured in the spectrometer by down-converting the UV light with a phosphor to longer wavelengths, it could be observed that at wavelengths below 300 nm, the dark output increased after long-term UV exposure (3 years). This may be explained by UV-radiation penetrating through the phosphorous

coating used for down-converting UV light to visible light for more efficient light detection, resulting, as with the PDAs, in an increased dark output.

FOS-II

Legend A:
—□— 13 ms
—○— 50 ms
—△— 99 ms
—▽— 204 ms
—◇— 409 ms

Legend B:
—□— 6.0 °C   —○— 9.4 °C
—△— 14.3 °C —▽— 19.6 °C
—◇— 24.6 °C —+— 28.2 °C
—×— 34.2 °C —✳— 38.7 °C
—— 43.1 °C
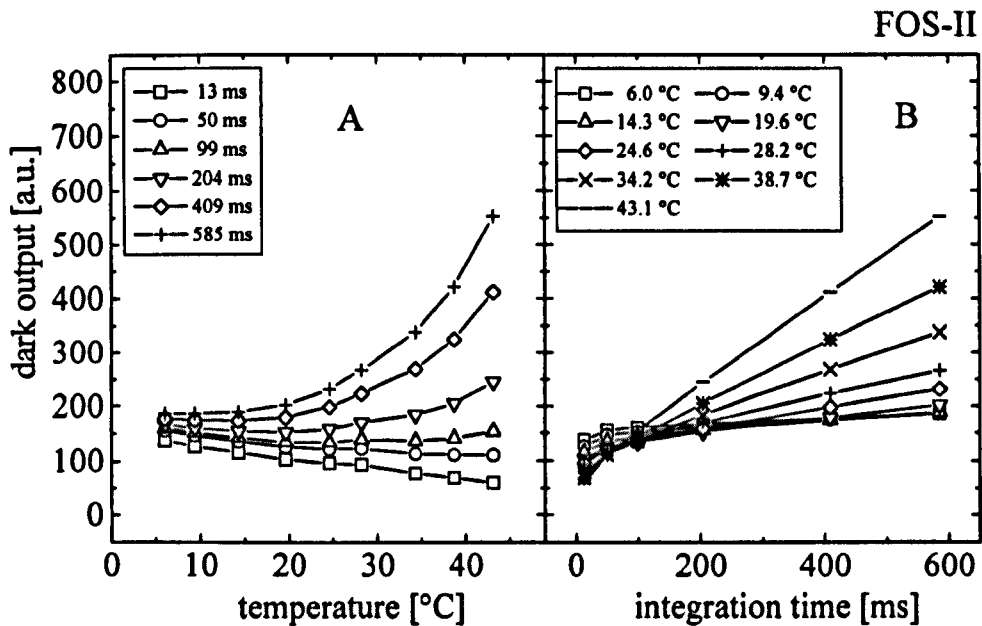
Fig. 3-2: Dark output of FOS-II at 203 nm wavelength as a function of temperature with integration times ranging from 13 ms to 585 ms (A) and as a function of temperature between 6 °C and 43.1 °C (B).

From the exponential nature of the dark output of both spectrometers, it should be pointed out that the relative change of dark output caused by a small temperature variation of the spectrometers, again exponentially increases with temperature, thus increasing the potential measurement error. Particularly when working with low light levels slightly above the dark output, such as is obtained in fluorescence measurements, these temperature-dependent fluctuations have to be monitored and compensated. Furthermore, to avoid the problem of photoresponse non-uniformity of the individual diode array elements, it is suggested that the dark output of each detector element should be subtracted from the corresponding signal output to maximize measurement precision.

3.4.2 Variation of noise levels of the dark output at different temperatures

A crucial parameter in the accuracy of spectrometers is the noise of their intensity output. To estimate the basic noise of FOS-I and FOS-II, 10 samples of the dark output were taken for each experiment. Thus, the dark output and its noise could be calculated at both varying temperatures and integration times for each individual element. The noise level, defined by the standard deviation of the dark output, is shown for FOS-I and FOS-II at three temperatures, as a function of wavelength, in Fig. 3-3 and Fig. 3-4 respectively. To express this noise level more clearly, its mean and standard deviations over the individual elements were calculated, where the latter were then termed the so-called averaged noise level.
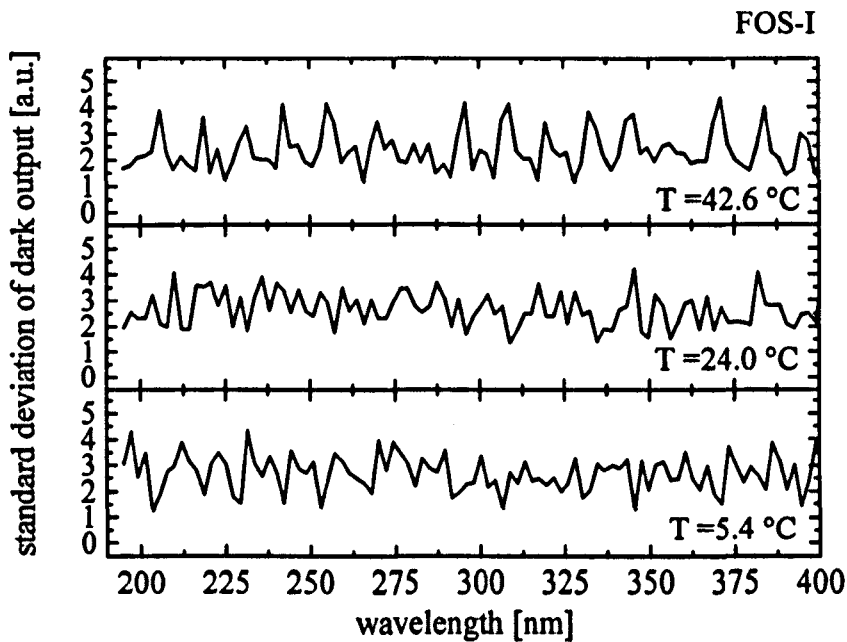
Fig. 3-3: Standard deviation of the dark output of FOS-I at an integration time of 585 ms as a function of wavelength at 42.6 °C, 24.0 °C and 5.4 °C.
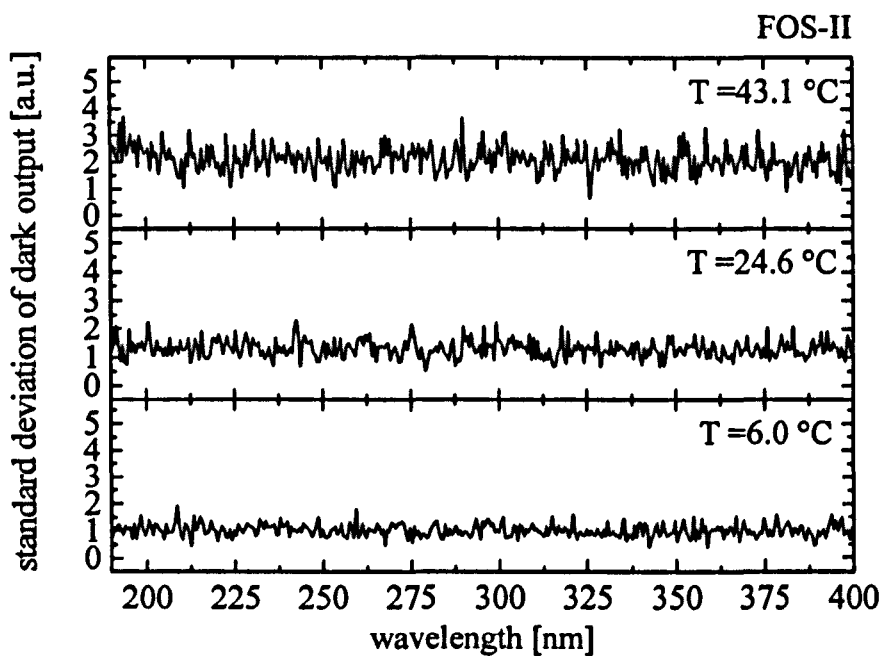
Fig. 3-4: Standard deviation of the dark output of FOS-II at an integration time of 585 ms as a function of wavelength at 43.1 °C, 24.6 °C and 6.0 °C.
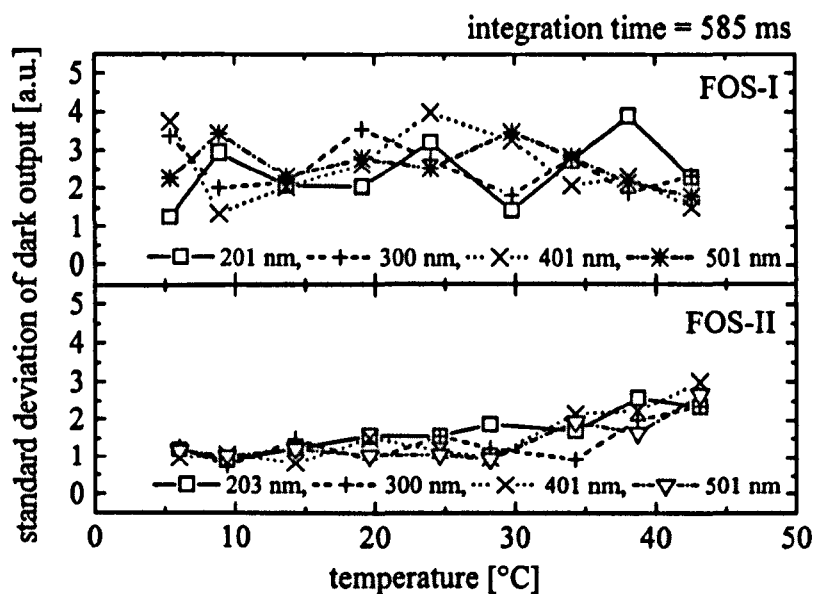
Fig. 3-5: Standard deviation of the dark output of FOS-I and FOS-II at an integration time of 585 ms as a function of temperature at several wavelengths.

Experimental Characterization of Fibre Optic based Spectrometers ...

For FOS-I, which was optimized for highest sensitivity and grounded to the metal case of the PC to reduce noise, averaged noise levels of 2.6 ± 0.7 a.u., 2.7 ± 0.6 a.u. and 2.4 ± 0.8 a.u. were found at 5.4 °C, 24.0 °C, 42.6 °C respectively. The temperature range of 5 °C to 42 °C and the use of integration times varying between 13 ms and 585 ms appeared to have no influence on these averaged noise levels. FOS-II was found to have an averaged noise level of 1.0 ± 0.2 a.u., 1.3 ± 0.3 a.u. and 2.0 ± 0.5 a.u. at 6.0 °C, 24.6 °C, 43.6 °C respectively, indicating a dependence of temperature and averaged noise level. The effect of temperature on the standard deviation of the dark output of FOS-I and FOS-II is shown in Fig. 3-5. However, it should be noted that the overall noise level found for FOS-II was still lower at 43.6 °C than the noise level of FOS-I throughout the experiments. In a similar way to FOS-I, the averaged noise level of FOS-II did not vary as a function of integration time within the range of 13 ms to 585 ms, that accessible by both spectrometers. However, increasing the integration time, and therefore the sensitivity of FOS-II at room temperature, up to 3600 ms, an increase in the averaged noise level to 2.0 ± 0.5 a.u. was found.

3.5 Effects of temperature variations on the wavelength stability

Absolute wavelength accuracy as a function of lifetime and ambient temperature is a crucial requirement of a spectrometer to secure reproducible results of a wavelength-resolved absorbance or emission spectra. The traditional spectrometer rotates a diffraction grating or prism which scans dispersed light across a slit in front of a single element detector. This detector records each intensity value at discrete wavelengths. Such a system can be calibrated by recording a number of known monochromatic emission lines, such as are emitted by low pressure mercury lamps, at their peak intensity. This is possible because the position of the dispersing element can be continuously adjusted. However, in detector-array-based systems such as FOS-I and FOS-II, the exit slit is removed and the entire spectrum is measured simultaneously by the array. Thus the spectral range is limited by the length of the detector array and the linear dispersion of the spectrometer. Its spectral resolution can be described by two major terms. The so-

called Rayleigh criterion, $\Delta\lambda_{Rayleigh}$, defines the ability of the instrument to distinguish between two adjacent peaks as individual lines [24]. The linewidth, $\Delta\lambda_{FWHM}$, describes the expansion of a monochromatic line by the spectrometer, denoting the sharpness of a monochromatic peak, which is defined as the full width at half maximum (FWHM) of the peak. For a given spectral range recorded onto the detector array, the spectral width of a pixel is determined by dividing the spectral range by the number of pixels in the detector array. With an array-based spectrometer, the spectral width of a detector pixel is theoretically the limiting factor in the spectral resolution. However, to satisfy the Nyquist condition, a minimum of two pixels has to be used to detect a line [25]. However, more important is the optical resolution of the instrument, which is dependent on a range of parameter, such as the entrance slit width, the dispersion of the grating and its ability to produce a flat optical field on the detector.

The objective of this section is to investigate the wavelength accuracy and temperature dependence of FOS-I and FOS-II. After reviewing a number of calibration algorithms, a wavelength-resolution dependent calibration algorithm for array-based spectrometers will be introduced and the effect of temperature variations on the wavelength accuracy of FOS-I and FOS-II investigated.

3.5.1 Review of wavelength calibration methods for detector array based spectrometers

The calibration of detector array-based spectrometers has been discussed by several authors [15, 25, 26, 27, 28, 29, 30, 31, 32, 33]. There are two commonly used approaches for wavelength calibration of multichannel detectors. The first is to calculate the relationship between the wavelength and the pixel position by using the geometrical relationships in the spectrometer, as for example described by Lindrum and Nickel [26]. The second and far more common approach is based on the derivation of a functional relationship between wavelength and pixel index (position) of the detector array. This can be achieved either by using line emission sources, such as low pressure mercury discharge lamps in the ultra violet or visible [27, 28] or by using neon discharge

lamps in the visible and near infrared part of the light spectrum [27, 29]. For simple calibrations or tests, even the weak mercury peaks emitted by fluorescence discharge lamps, situated at 435.83 nm and 546.08 nm, or the characteristic peak at 656.1 nm of a deuterium lamp may be used [27]. Furthermore various solid and liquid filters, giving fairly sharp absorption peaks caused by electronic transitions of incomplete f orbitals of rare earth salts and oxides (Ho, Sm, Dy, Eu, Nd, etc.) are often recommended for calibration and verification purposes [28, 30]. However, their potential is limited because of the asymmetry found with some of their absorption peaks [28].

In order to achieve an accurate wavelength calibration, the pixel position of known emission lines or absorption bands must first be estimated to fractions of a pixel. Scopatz *et al* [31] employed a sub-pixel assignment technique to determine the centroid wavelength of a spectral line and calibrated a 1024 element intensified diode array spectrometer with four to six atomic lines emitted by either mercury or neon discharge lamps. With the use of a third-order polynomial fit and a spectral pixel width of 0.3 nm, he achieved a repeatability of 0.06 nm over a period of 8 months.

Berlot and Locascio [28] have developed a generalized calibration procedure for ultraviolet-visible diode-array spectrometers, including formulae to determine the central locations of spectral lines imaged on multiple diodes. Two diode array spectrometers were calibrated. One was equipped with a detector array of 32 elements covering the wavelength range between 340-700 nm and the other a 328-element detector covering the wavelength range from 190-730 nm. Several calibration standards, such as the spectral lines from a low pressure mercury discharge lamp or the absorption peaks of holmium and didymium glass filters as well as holmium and samarium perchlorate solutions, were evaluated. Applying a linear regression analysis for wavelength calibrations, a standard error or estimate of 1.7 nm and of 0.52 nm could be found for the 32- and the 328-element respectively. Using the rare earth glasses or solutions, standard errors or estimate were found to increase 2-3 times.

The wavelength-pair calibration method described by Brownrigg [32] was designed for low-resolution (~10 nm spectral bandwidth) instruments and requires two calibration wavelengths and their positions on the array. A 38-element detector was used to observe the wavelength coverage from 340-690 nm or from 380-730 nm respectively of the spectrometers used. Brownrigg found that the greatest source of error derives from establishing accurately the positions of the two calibrations lines on the array element and that the error sensitivity increases as the line separation of the wavelength pair decreases. When determining the line position of the wavelength pair with an accuracy better than 1/30th of an element and a calibration line separation >100 nm, a wavelength accuracy of ±1 nm could be achieved.

Bellon *et al* developed a fibre-coupled NIR spectrometer to determine the sugar content in peaches and sort them into three maturity classes [15]. A CCD camera with 500*582 pixels was used to observe the light spectra with a wavelength coverage between 809 and 1082 nm. As the outputs of several pixels were averaged, the spectrum was observed in 2.4 nm steps with a spectral resolution (FWHM) of approximately 8 nm. A fibre bundle consisting of 20 input fibres was assembled and formed into a cross section converter at the entrance slit of the spectrometer. As the wavelength-resolved light of the entrance slit was imaged horizontally on two dimensional CCD camera, the intensity found at its vertical pixels could be related to the individual input fibres, representing 20 different input channels. Four spectral lines from a mercury and three spectral lines from a cadmium calibration source were mapped to the pixel with the highest intensity and a linear regression was applied to obtain a wavelength calibration function. No long term or temperature wavelength drifts were found when the system was tested between 11 °C and 40 °C in steps of 5 °C, thus indicating that the wavelength stability might have been better or equal to 0.6 nm, the spectral width of one pixel.

Cho *et al.* [33] developed a wavelength calibration method for a seven-channel fiber-optic CCD spectrograph. From the matrix of 1152 horizontal pixels by 298 vertical pixels available, three horizontal and two vertical pixels were "binned" into a superpixel

to increase sensitivity. Thus a wavelength coverage between 190 nm and 450 nm with a spectral bandwidth of 1 nm was created. The sub-pixel position of five mercury peaks was interpolated from a cubic polynomial fit across the tops of peaks. Then a linear, a quadratic, a cubic and two trigonometric functions were tested for least square fitting of pixel numbers with known wavelengths of the mercury emission lines. Cho *et al.* found that the linear calibration model gave the largest averaged calibration error of 0.268 nm and the quadratic and the first trigonometric model reduced the error slightly to 0.237 nm and 0.254 nm. However, the cubic model and the second trigonometric model, based on a Fourier series approximation, gave the lowest calibration errors of 0.144 nm and 0.139 nm respectively, thus indicating the non-linear pixel vs. wavelength relationship of the spectrometer.

Sadler *et al.* developed a procedure to reduce the line registry effect associated with the undersampling of spectral images by a CCD in a spectrograph [25]. By tilting the image of the entrance slit across a number of rows of a two-dimensional array, he reconstructed the spectral profile with a sub-pixel spatial resolution. For a spectral line with an FWHM of 2.0 pixels, simulations showed that the peak height, with the use of upright slits, may vary by 15 % depending on the position of the spectral line. However, by implementing the tilted-slit procedure, this variation in peak height could be reduced to 3 %.

From the wavelength calibration techniques described above, it was concluded that the absolute wavelength position of, for example, an emission peak of a low pressure mercury light source could be estimated to a fraction of a pixel on the array detector of FOS-I and FOS-II respectively by using a least square fitting function. After determining the exact position of the emission peak, a quadratic or cubic calibration curve relating wavelength and pixel position could be calculated with a sub-pixel precision, thus enabling the study of wavelength drifts of FOS-I and FOS-II at varying temperatures.

3.5.2 Development of a wavelength resolution-dependent wavelength calibration algorithm

Wavelength position and irradiance levels of the numerous spectral lines emitted by low pressure mercury lamps have been investigated and published by many authors [34, 35, 36]. They are commonly used for wavelength calibration of ultraviolet and visible spectrometer systems [25, 30, 27, 28, 29, 31, 32, 15, 33]. As the wavelength position and number of mercury emission lines differ slightly between the different authors, the latest wavelength data obtained by Sansonetti *et al.* [35], partially shown in Tab. 3-2, was used as a reference. Fig. 3-1 shows the line emission spectra of the low pressure mercury lamp, I_{Hg}, recorded by FOS-I and FOS-II with an integration time of 50 ms.
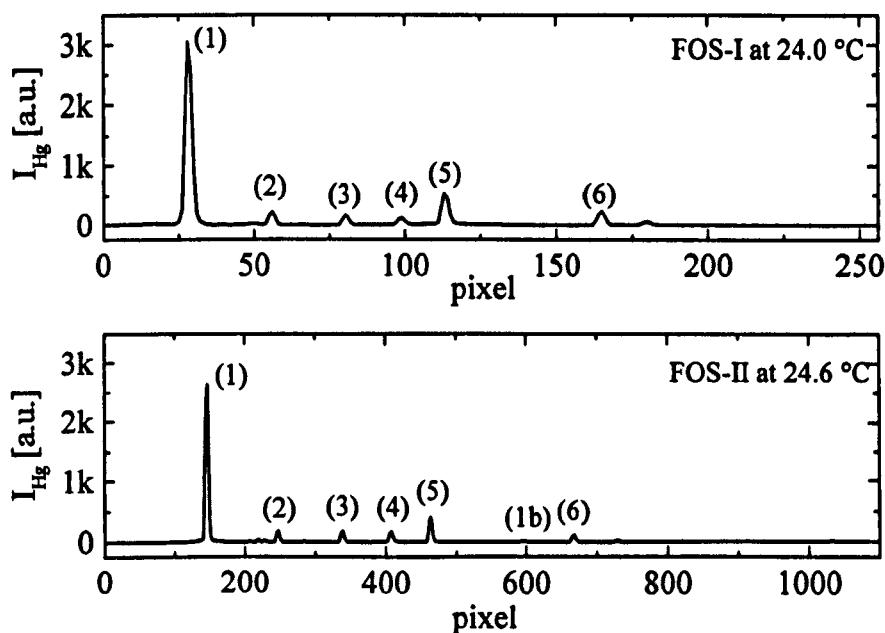
Fig. 3-1: Line emission spectra of a low pressure mercury lamp, I_{Hg}, recorded by FOS-I and FOS-II with an integration time of 50 ms. The numbered peaks (1..6) were found useful for wavelength calibration. Peak (1b) is the second order peak of peak (1) attenuated by approximately 23 dB.

The numbered peaks (1..6) were found useful for wavelength calibration. Peak (1b), only found with FOS-II, is the second-order peak of peak (1) attenuated by approximately 23 dB. This peak was not found with FOS-I, because of its second-order dielectric cut-off filter coated directly on its diode array detector.

peak number	wavelength [nm]	intensity [a.u.]
1	253.6521	300000
2	312.5674	2800
2	313.1555	1900
2	313.1844	2800
3	365.0158	5300
3	365.4842	970
3	366.2887	110
3	366.3284	650
4	404.6565	4400
4	407.7837	270
5	434.7506	34
5	435.8335	10000
6	546.0750	10000

Tab. 3-2: Recommended wavelength (air) of mercury emission lines selected for wavelength calibration from Ref. [35]. The intensities are relative values based on irradiance values from Ref. [36] with the intensity of 436 nm set arbitrarily to 10000.

Assuming the instrumental line profiles of FOS-I and FOS-II are of Gaussian shape, a line emission peak of a mercury calibration source, $I_{Hg}(p)$, recorded by a spectrometer can be described as

$$$$

(3.5-1)

with p, being a pixel number of the detector array, p_c being the pixel position of the peak maximum, w being its standard deviation in pixel units, I_{Hg0} being its intercept describing the dark output and the background continuum emitted by the mercury lamp and the area, A, covered by the Gaussian-shaped peak. Thus, the resolution of a spec-

trometer could be described by the full width at half maximum (FWHM) criterion as a function of pixels, as p_{FWHM}, and as a function of wavelength, as λ_{FWHM}, to be

$$\Delta p_{FWHM} = w\sqrt{-2\ln(0.5)} \qquad (3.5\text{-}2)$$

$$\Delta \lambda_{FWHM} = \Delta \lambda_p * p_{FWHM} = \Delta \lambda_p w\sqrt{-2\ln(0.5)} \qquad (3.5\text{-}3)$$

with $\Delta \lambda_p$ as the pixel dispersion, if the linewidth of the emission line is substantially smaller than the spectral resolution of the spectrometer.

With these conditions, the spectral resolution $\Delta \lambda_{FWHM}$ was estimated at the 253.65 nm emission line with a Gaussian least square fit to be 5.6 nm and 3.4 nm for FOS-I and FOS-II respectively for this experimental arrangement, as shown in Fig. 3-2.
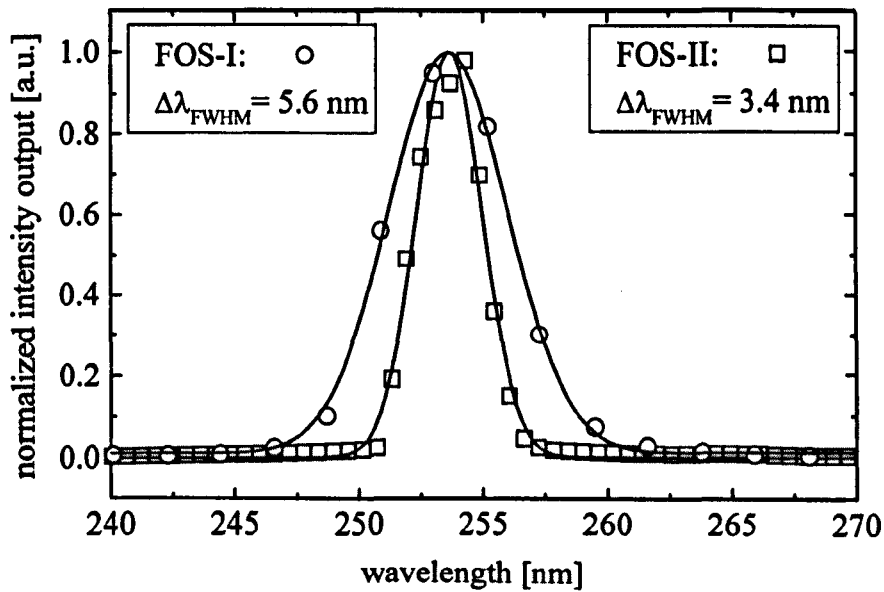
Fig. 3-2: Linewidth, $\Delta \lambda_{FWHM}$, of FOS-I and FOS-II with FOS-II having an input fiber with a core-diameters of 50 μm, determined with a low pressure mercury calibration lamp at λ=253.65 nm.

It may be noted again, that an input fibre with a core diameter of 50 μm was connected permanently to FOS-II throughout this and the following experiments. The least-squares method was chosen because of its property to minimize the squares of the residuals, with the residuals being the difference between the true intensity value and its calculated value from the fitting function. However, with the spectral resolution (FWHM) achieved by FOS-I and FOS-II, it is only the emission lines at 253.65 nm and 546.08 nm of a low pressure mercury lamp that may be seen as single lines, and are potentially useful for wavelength calibration. The emission lines situated around 313 nm, 365 nm, 405 nm and 436 nm, described in

Tab. 3-2, were found to be doublets or multiplets which could not be resolved with FOS-I and FOS-II [35]. Thus a method had to be developed to estimate the centroid of these multiplets, recorded by the spectrometers as a single emission line. The individual lines of the multiplets were convolved with the instrumental line profiles of the spectrometers and superimposed to simulate the emission lines they would detect. A Gaussian least squares fit was performed to determine the wavelength position at the peak maximum of these simulated emission lines for FOS-I and FOS-II respectively. Tab. 3-3 shows the peak position of these superimposed emission lines, taking the instrumental profiles of FOS-I and FOS-II into account.

FOS-I (24.0 °C)			FOS-II (24.6 °C)		
convolved calibration wavelength [nm]	pixel position, p_c	relative wavelength accuracy $\delta\lambda = \Delta\lambda_p\,\Delta p_c$ [nm]	convolved calibration wavelength [nm]	pixel position, p_c	relative wavelength accuracy $\delta\lambda = \Delta\lambda_p\,\Delta p_c$ [nm]
253.65	28.267 ± 0.026	0.06	253.65	145.928 ± 0.090	0.05
312.95	55.926 ± 0.077	0.17	312.95	247.008 ± 0.061	0.04
365.22	80.316 ± 0.054	0.12	365.21	337.952 ± 0.051	0.03
404.78	98.790 ± 0.075	0.16	404.72	407.852 ± 0.102	0.06
435.83	113.283 ± 0.037	0.08	435.83	463.544 ± 0.077	0.04
546.08	164.754 ± 0.081	0.17	546.08	667.144 ± 0.129	0.07

Tab. 3-3: Convolved calibration wavelength, pixel position, p_c, and relative wavelength accuracy, $\delta\lambda$, of FOS-I and FOS-II at 24.0 °C and 24.6 °C respectively.

To calibrate the spectrometers, the pixel position on their detector array had to be related with the wavelengths of the mercury emission lines with a sub-pixel precision. As an isolated spectral emission line was found to reach five of more detector elements, a Gaussian least squares fit was found to be a very accurate method to determine the exact position of the peak on the pixel. Its special advantage relied on the fact that the instrumental profile was assumed to be Gaussian, and far more important, that the maximum position of the mercury multiplets had also been estimated with a Gaussian fit, thus partially compensating the errors caused by this assumption. Twenty-five samples of the mercury emission spectra and the dark output were taken. Their means and standard deviations were calculated. The signal to noise ratio, $SNR(p)$, of the pixels, p, used for calibration was estimated to be

$$\blacksquare \tag{3.5-4}$$

with the mean sample output, $\bar{I}_{Sam}(p)$, the dark output, $\bar{I}_{Drk}(p)$ and the standard deviation of the sample output, $\Delta I_{sam}(p)$. The SNR of FOS-I and FOS-II as a function of pixel number, p, is shown in Fig. 3-3 for the selected calibration peaks. Only pixels having an SNR>6 dB were selected for a Gaussian least squares fitting procedure to determine the sub-pixel position of the emission lines emitted by the low pressure mercury lamp. The results of such a fit, performed for the outputs of FOS-I and FOS-II at 24.0 C and 24.6 C respectively, are shown in Tab. 3-3. With this fitting procedure, the centroid position of the mercury singlets or multiplets could be estimated with a precision 0.08 pixels for FOS-I and 0.13 pixels for FOS-II in the worst case. This resulted in a worst case wavelength accuracy of 0.16 nm for FOS-I and 0.07 nm for FOS-II to determine the maximum position of a single peak, as shown in Tab. 3-3.
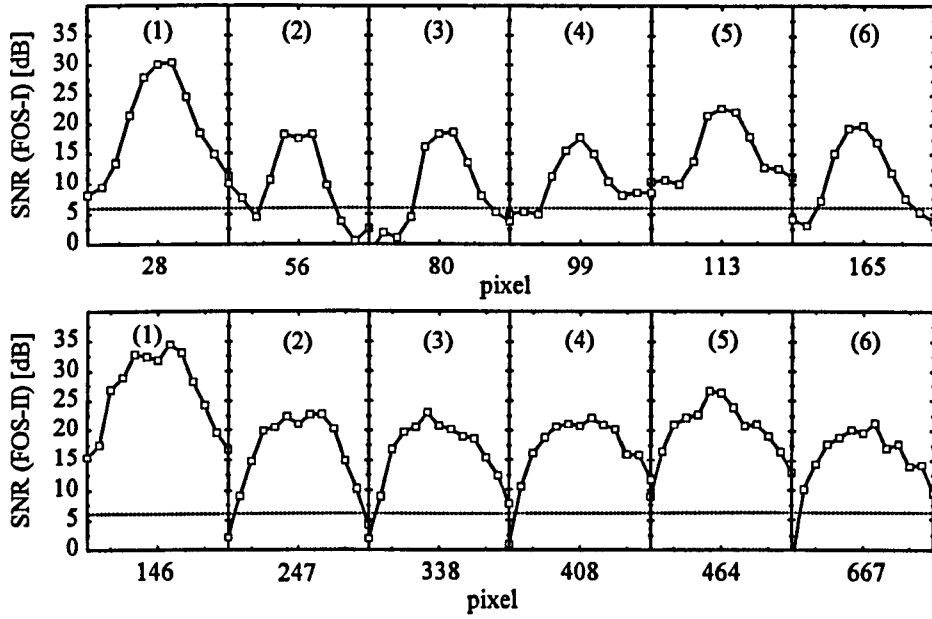
Fig. 3-3: Signal to noise ratio (SNR) line spectra, illuminated by the emission lines of the low pressure mercury lamp at the recorded peaks 1-6, shown in Fig. 3-1.

As discussed previously, a common approach to calibrate a detector-array-based spectrometer is to determine an equation which relates the sub-pixel positions obtained with the calibration wavelength emitted by the mercury lamp. The simplest form of such an equation is a polynomial, such as

$$\qquad\qquad\qquad\qquad\qquad\qquad\qquad\qquad\qquad\qquad\qquad\qquad \text{(5.4)}$$

where p are the detector element indices, and the coefficients A, B_1, B_2, ...B_n, are to be determined by a least squares fit. To evaluate the quality of the fit, the standard error of estimate, SEE, can be calculated, which may essentially be seen as the standard deviation of the residuals about the regression curve. The SEE can be written as [32]

$$SEE = \sqrt{\rule[-1.5em]{4em}{3em}}$$

(5.5)

where $\lambda(p_c)$ and λ_c are the calculated and the true wavelength and n_c and n_p are the number of calibration wavelength and the number of coefficients in the polynomial respectively. Quadratic, cubic and quartic models were tested for least squares fitting. The cubic model was found to be sufficient, because it produced with the minimum number of polynomial coefficients a reasonable SEE and more importantly the SEE could not be improved significantly by increasing the number of polynomial coefficients.

3.5.3 Wavelength stability of FOS-I and FOS-II at varying temperatures

The objective of this section is to investigate the wavelength stability of FOS-I and FOS-II as a function of temperature. To accomplish this, both spectrometers were situated in an air conditioned cabinet, as described in Section 3.1. A low pressure mercury vapour lamp (HG2, Cathodeon Ltd.) was fixed on an optical bench outside the cabinet. The lamp was allowed to warm up for at least 1 hour before measurements were made. FOS-I was connected to a fibre with a core/cladding diameter of 600/660 μm and a length of 3.7 m. FOS-II was connected to a fibre with a core diameter of 50 μm and a length of 2 m, defining its entrance slit and therefore its wavelength resolution. Light from the low pressure mercury lamp was coupled into both fibres with a low NA in such a way that about a 75 % full range peak intensity of the 253.65 nm emission peak was obtained in both spectrometers running with an integration time of 50 ms. The temperature in the cabinet was varied between 0 °C and 50 °C in steps of approximately 5 °C with a precision of ±1 °C.

The line emission spectrum of the low pressure mercury lamp was recorded by FOS-I and FOS-II for each of these temperatures, as for example shown in Fig. 3-1. A Gaussian least squares fit was performed at each temperature for the peaks 1..6 to determine

their sub-pixel position on the detector arrays of FOS-I and FOS-II. Then a calibration function, based on a cubic polynomial, was calculated by using a least squares regression to relate the sub-pixel positions obtained with their corresponding calibration wavelengths. Finally, the standard error of estimate, SEE, was calculated for each regression line.

FOS-I	$\lambda(p) = A + B_1 p + B_2 p^2 + B_3 p^3$				
temperature [°C]	A [nm]	B_1 [nm]	B_2 [(E-5) nm]	B_3 [(E-8) nm]	SEE [nm]
5.4	192.80 ± 0.08	2.1535 ± 0.0083	-12.4 ± 4.2	39.0 ± 14.4	0.020
8.9	192.89 ± 0.04	2,1499 ± 0.0018	-8.0 ± 2.1	24.9 ± 7.2	0.010
13.7	192.93 ± 0.10	2.1487 ± 0.0044	-7.1 ± 5.2	23.0 ± 17.8	0.025
19.1	192.85 ± 0.10	2.1523 ± 0.0042	-10.8 ± 5.0	34.5 ± 17.1	0.024
24.0	192.98 ± 0.03	2.1474 ± 0.0014	-4.9 ± 1.6	14.0 ± 5.6	0.008
27.8	192.97 ± 0.09	2.1489 ± 0.0040	-7.2 ± 4.8	22.9 ± 16.4	0.023
34.1	192.96 ± 0.12	2.1504 ± 0.0053	-9.2 ± 6.3	29.9 ± 21.7	0.030
38.1	193.01 ± 0.03	2.1479 ± 0.0014	-5.6 ± 1.7	16.3 ± 5.8	0.008
42.6	193.03 ± 0.09	2.1478 ± 0.0038	-5.4 ± 4.5	15.4 ± 15.3	0.021

Tab. 3-4: Coefficients and SEE of third order polynomial least squares fit for FOS-I at temperatures ranging from 5.4 °C to 42.6°C.

FOS-II	$\lambda(p) = A + B_1 p + B_2 p^2 + B_3 p^3$				
temperature [°C]	A [nm]	B_1 [nm]	B_2 [(E-5) nm]	B_3 [(E-8) nm]	SEE [nm]
6.0	168.42 ± 0.01	0.60990 ± 0.00013	-6.08 ± 0.04	-0.06 ± 0.03	0.002
9.4	168.10 ± 0.06	0.60882 ± 0.00062	-5.77 ± 0.17	-0.29 ± 0.14	0.011
14.3	167.64 ± 0.16	0.60792 ± 0.00154	-5.51 ± 0.43	-0.48 ± 0.35	0.027
19.6	166.88 ± 0.16	0.60848 ± 0.00154	-5.58 ± 0.43	-0.42 ± 0.35	0.027
24.6	166.00 ± 0.19	0.60898 ± 0.00181	-5.64 ± 0.50	-0.37 ± 0.41	0.031
28.2	165.31 ± 0.12	0.60996 ± 0.00112	-5.82 ± 0.31	-0.25 ± 0.25	0.019
34.3	164.24 ± 0.25	0.60930 ± 0.00238	-5.58 ± 0.65	-0.41 ± 0.53	0.040
38.7	163.14 ± 0.23	0.61052 ± 0.00215	-5.89 ± 0.58	-0.16 ± 0.47	0.036
43.1	162.04 ± 0.22	0.61110 ± 0.00205	-6.00 ± 0.56	-0.05 ± 0.45	0.034

Tab. 3-5: Coefficients and SEE of third order polynomial least squares fit for FOS-II at temperatures ranging from 6 °C to 43.1 °C.

Thus a calibration function was obtained for each spectrometer at a number of different temperatures. Tab. 3-4 and Tab. 3-5 show the results of the wavelength calibration procedure for FOS-I and FOS-II respectively. Observing the SEE of the calibration model for both spectrometers over the entire temperature range, a wavelength accuracy of 0.03 nm and 0.04 nm can be obtained for FOS-I and FOS-II respectively. It should be pointed out that the results of the fit improved approximately fivefold by using the calibration wavelength obtained by convoluting the mercury multiplets with the instrumental profile of each instrument, compared to using the mercury calibration wavelength found in literature. Fig. 3-4 and Fig. 3-5 show the coefficients of the cubic fitting functions including their error bars as a function of temperature. Only the intercept, A, of the calibration functions of FOS-I and FOS-II was found to vary with temperature.
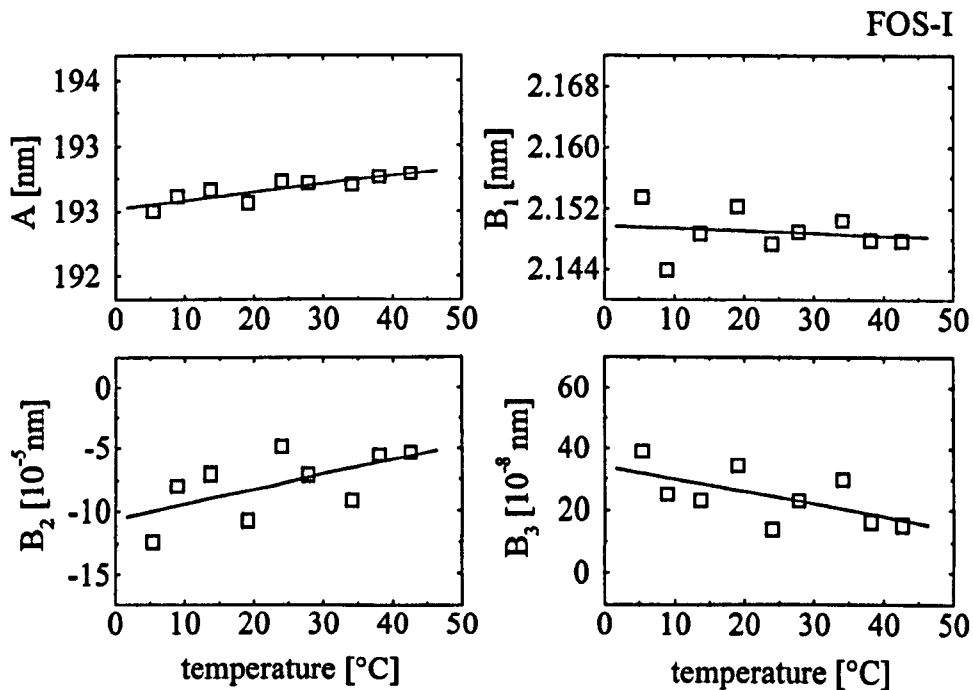
Fig. 3-4: Coefficients of the cubic least squares regression fit of FOS-I as a function of temperature
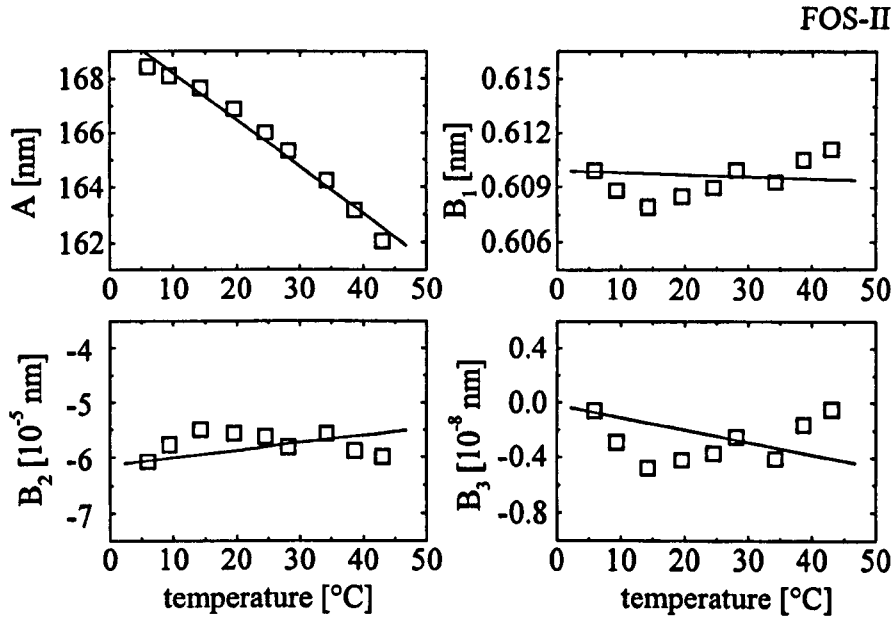
Fig. 3-5: Coefficients of the cubic least squares regression fit of FOS-II as a function of temperature

Over the entire temperature range, a drift of approximately 0.2 nm and 6.4 nm could be observed with FOS-I and FOS-II respectively. This is equivalent to a drift of approximately 0.006 nm $°C^{-1}$ for FOS-I and approximately 0.17 nm $°C^{-1}$ for FOS-II. A simple relationship between temperature and the changes of the coefficients B_1, B_2 and B_3 of the cubic least squares fit could not be found. Although these coefficients change slightly, their absolute values stay approximately within the error of prediction over the entire temperature range. However, the effect of the wavelength accuracy and drift on a spectrometer should be discussed in context, with its wavelength resolution and the linewidth of the emission or absorption peak observed. Assuming a single wavelength detection procedure to determine the magnitude of an emission or absorption peak of Gaussian shape, the lowest error caused by wavelength drift may be found when observing the magnitude at the peak maximum, as its rate of change, described by its slope, is close to zero but increases gradually. However, at the inflection point, where the slope of the Gaussian shaped peak reaches its maximum, the highest change in magnitude and therefore the highest measurement error can be expected. Furthermore

the magnitude of the slope of the peak, its first derivative, is dependent on its linewidth and grows approximately exponentially with the decrease in linewidth. Thus, the measurement error induced by wavelength shift is increasing approximately exponentially in respect to the decrease in linewidth of the peak observed. This indicates that a measurement error caused by wavelength drifts increases approximately exponentially in respect to the increase an wavelength resolution, as discussed below.

3.5.4 Effect of wavelength drift on spectrometer measurements

In a laboratory based environment, the temperature could be assumed to vary by about 1 °C. Thus, with an emission peak, such as emitted by a low pressure mercury lamp, and recorded by FOS-I and FOS-II with an arbitrary magnitude of 100 % and a linewidth of approximately their instrumental profiles, 5.6 nm and 3.4 nm, an error induced by measuring the magnitude of 0.00032 % and 0.71 % may be observed at the top of the peak, but of 0.15 % and 7.22 % at their inflection points respectively.

In field-based applications, the temperature of the instruments could vary by up to 40 °C. Then, an error in measuring the magnitude of the peaks caused by wavelength drift of up to 0.52 % and 6.2 % may be observed in FOS-I at the top of the peak and its inflection point respectively. With FOS-II it would not be possible to detect the peak, as its FWHM is smaller than the actual wavelength drift. However, a simple correction algorithm may by applied to correct the wavelength drift, found with FOS-II, when working with a deuterium light source commonly used in ultra violet spectroscopy. As the 656.1 nm peak of the deuterium lamp is a monochromatic peak [27], similar to the mercury emission lines used for the wavelength calibration, it can be used to recalculate the intercept, A, of the calibration curve and thus compensating its temperature dependent drift. By selecting the calibration coefficients B_1, B_2 and B_3, obtained for FOS-II at 24.6 °C as a reference, the intercept, A, could be recalculated, because wavelength and pixel position were known. Using this technique, an SEE ≤ 0.6 nm could be achieved for FOS-II over the entire temperature region without the necessity of knowing the instrument's temperature. Estimating the wavelength

drift with the obtained SEE of 0.6 nm of the wavelength corrected calibration curve, an error of magnitude of 8.4 % and 25 % may be observed at the top of the peak and the inflection point respectively over the entire temperature range with an emission line recorded by FOS-II close to its spectral resolution.

However, the absorption peaks usually observed in water analysis based on ultraviolet spectroscopy are far broader than the wavelength resolution of FOS-I and FOS-II. For example, the absorption spectrum of nitrate, NO_3^-, has its peak maximum situated at around 203 nm with an FWHM of approximately 30 nm. Consequently the slope of such an absorption peak function and therefore the induced error caused by wavelength drifts is far lower. Assuming such a broad peak with a magnitude of 1 AU in a laboratory with a temperature variation smaller than 1 °C, negligible absorption variations of 0.01 mAU and 0.3 mAU at the peak and the inflection point respectively may be found with FOS-I. With FOS-II, absorption variations of 0.08 mAU and 8 mAU may be observed in such an environment at the top of the absorption peak and its inflection point respectively. Assuming absorption errors of 2 mAU to 10 mAU, caused be the signal to noise ratio of the detector electronics, commonly found with such spectrometer modules, it may be concluded that the temperature variations found in a laboratory (<1 °C) have a minor effect on the performance of the instrument.

However, using FOS-I in a field trial with temperature variations as high as 40 °C its absorption could vary by 0.2 mAU and 10 mAU at the peak and the inflection point respectively. With FOS-II, such temperature changes could create absorption variations as high as 120 mAU and 310 mAU for peak and inflection point respectively, if the spectrometer is not temperature corrected, and 1 mAU and 30 mAU respectively, if the wavelength calibration curve is temperature compensated as described above. Comparing these potential measurement errors with the minimum absorption errors of 2 mAU and 10 mAU caused be the detector electronics, it may be necessary in such rather harsh environments to stabilize the temperature of the spectrometer modules.

3.6 Spectral sensitivity in the ultraviolet - system test

The cross-comparison work discussed herein has been carried out with the same primary optical system, configured into a fibre optical nitrate monitor, reflecting one of the most relevant pollution monitoring issues in the water industry [17, 18]. In this way, the essential difference in the systems cross-compared will be due to the influence of the miniature spectrometer FOS-I and FOS-II. In particular, the sensitivity in the ultraviolet part of the light spectrum at wavelength between 200 nm and 300 nm will be investigated. A simple experimental arrangement, as shown in Fig. 3-6, essentially comprising a deuterium lamp light source, DL, with its power supply, PS, a light coupling system, LS, a mode scrambler, MS, input and output optical fibres, FI of a length of 4 m and FO of a length of 1 m, both having core/cladding diameter of 600/660 µm, a highly sensitive absorption cell in the form of a liquid core waveguide, LCW, having an optical pathlength of 196 mm and a fibre-optic shutter, SH, was used. The input fibres FC-I, being the cross-section converter of FOS-I, and FC-II being an ultraviolet improved silica/silica fibre, having a core/cladding diameter of 100/110 µm with a length of 1 m, were connected to whichever of the miniature spectrometers FOS-I or FOS-II was being used to the sensor system. A personal computer, PC, with appropriate interface cards collected and stored spectral data obtained from the two miniature spectrometers. A detailed description of the sensor arrangement can be found in Chapter 5. To avoid the problems with wavelength calibrations investigated in Section 3.4, the system was specially calibrated for FOS-II before the nitrate analysis by replacing the deuterium light source with the low pressure mercury light source used previously. A key factor in optimizing such a sensor system is the light power budget, to obtain a satisfactory signal to noise ratio of the optical signal finally detected. As a result, the silica-lens-based light coupling system, as described in Chapter 2 and published in [6], which shows some wavelength-dependence in the coupling efficiency, was used to compensate the increasing light losses at wavelengths below 250 nm which occur in the optical fibres FI, FO, FC-I and FC-2, in the liquid core waveguide, LCW, and also arise from the decreasing sensitivity of the spectrometers FOS-I and FOS-II. A key feature of the work was that UV-improved optical fibres (UVI-fibres), described in Chapter 2 and

elsewhere [7, 8, 9] were employed to ensure a stable UV light flux at wavelengths below 250 nm, to and from the sensor cell through those fibres.
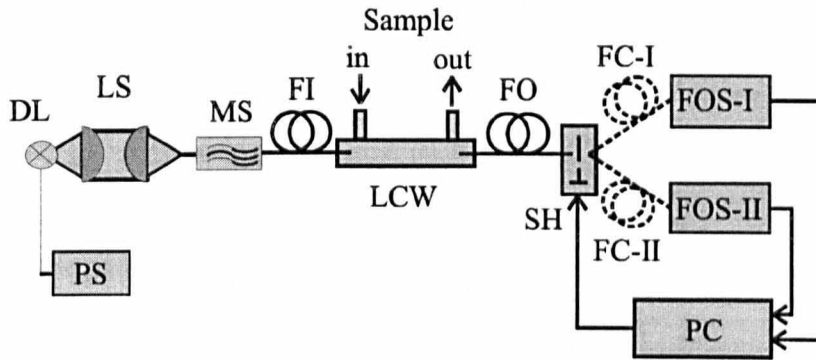
Fig. 3-6: Experimental arrangement used to compare the sensitivity of FOS-I and FOS-II. The sensor system comprises a deuterium lamp, DL, with its power supply, PS, a lens system, LS, input and output fibres, FI and FO, a mode scrambler, MS, a liquid core waveguide, LCW, as the absorption cell, a fibre-optic shutter, SH, the input fibres FC-I and FC-II for the two miniature spectrometer systems, FOS-I and FOS-II and an IBM-compatible personal computer, PC.

The liquid core waveguide, which will be described in Chapter 5, was used as the optical sensor cell in this demonstration, shows the major advantage of a relatively low light loss at long pathlengths, since the optical energy coupled into the LCW is confined to and guided by its core and contains the analyte on which the measurements are to be carried out. The applicability of the LCW has been tested in the visible [18 ,37] and the UV regions of the spectrum [17, 18]. A detailed description of its construction and performance can be found in Chapter 5 and elsewhere [5, 18, 37].

3.6.1 Signal to noise ratio at wavelength below 300 nm

The deep ultraviolet region of the light spectrum is of particular interest in water quality analysis and process monitoring. Thus, the applicability of FOS-I and FOS-II in a fibre-optic-based sensor arrangement, as described above, to perform measurements below 300 nm and especially 230 nm with a reasonable signal to noise ratio was investigated.

A nitrate ion, NO_3^-, standard solution, prepared by dissolving sodium nitrate ($NaNO_3$) in de-ionized water, was used for preparing aqueous nitrate solutions, at concentrations ranging from 0.067 mg l^{-1} to 0.51 mg l^{-1}. Nitrate, an important water pollutant, was chosen because of its characteristically absorption peak situated around 203 nm wavelength with a linewidth of approximately 30 nm. The LCW was filled with de-ionized water and a varying attenuation, realized by doping the solution with nitrate concentrations ranging from 0.067 mg l^{-1} to 0.51 mg l^{-1}, introduced to investigate its effect on the intensity spectrum and the SNR of both spectrometers. The dark output-corrected intensity spectra and the resulting SNR, obtained by dividing the dark output-corrected intensity spectra by its standard deviation is shown in Fig. 3-7 and Fig. 3-8 for FOS-I and FOS-II respectively. Both figures clearly indicate that a stable transmission of ultraviolet light is possible at wavelength below 240 nm, which is the envisaged wavelength region of this work. However, it was found that the intensity values measured at wavelengths below 240 nm of FOS-I were significantly higher than those of FOS-II, thus showing a higher sensitivity in this wavelength region. Thus it may be concluded that FOS-II will be far more sensitive to stray light effects, distorting the results of analytical experiments, than FOS-I. Additionally, although the noise level of FOS-I was determined to be significantly higher than that of FOS-II, the signal to noise ratio of FOS-I was still higher than that of FOS-II. Reducing the intensity signal in the sensor system at a wavelength of 203 nm to, for example, 10% of its original signal at an equivalence of 1 AU, a SNR of more than 10 dB could still be observed with FOS-I and FOS-II.
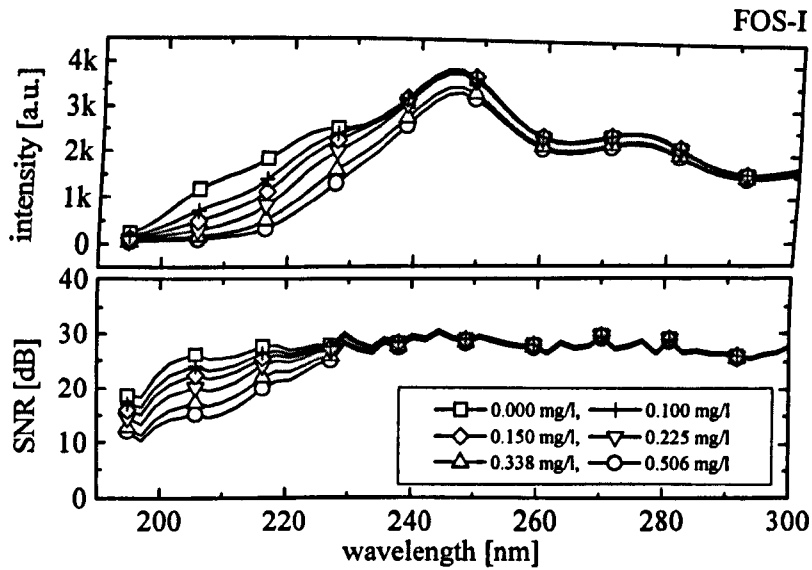
Fig. 3-7: Intensity output and SNR of FOS-I as a function of wavelength ranging from 190 nm to 300 nm with NO_3^- induced absorption.
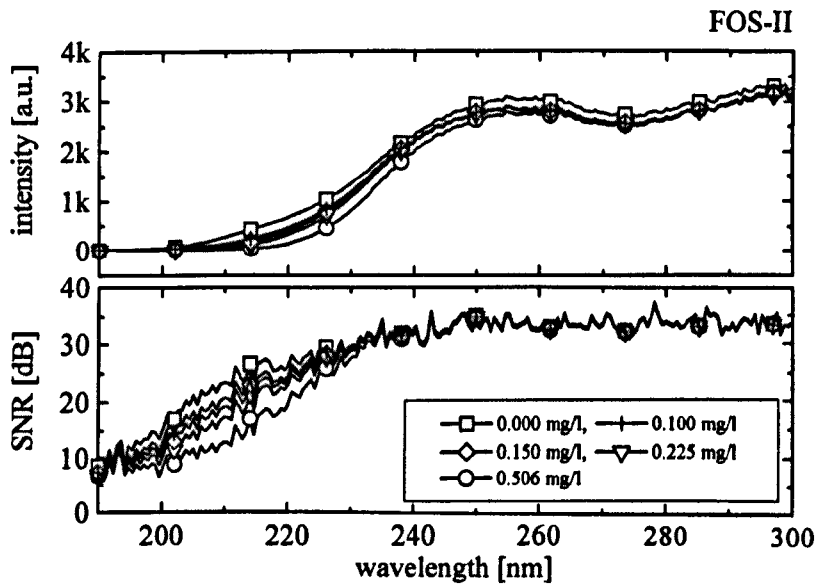
Fig. 3-8: Intensity output and SNR of FOS-II as a function of wavelength ranging from 190 nm to 300 nm with NO_3^- induced absorption.

However, investigating the spectrum of FOS-II further, it was found that stray light effects in the spectrometer already reduced the absorption to 0.8 AU. In further experiments, spectrometer FOS-I was chosen as the wavelength resolving detector element, in view of the above discussion.

3.7 Summary and Discussion

Two inexpensive fibre-optic-based spectrometer modules have been investigated for potential use in field applications as an integral part of a UV sensor system. The influence of temperature variations on the dark output and their wavelength stability has been studied. It was found that the dark output of FOS-I followed an exponential law, doubling each time the temperature of the spectrometer is increased by approximately 7 °C. With FOS-II, a non-linear and therefore less predictable relationship was found, mainly caused by the pre-amplifier electronics. However, the optical dark output data obtained was found to double each 9 to 10 °C, when fitting the data to an exponential function. With this kind of system, the main source of noise was found to arise in the spectrometer itself. An averaged noise level of 2.7 ± 0.6 a.u. was found at 24 °C. Within the temperature range of 5 °C to 42 °C, the use of integration times varying between 13 ms and 585 ms appeared to have no influence on these averaged noise levels. However, FOS-II was found to have a lower averaged noise level varying from 1.0 ± 0.2 a.u. to 2.0 ± 0.5 a.u. at temperatures ranging from 6.0 °C to 43.6 °C, indicating a clear temperature dependence in the averaged noise level. A wavelength drift induced by temperature variations, typically found in field applications, was investigated with a specially developed calibration algorithm. A drift of approximately 0.006 nm K^{-1} for FOS-I and approximately 0.17 nm K^{-1} for FOS-II could be observed. However, using the 656.1 deuterium peak for on-line correction, FOS-II could be stabilized to a wavelength accuracy of 0.7 nm within the above temperature range. Finally, the sensitivity of the detector arrays of FOS-I and FOS-II was investigated in the ultraviolet at wavelengths between 200 nm and 300 nm, when connected to a typical sensor arrangement. In particular below 240 nm, FOS-I showed a clear advantage compared to FOS-II. However, it should be mentioned that the effect of stray light on the performance of

both spectrometers has not been investigated, but that such data would be valuable to compare more fully the range of both instruments. Good system design should help to minimize its effect. However, the work described in this Chapter shows that the spectrometers investigated can be used successfully as polychromatic detectors in fibre-optic based UV sensors. Two sensor applications, specifically designed for deep ultraviolet applications are discussed in Chapters 4 and 5.

3.8 References

1 W. R. Seitz, "Chemical sensors based on fiber optics", Analytical Chemistry, (1984), Vol. 56, No. 1, 16-34.

2 J. O. W. Norris "Multimode optical fibre chemical sensors" in Optical Fiber Sensor Technology Eds: K. T. V. Grattan & B. T. Meggitt, Chapman & Hall, London, (1995), 161-196.

3 L. W. Burgess, "Absorption based sensors", Sensors & Actuators B, (1995), Vol. 29, 10-15.

4 Z. Mouaziz, R. Briggs, I. Hamilton and K. T. V. Grattan, "Design and implementation of a fibre-optic-based residual chlorine monitor", Sensors and Actuators B, (1993), Vol. 11, 431-440.

5 P. Dress, H. Franke, "A cylindrical liquid-core waveguide", Appl. Phys. B63 No.1, (1996), 12-19.

6 M. Belz, W. J. O. Boyle, K. -F. Klein, K.T.V. Grattan: "Smart sensor approach for a fiber-optic based residual chlorine monitor". Paper presented at Europt(r)ode III, (Zürich), Book of Abstracts, 194, published in Sensors and Actuators B, (1997), Vol. 39-123, 380-385.

7 K.-F. Klein, P. Schließmann, E. Smolka, G. Hillrichs, M. Belz, W.J.O. Boyle, K.T.V. Grattan: "UV-stabilized silica based fiber for applications around 200 nm wavelength", Paper presented at Europt(r)ode III (Zürich), Book of Abstracts (1996), 160, published in Sensors and Actuators B, (1997), Vol. 39-123, 305-309.

8 M. Belz, W.J.O. Boyle, K.-F. Klein and K.T.V. Grattan: "Water Quality Measurement using fibre optics at wavelength below 250 nm", in: J. Halttunen (ed.), Proceedings of the XIV IMEKO World Congress (Tampere 1-6. June 1997), Finnish Automation Support, Helsinki, (1997), Vol. XA, 151 - 155.

9 K.-F. Klein, S. Hüttel, U. Kaminski, J. Kirchhof, S. Grimm, G. Nelson, "Stability and life-time improvements of UV-fibers for new applications", SPIE Proc. , (1998), Vol. 3262, paper 3262 C-32.

10 H.-F. Tseng, J. R. Ambrose, M. Fattahi, "Evolution of the Solid-State Image Sensor", Journal of IMAGINE SCIENCE, (1985), Vol. 29, No. 1, 253-259.

11 L. Placentino, E. Pace, G. Naletto, G. Tondello, "Performance if metachrome II as a scintillator for the far and vacuum ultraviolet spectral region", Opt. Eng., (1996), 35 (11), 3342-3347.

12 P. Lee, A. Simoni, A. Sartori, G. Torelli, "A photosensor array for pectrophotometry", Sensors and Actuators A, (1995), Vol. 46-47, 449-452.

13 Y. Qui, X. Z. Qu, X. Q. Song, "Construction of a CCD Mulitchannel Fiber Optic Spectrometer and its Application", Instrumentation Science and Technology, (1996), Vol. 24(2), 143-150.

14 Y. M. Yee, N. I. Maluf, P. A. Hing, M. Albin, G. T. A. Kovacs, "Miniature spectrometers for biochemical analysis", Sensors and Actuators A, (1997), Vol. 58, 61-66.

15 V. Bellon, J. L. Vigneau, M. Leclercq, "Feasibility and Performance of a New, Multiplexed, Fast and Low-Cost Fiber-Optic NIR Spectrometer for the On-Line Measurement of Sugar in Fruits", Applied Spectroscopy, (1993), Vol. 47, No. 7, 1079-1083.

16 X. Wang, D. E. Vaughan, V. Pelekhaty, "A novel miniature spectrometer using an integrated acousto-optic tunable filter", Rev. Sci. Instrum., (1994), Vol. 65 (12), 3653-3656.

17 M. Belz, P. Dress, K.-F. Klein, W.J.O. Boyle, H. Franke and K.T.V. Grattan: "Liquid Core Waveguide with Fiber Optic coupling for Remote Pollution Monitoring in the deep Ultraviolet". Poster presented at 7'th IAWQ Workshop on Instrumentation, Control and Automation and Wastewater Treatment and Transport Systems, Brighton (UK), (July 1997), published in Water Science and Technology, (1998), Vol. 37, No. 12, 279-284.

18 P. Dress, M. Belz, K.-F. Klein, K.T.V. Grattan, H. Franke, "Water-core-waveguide for pollution measurements in the deep ultra-violet", APPLIED OPTICS, (1998), Vol.37, No.21, 4991-4997.

19 Jobin Yvon/Spex, "Matching a Spectrometer to a Light Source", Guide for spectroscopy, Jobin Yvon/Spex publication L-269/25/5-94, ISA Ltd, Stanmore, Middlesex, UK.

20 D. Falkin, M. Vosloo, "Charge coupled devices for spectroscopy", Spectroscopy Europe, (1993), 5/5, 16-22.

21 A. Rogalski, M. Razeghi, "Semiconductor ultraviolet photodetectors", Opto-Electr. Rev., (1996), Vol. 4, N 1/2, 13-30.

22 P. J. Starks, E. A. Walter-Shea, F. R. Schiebe, B. L. Markham, "Temperature Sensitivity Characterization of a Silicon Diode Array Spectrometer", Remote Sens. Environ., (1995), Vol. 51, 385-389.

23 "N-MOS Linear Image Sensors Application Note", Technical Information, SD-26, Hamamatsu, 1998.

24 J. F. James, R. S. Sternberg, "The Design of Optical Spectrometers", Chapman and Hall, (1969), 10.

25 Sadler, D. Littlejohn, R. Riley, C. V. Perkins, "Improvements in Spectral Line Shape Reproduction from Spectrographs with CCD Detection", Applied Spectroscopy, (1996), Vol. 50, No. 4, 504-510.

26 M. Lindrum, B. Nickel, "Wavelength Calibration of Optical Multichannel Detectors in Combination with Single- and Double-Grating Monochromators", Applied Spectroscopy, (1989), Vol. 43, No. 8, 1427-1431.

27 American Society for Testing and Materials, "Standard Practice for Measuring Practical Spectral Bandwidth of Ultraviolet-Visible Spectrophotometers", Annual Book of ASTM Standards, (1997), Vol. 03.06, E 958-93, 786-790.

28 P. E. Berlot, G. A. Locascio, "Ultraviolet-Visible Photodiode Array Spectrophotometer Wavelength Calibration Method. A Practical Computer Algorithm", Analyst, (1991), Vol. 116, 313-316.

29 C. H. Tseng, J. F. Ford, C. K. Mann, T. J. Vickers, "Wavelength Calibration of a Multichannel Spectrometer", Applied Spectroscopy, (1993), Vol. 47, No. 11, 1808-1813.

30 American Society for Testing and Materials, "Standard Practice for Describing and Measuring Performance of Ultraviolet, Visible, and Near-Infrared Spectrophotometers", Annual Book of ASTM Standards, (1997), Vol. 03.06, E 275-93, 708-717.

31 S. Scopatz, G. Neel, E. Romesburg, M. Zivitz, "Calibrating a detector array based spectroradiometer with sub-pixel precision", in Raman Scattering, Luminescence, and Spectroscopic Instrumentation in Technology, (1989), SPIE Vol. 1055, 306-313.

32 J. T. Brownrigg, "Wavelength Calibration Methods for Low-Resolution Photodiode Array Spectrometers", Applied Spectroscopy, (1993), Vol. 7, 1007-1014.

33 J. Cho, P. J. Gemperline, D. Walker, "Wavelength Calibration Method for a CCD Detector and Multichannel Fiber-Optic Probes", Applied Spectroscopy, (1995), Vol. 49, No. 12, 1841-1845.

34 C. B. Childs, "Low pressure mercury arc for Ultraviolet Calibration", Applied Optics, (1962), Vol. 1, No. 6, 711-716.

35 C. J. Sansonetti, M. L. Salit, J. Reader, "Wavelength of spectral lines in mercury pencil lamps", Applied Optics, (1996), Vol. 35, No. 1, 74-77.

36 J. Reader, C. J. Sansonetti, J. M. Bridges, "Irradiances of spectral lines in mercury pencil lamps", Applied Optics, (1996), Vol. 35, No. 1, 78-83.

37 P. Dress, H. Franke, "Increasing the accuracy of liquid analysis and pH-value control using a liquid-core-waveguide", Rev. Sci. Instrum. Vol. 68, No. 5, pp. 2167-2171, 1997.

4. Design of a fibre-optic nitrate sensor
based on a reflectance cell

4.1 Abstract

Most spectroscopic applications in the visible and ultraviolet part of the optical spectrum using fibre optics have been restricted to the wavelength range above 230 nm up to now. Ultraviolet (UV) light, especially that below 230 nm, damages standard silica fibres with an undoped core and fluorine-doped cladding so quickly that a stable UV light transmission is essentially impossible. As a result, the fiberization of many conventional spectroscopic devices which has been seen in the visible and near infra-red parts of the spectrum has not been expanded to these short wavelengths.
After discussing the advantages of ultraviolet-improved fused silica fibres in Chapter 2, the coupling of UV light into such fibres in Chapter 2 and the applicability of miniature optical spectrophotometer modules in that wavelength region in Chapter 3, the applicability of an UV-optimized fibre-optic remote sensor for the determination of nitrate (NO_3^-) is studied. The system has an input and an output fibre of length 4 m respectively and a detection limit of 2.0 mg l^{-1} NO_3^- at a wavelength of 203 nm, based on a reflectance cell, and is described and its performance discussed in this Chapter.

4.2 Introduction

There has been an increase in demand for chemical sensors in recent years, especially since stricter national and international regulations have been introduced for pollutants present in process and waste waters. As a result, a range of different techniques for optically-based sensors has been developed by a wide range of laboratories and research institutions, as reviewed by Briggs and Grattan [1]. However, a survey carried out by Crossley [2] has shown that the market is still, to a large extent, dominated by conventional optical and spectrophotometric methods, such as fluorescence, absorption and kindred techniques. As a typical example, selective and simple methods for the deter-

mination of ammonia, nitrate and nitrite and organic matter in water are increasingly required to serve the rising interest that has been shown in monitoring the quality of drinking and sewage water, since high concentrations of these pollutants are indicative of poor water quality. However, ammonia, nitrate and nitrite and organic matter can be monitored optically due to their strong and broad absorption peaks centered around 180 nm, 203 nm 210 nm and 254 nm respectively [3, 4]. Methods to determine the concentration of nitrate in water range from nitrate-selective electrodes and colorimetric methods to direct UV absorption spectroscopy [5, 6, 7, 8, 9, 10, 11]. Detection limits of conventional spectrometer-based sensor systems equipped with standard absorption or reflectance cells with an optical pathlength of 10 mm, as cited above, were found to be around 0.5 mg l^{-1} of NO_3^-, when using the broad and strong absorption peak centered around the 203 nm wavelength. However, for continuous monitoring, the optical elements of the sensor which are immersed in the sample solution must be regularly cleaned due to biofilm formation and as well, analysis techniques like multivariate data analysis have to be used to determine nitrate concentrations in municipal waste water [11].

Several remote sensing systems with fibre optics have been developed for chemical sensing. They rely on the advantage of fibre optics to separate the sample cell, which could be situated in a hazardous environment, and the measurement equipment by guiding light to the sensor from a light source and from the sensor to the detector (remote sensing). These sensors have traditionally been constructed for the visible and near infrared part of the light spectrum, where losses in fibres are low. However, attempts to extend the usage of such sensor systems to measure water pollutants, such as ammonia, nitrate and nitrite, directly, have suffered from the problem that the reliable transmission of UV light below the 230 nm wavelength was not possible with commercially available fused silica fibres with a high OH content. The reason for this adverse behaviour in standard fibres is the generation of UV-induced colour centres, with resulting absorption bands in the transmission range concerned, as discussed in Chapter 2 and in the literature [12, 13, 14].

Fibre-optic nitrate sensing in the visible part of the light spectrum, based on colourimetric techniques, has been reported by Zaho *et al* [15] and Waterbury *et al* [16]. Nevertheless, early nitrate measurements using fibre optics in the ultra violet with a short fibre length and a conventional absorption cell having an optical pathlength of 1 cm were performed by Mouaziz *et al* [17]. He utilized a mercury-iodine light source with its intensity peak situated around 206 nm wavelength to measure the absorbance generated by nitrate and referenced the measurement by removing nitrate in the sample with an IMAC HP441 ion exchange resin in a second measurement cycle. Further work was carried out by Stanley *et al* [18] who determined the concentration of nitrate in the range 0.4 to 30 mg l^{-1}, using several metre long fibres. His complex optical system included a mechanically rotating filter wheel, a fragile deuterium lamp arrangement and it required a photomultiplier tube (PMT) detector. Although coupling light from a deuterium light source into standard fused silica fibres with a high OH content, he did not report any light losses induced by the generation of E'centres, perhaps caused by the fact that only very low light intensities were coupled into the optical system. He compared the absorption at 220 nm and 275 nm with a UV-sensitive PMT and two interference filters centred around the wavelengths mentioned.

A more generic approach to develop a polychromatic sensor for water analysis in the wavelength region from 196 nm to the visible light region is described in this Chapter. A primary aim is to have available both more and specific data, resulting in a reduction in the interference effects from other species, with a greater independence of the type of source water. This is designed to identify species, based on information from spectral features and hence obviate the need for a more service-intensive reagent-based system. The sensor system envisaged comprises a miniature diode array spectrometer (Chapters 3), an effective optical fibre coupling system (Chapter 2) to maximize optical efficiency and hence compensate for lower signal levels at a diode array detector compared to the use of a phase-locked UV-enhanced silicon diode detector and employing ultraviolet-improved fused silica/silica fibres as a stable waveguide at wavelengths be-

low 230 nm (Chapter 2). A reflectance cell with an optical pathlength of 1 cm is used in this sensor arrangement to detect the concentration of nitrate (NO_3^-) at the 203 nm wavelength, showing its applicability in practical optical instrumentation. In particular, the non-linear behaviour of the UV-improved fibres during the "warming up" period of the sensor and the signal to noise ratio after stabilization are discussed. Finally, results on the measurement of NO_3^- in de-ionized water are shown.

4.3 Optical properties of water in the ultraviolet

Due to the increased absorption of water in the deep UV region (200-250 nm) the losses of any optical cell filled with H_2O will increase with reducing wavelength. This section outlines the change of refractive index and attenuation of water at different wavelengths, which can be described by its complex refractive index. The complex refractive index of water, $n(\lambda) + jk(\lambda)$, is an important parameter for design and modelling of fibre-optic sensor cells intended for use with aqueous solutions. Although several hundreds of publications could readily be cited, only the work of Querry *et al.* and Huibers, who compiled most of the published data will be referenced [19, 20]. The interested reader may consult the extensive literature research cited in these articles. The absorption or better the attenuation of water, $a(\lambda)$, can be calculated from the complex part of the refractive index, $jk(\lambda)$

$$a(\lambda) = 4\pi \frac{k(\lambda)}{\lambda}$$
(4.3-1)

which can be used to describe the decrease of light power, $P(z,\lambda)$, caused by water in a sensor arrangement as a function of distance, z, and wavelength, λ

$$P(z,\lambda) = P(0,\lambda)e^{-a(\lambda)z} = P(0,\lambda)e^{-4\pi \frac{k(\lambda)}{\lambda}z}$$
(4.3-2)

Thus, the loss of light, $L_w(z,\lambda)$, in dB as a function of wavelength, λ, and distance, z, induced into an optical sensor by the absorption of water can be calculated by use of the following equation

$$L_w(z,\lambda) = 10\log_{10}\left(\frac{P(0,\lambda)}{P(z,\lambda)}\right) = \frac{40k(\lambda)\pi}{\lambda\ln(10)}z \qquad (4.3\text{-}3)$$

Refractive index, n, and the loss of light, $L_W(z, \lambda)$, induced by absorption water are shown in Fig. 4-1. It can be clearly seen that although n and $L_W(z, \lambda)$ increase in the ultraviolet, a transportation of light through water is possible. Losses as low as 0.3 dB cm^{-1} and 0.007 dB cm^{-1} at 200 nm and 300 nm wavelength respectively have to be expected in this wavelength region.
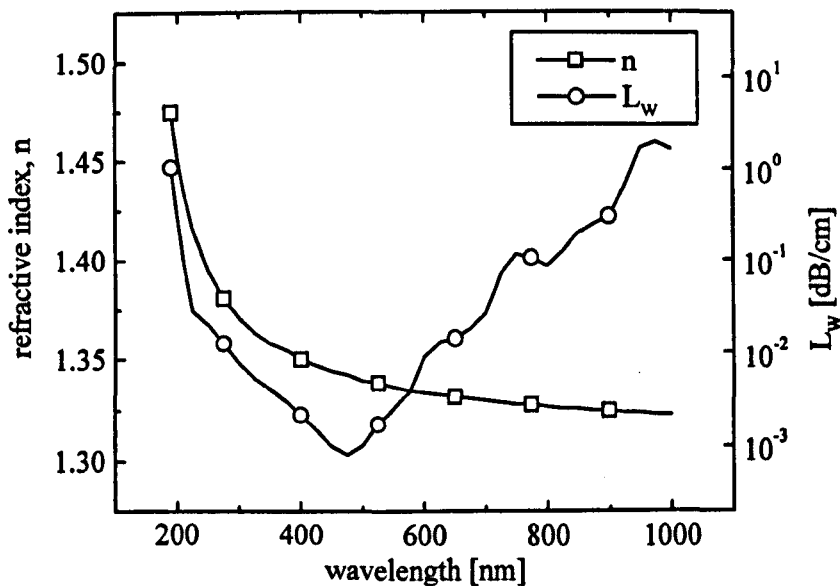
Fig. 4-1: Refractive index, n, and loss [dB cm^{-1}] of water as a function of wavelength, λ.

4.4 Experimental set-up

A simple fibre-optic based sensor arrangement to measure nitrate concentration in water by UV absorbance was developed. A range of different factors have to be taken into account when a fibre-optic sensor system for UV-C light ($\lambda \leq 250$ nm), comprising a deuterium lamp (DL), a lens system (LS), input and output fibres (FI, FO), having a core/cladding diameter of 410/440 µm and 2 m length respectively, a reflectance cell (RC), an optical shutter (SH) and a fibre-optic spectrometer (FOS), as shown in Fig. 4-2, is assembled.
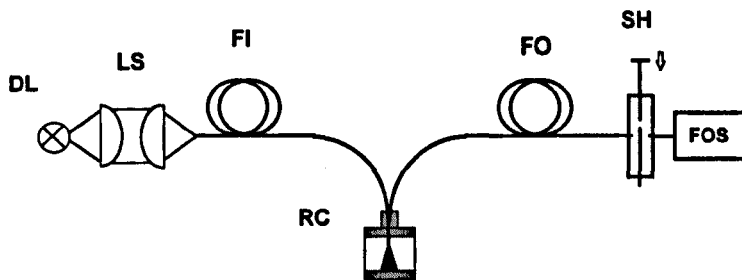
Fig. 4-2: Experimental set-up for a UV-C sensor, comprising a deuterium lamp (DL), a lens system (LS), input and output fibres (FI, FO), a reflectance cell (RC), an optical shutter (SH) and a fibre-optic spectrometer (FOS).

The key factor when designing such a sensor system is the power budget P_B, which could be defined as $P_B = 10 \log (P_{in} P_{out}^{-1})$ where P_{in} is the spectral input power of the sensor, emitted by the light source and P_{out} in the spectral power received by the spectrometer. Therefore a range of effects comprising the spectral distribution of the light source, the ease of coupling light from one optical component to the other, the spectral dependence of the lens-optics - coupling light from the light source into the input fibre, FI - , basic and induced light losses in FI and FO below the 250 nm wavelength, the spectral efficiency of RC, the sensitivity of the spectrometer, and the overall degradation of the equipment when exposed to UV light have to be taken into account when optimizing the power budget of such a sensor system.

A deuterium discharge lamp, type 208/05R manufactured by Heraeus [21], with a source diameter ≈ 0.5 mm, a NA ≈ 0.34 and a typical lifetime of 1000 hours was im-

plemented in the sensor system. This light source has a high radiant flux output combined with a relatively uniform spectral distribution in the ultra violet between 200 nm and 400 nm wavelength. As discussed in Chapter 2, its combination of a small emitting area and numerical aperture enabled wavelength-selective light coupling to the input fibre, FI, by a lens system comprising two plano-convex fused silica lenses. The chromatic aberration of the fused silica in the UV was used to tailor the spectral distribution of the source, through the optical system, to match the spectral sensitivity of the fibre-optic spectrometer and therefore to optimize its signal to noise ratio in the deep UV.

A reflectance cell with a variable pathlength (0 .. 12 mm), as outlined in Fig. 4-2, was designed and manufactured. Input (FI) and output (FO) fibres were placed 5 mm from a mirror, prepared from stainless steel with a polished surface finish. This arrangement resulted in an optical path length of 10 mm and the measurement results obtained could be compared to those obtained by using a commercially available UV-VIS spectrometer.

4.5 "Warming-up" time of the sensor system

The "warming up" period and thus the stability of the proposed sensor system was investigated. Intensity drifts were found in the first minutes of operation, which are believed to result from the warming-up period of the deuterium lamp and transient effects inside the UV-improved fibre material (see Chapter 2). The attenuation in the fibres can be explained by two independent effects, these being a basic level of attenuation, mainly determined by UV-intrinsic losses and Rayleigh-scattering and an UV-induced attenuation, caused by the generation of so called E'-centres, as discussed in Chapter 2 and in several references [12, 13, 14]. Although the generation of these E'-centres is greatly reduced in UVI fibres and therefore transportation of UV light is possible, it is not completely suppressed. However, in contrast to the up to 20 dB m^{-1} loss in standard fibres after 10 hours of UV exposure, only a decrease in light transmission

of about 10% at the absorption peak of the induced loss at 214 nm was found for this sensor arrangement, as shown in Fig. 4-3.
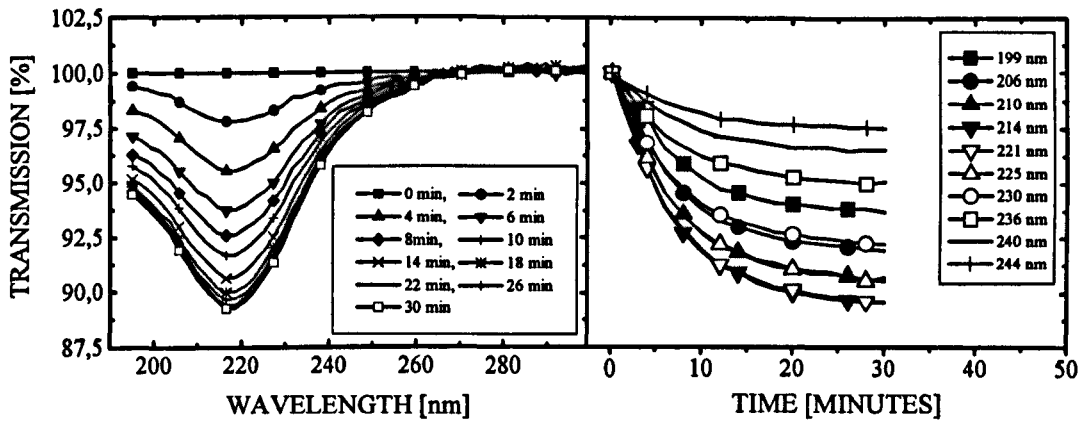
Fig. 4-3: Transmission loss in UV-improved fibre as function of wavelength and time, when the light source is switched on
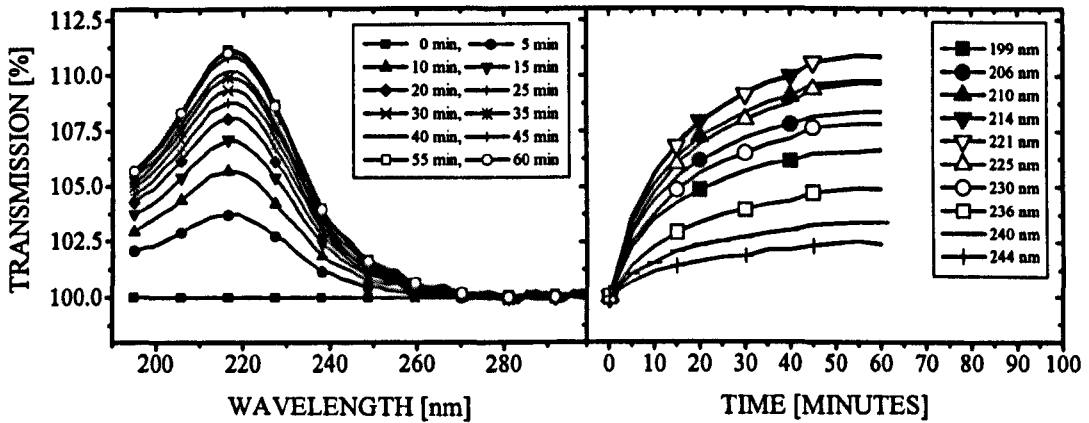
Fig. 4-4: Recovery of transmission in UV-improved fibre as function of wavelength and time, when the light source is switched off.

This loss was found to be time dependent and is induced in the optical fibres of the sensor system in the first 30 minutes of exposure. After this initial "warming up" period, the fibres appear to have a stable transmission of UV-light down to a wavelength

of 195 nm, the lower wavelength limit of the spectrometer. However Fig. 4-4 shows that the induced loss is reversible because the fibre returns to its original level of loss within a period of 60 minutes, when the UV-light into the fibre is switched off. These UV-improved fibres, described in Chapter 2, have been developed and tested over a period of 180 hours. Thus, after a "warming up" time of 30 minutes, the sensor system was found to have a stable UV-transmission and could be used in spectroscopic applications such as the determination of nitrate concentration discussed in the following section.

4.6 Experimental results

After stability investigations, the sensor system, as shown in Fig. 4-2, was optimized for nitrate measurements by altering the wavelength-dependent coupling efficiency of the lens system [12] to the 200 nm wavelength region. A standard nitrate ion (NO_3^-) solution, prepared by dissolving sodium nitrate ($NaNO_3$) in de-ionized water, was used for preparing aqueous nitrate solutions, having concentrations of 31.4, 15.7, 7.84, 3.92, 1.96 and 0.98 mg l^{-1} of NO_3^- ions. Taking 10 individual measurements for each sample with a spectrometer integration time of 150 ms, approximately 1.5 s were needed to measure the absorption spectra of one NO_3^- sample between 195 nm and 730 nm wavelengths. All experiments were performed in the laboratory at room temperature (21 °C), to avoid measurement error which may be caused by temperature drifts, as described in detail in Chapter 3. The intensity spectrum and its associated signal to noise ratio, defined as the mean of the dark output corrected intensity signal divided by its standard deviation (Chapter 1), are shown in Fig. 4-5 and Fig. 4-6 respectively. From both figures, it can be clearly seen that reliable measurements are possible in the most interesting wavelength region between 196 nm and 250 nm with the sensor system from the SNR point of view, defining the detection limit of the sensor system. According to the Bouger-Lambert-Beer Law, the concentration of a chemical species can be related to a the absorbance of light at a specific wavelength.
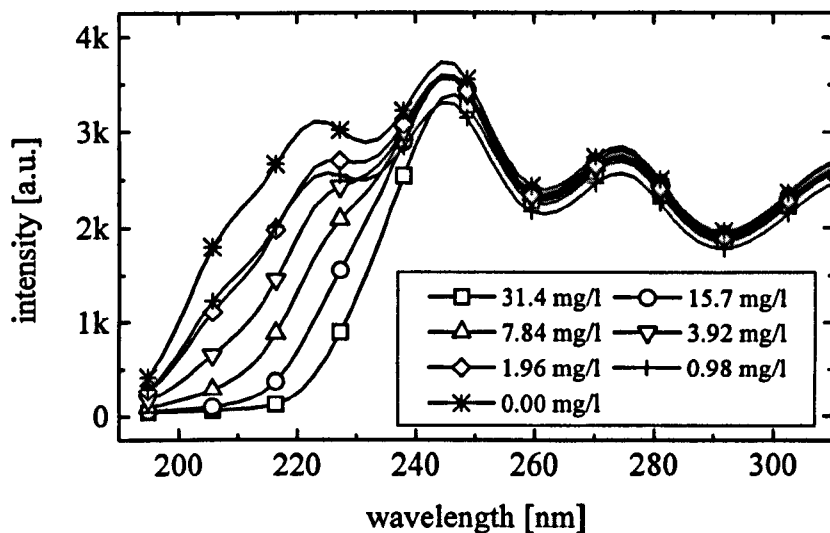
Fig. 4-5: Intensity spectra of NO_3^-, containing 31.4, 15.7, 7.84, 3.92, 1.96 and 0.98 mg l^{-1} NO_3^- in de-ionized water obtained with the reflectance cell having an optical pathlength of 10 mm.
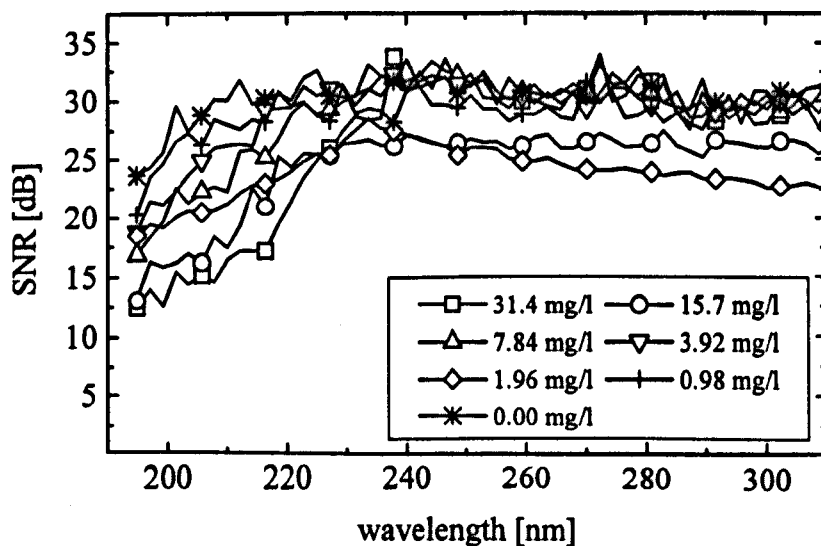
Fig. 4-6: Nitrate (NO_3^-) absorption measured with reflectance cell having an optical pathlength of 10 mm, containing 31.4, 15.7, 7.8, 3.9, 2.0 and 1.0 mg l^{-1} NO_3^- in de-ionized water.

The absorbance spectra of nitrate, with concentrations ranging from 0.98 mg l^{-1} to 31.4 mg l^{-1} are shown in Fig. 4-7. A shift of the absorbance maximum to higher wavelengths, caused by stray light effects (Chapter 1) can be observed at higher concentrations.
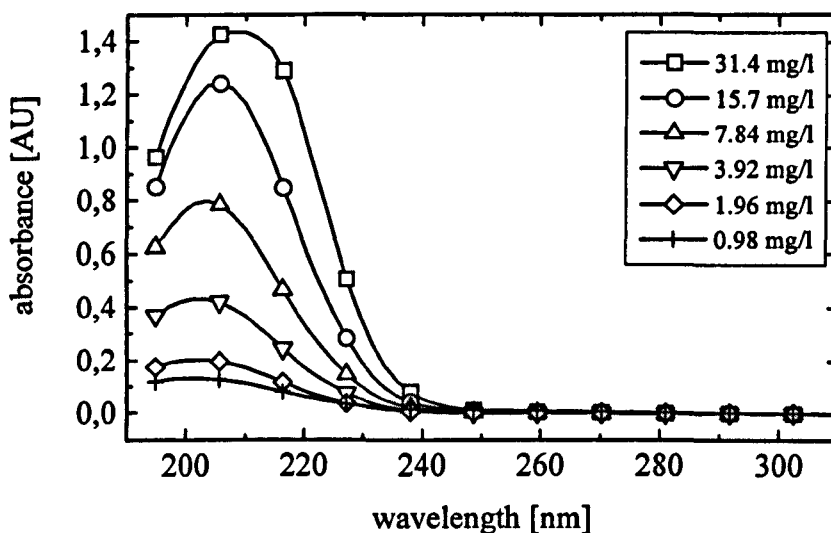
Fig. 4-7: Nitrate (NO3) absorption measured with reflectance cell having an optical pathlength of 10 mm, containing 31.4, 15.7, 7.8, 3.9, 2.0 and 1.0 mg l^{-1} NO3^{-} in deionized water.

The performance of the sensor system at a specific wavelength can be expressed mathematically in terms of a linear regression, where the slope of the regression line represents the sensitivity and the standard deviation its limit of detection. Such regression lines, relating absorbance and concentration of NO3^{-} have been calculated for 199 nm, 203 nm, 210 nm and 220 nm wavelengths. Up to a concentration of 3.9 mg l^{-1}, the measured absorbance values of all wavelength follow a straight line as indicated in Fig. 4-8.
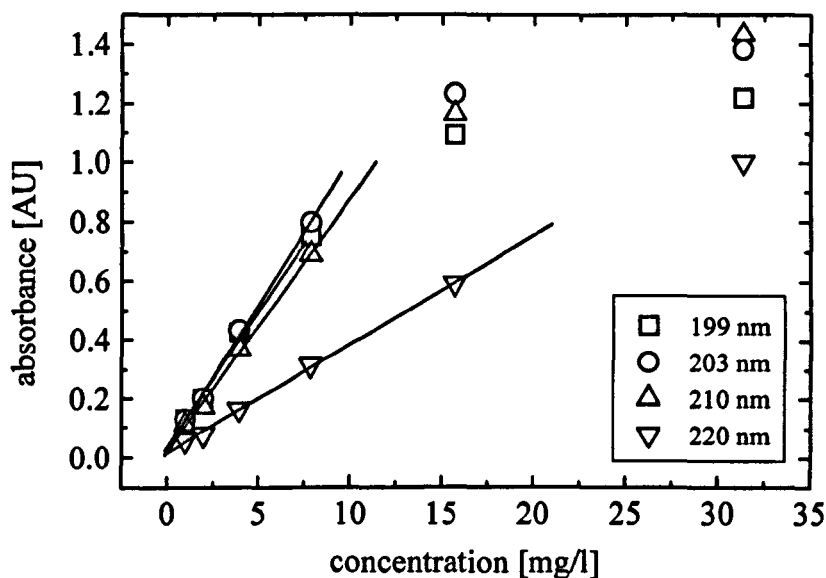
Fig. 4-8: Calibration curves for NO_3^- concentrations at 199 nm, 203nm, 210 nm and 220 nm wavelengths

wavelength [nm]	A [AU]	B [AU (mg/l) -1]	R	SD [AU]	$\Delta c = \dfrac{SD}{B}$ [mg l-1]	cLimit [mg l-1]
199	0.038	0.092	0.9978	0.023	0.25	0.50
203	0.027	0.099	0.9987	0.019	0.20	0.40
210	0.020	0.086	0.9990	0.014	0.16	0.32
220	0.017	0.037	0.9994	0.009	0.53	1.06

Tab. 4-1: Parameters of linear regression (A + B*concentration), correlation (R), and standard deviation (SD), of NO_3^- absorption at 200 nm, 203 nm, 210 nm and 220 nm as a function of concentration.

Then, the linear range of the 199 nm calibration curve is exceeded. Linear calibration curves for 203 nm and 210 nm wavelength were found until a value of 7.8 mg l-1. Only the calibration curve calculated at the 220 nm wavelength includes all concentration

measurements. Although from the signal to noise point of view, the range of the calibration curves should be within the envisaged concentration region, stray light is severely limiting the range of the sensor at lower wavelengths. In certain circumstances, a polynomial curve fit may be used to compensate the effects of stray light, enlarging the range of the measurement. Tab. 4-1 shows the intercept, A, the slope, B, as well as the correlation factor, R, and the standard deviation, SD, of the calibration fit for the defined wavelengths. The intercept of the calibration curves, A, differs by about the same magnitude as the standard deviation, indicating a stable transportation of UV light in the sensor system throughout the experiments. The highest sensitivity, represented by the slope, B, of the calibration curves was found at the absorption peak at the 203 nm wavelength to be 0.099 AU (mg/l) $^{-1}$. However, all four linear regressions present a good fit to the experimental data, as shown by their correlation factor, R. The concentration error, Δc, caused by the noise of the detection system, can be calculated from the standard deviation, SD, of the fit to be $\Delta c = SD\ B^{-1}$, clearly indicating that c_{Limit} is dependent on both SD and B. The result of this calculation can then be used to estimate the detection limit, c_{Limit}, which can be defined as twice the concentration error. Both concentration error and detection limit for the calibration fits performed are shown in Tab. 4-1. The lowest detection limit, c_{Limit}, of 0.32 mg l^{-1} could be achieved at the 210 nm wavelength, indicating that the lower slope, B, was compensated by the improved standard deviation of the fit.

4.7 Summary and discussion

A fibre-optic nitrate sensor, optimized for the deep ultraviolet part of the light spectrum, has been developed. Ultraviolet improved fibres (UVI fibres) have been used to enable a transfer of UV light to and from the sensor cell. The sensor system was found to be stable after a "warming up" period of 30 minutes. Four calibration curves, situated at 199 nm, 203 nm 210 nm and 220 nm wavelengths, featuring a detection limit of 0.50 mg l^{-1}, 0.40 mg l^{-1}, 0.32 mg l^{-1} and 1.06 mg l^{-1} NO$_3^-$ have been calculated. However, only small optical pathlengths can be realized with the sensor cell used because of the high optical losses found in this optical cell arrangement To expand the optical

pathlength and therefore the sensitivity of the sensor cell, waveguide principles can be employed; these are described in Chapter 5.

4.8 References

1 R. Briggs, K.T.V. Grattan, "The Measurement and Sensing of water quality: a review", Trans. Inst. MC, (1990), Vol. 12(2), 65-84.

2 S. Crossley, "Commercially available optical sensors - a global product review", Optical Sensors Collaborative Associations (ASCA), UK, Document 94/19F.

3 R. M. Dowdeswell, K. G. Carr-Brion, W. J. O. Boyle, "Pollution breakthrough monitoring using optical sensing techniques and artificial neural network decision system", Meas. Sci. Technol., (1996), Vol. 7, 1212-1219.

4 K. C. Thompson, M. Blankley, "Automatic Continuous-flow Determination of Nitrate in Raw and Potable Waters, Rivers and Sewage Effluents by Ultraviolet Absorption Spectrometry", Analyst, (1984), Vol. 109, 1053-1056.

5 R. C. Hoather, R. F. Rackham, "Oxidised Nitrogen in Waters and Sewage Effluents Observed by Ultra-violet Spectrophotometry", Analyst, (1959), Vol. 84, 548-551.

6 F. A. J. Amstrong, "Determination of Nitrate in Water by Ultraviolet Spectrophotometry", Analytical Chemistry, (1963), Vol. 35, No. 9, 1292-1294.

7 J. H. Wetters, K. L. Uglum, "Direct Spectrophotometric Simultaneous Determination of Nitrite and Nitrate in the Ultraviolet", Analytical Chemistry, (1970), Vol. 42, No. 3, 335-340.

8 K. Nagashima, M. Matsumoto, S. Suzuki, "Determination of Nitrate and Nitrite by Using Second-Derivative Spectrophotometry", Analytical Chemistry, (1985), Vol. 57, 2065-2067.

9 N. Suzuki, R. Kuroda, "Direct Simultaneous Determination of Nitrate and Nitrite by ultraviolet second-derivative spectrophotometry", Analyst, (1987), Vol. 112, 1077-1079.

10 F. I. Ormaza-Gonzalez, A. P. Villalba-Flor, "The Measurement of Nitrite, Nitrate and Phosphate with Test Kits and Standard Procedures: A Comparison", Wat. Res., (1994), Vol. 28, No. 10, 2223-2228.

11 M. Karlsson, B. Karlberg, R.J.O. Olsson, "Determination of nitrate in municipal waste water by UV spectroscopy", Analytica Chimica Acta, (1995), Vol. 312, 107-113.

12 M. Belz, W. J. O. Boyle, K. -F. Klein, K.T.V. Grattan, "Smart sensor approach for a fiber-optic based residual chlorine monitor", Paper presented at Europt(r)ode III, Zürich, (April 1996), Book of Abstracts, 194, published in Sensors and Actuators B, (1997), Vol. 39-123, 380-385.

13 H. Fabian, U. Grzesik, K. H. Wörner, K.-F. Klein: "Optical fibers for UV-applications", ECO, Den Haag, SPIE-Proc., (1991), Vol. 1531.

14 K.-F. Klein, P. Schließmann, E. Smolka, G. Hillrichs, M. Belz, W.J.O. Boyle, K.T.V. Grattan, "UV-stabilized silica based fiber for applications around 200 nm wavelength",. Paper presented at Europt(r)ode III, Zürich, (April 1996), Book of Abstracts 160, published in Sensors and Actuators B, (1997), Vol. 39-123, 305-309.

Design of a fibre optic nitrate sensor ...

15 H. Zaho, H. Pedersen, "A fiber optic chemical sensor for in-situ monitoring of nitrate and nitrite", Proceedings of the 4'th Food Processing Automation Conference (FPAC IV), Chicago, (1995), CH. 66, 190-196.

16 W.S. Yao; R. H. Byrne, R. D. Waterbury, "Determination of nanomolar concentrations of nitrite and nitrate in natural waters using long path length absorbance spectroscopy", Environmental Science & Technology, (1998), Vol. 32, No. 17, 2646-2649.

17 R. Mouaziz, R. Briggs, K.T.V. Grattan, "Multi-parameter Fibre Optic Chemical Sensor for the Measurement of Nitrate ion, Ammonia and Organic Matter", Proceedings of the Symposium on Chemical Sensors II, (ed.: M. Butler, A. Ricco, N. Yamazoe), The Electrochemical Society Inc., New Jersey, USA, (1993), Vol. 93-7, p. 303-316.

18 M.A. Stanley, J. Maxwell, M. Forrestal, A. P. Doherty, B.D. MacCraith, D. Diamond, J.G. Vos, "Comparison of the analytical capabilities of an amperometric and an optical sensor for the determination of nitrate in river and well water" Analytica Chimica Acta, (1994), Vol. 299, 81-90.

19 M.R. Querry, D.M. Wieliczka, D.J. Segelstein, "Water (H2O)", Handbook of optical constants of solids II, ed. by E. D. Palik, Academic Press, San Diego, (1991), 1059-1077.

20 P. D. T. Huibers, "Models for the wavelength dependence of the index of refraction of water", Applied Optics, (1997), Vol. 36, No. 16, 3785-3787.

21 Heraus Noblelight GmbH: Brochure on D2 lamps, Hanau, (1996).

5. Development of long pathlength cells for fibre-optic UV-sensor systems

5.1 Abstract

Two fibre-optic-based sensor systems with high sensitivity in the deep ultraviolet, based on differential absorption spectroscopy, are discussed in this Chapter. Both comprise the UV-optimized sensor arrangement, discussed in Chapter 5, but include novel flow-through sensor cells with extended optical pathlengths to increase the sensitivity of the system. Their optical properties and efficiency in the ultraviolet are discussed. The first sensor cell, based on an aluminium coated fused silica capillary cell and having an optical pathlength of 43 cm, is demonstrated in the construction of a residual chlorine sensor. The second sensor cell, a Teflon AF-coated liquid-core waveguide (LCW), is illustrated when applied to monitoring of nitrates, chlorine and acetylsalicylic acid. The sensor systems exhibit low spectral loss between wavelengths of 200 nm and 400 nm and can be used for a wide range of analytical investigations to determine small concentrations of such impurities in water, showing the potentially wider applicability of the systems.

5.2 Introduction

A range of optical sensor cells have been developed for pollutant sensing in the visible, the infrared and the ultraviolet regions of the light spectrum. A major disadvantage most of these sensor cells have in common is that they feature high light losses over relatively short optical pathlengths, thus limiting the sensitivity of the sensor system. However, there are two ways to increase the sensitivity. Firstly, the noise present in the spectrophotometer system used could be decreased. Although most spectrophotometers have a noise level of some mAU, those for spectrophotometers used in liquid chromatography have been reduced to 100 µAU or less. This has been realized by im-

proving the quality of the components used, such as the optics, and optimizing the system, i.e. improving the mechanical structure, the thermal stability, the electronics, the light sources and the detector elements. However, it is difficult to achieve such low noise levels in field instrumentation, because mechanical vibrations, temperature variations or ambient light easily introduce noise levels greater than several mAU. A practical range for absorbance measurements was found to be 0.05 to 1 AU, corresponding to a 10% to 90% light attenuation by the sample. A second approach to increase the sensitivity of an absorbance-based optical sensor system is to increase the optical pathlength of its sensor cell. As defined by the Bouger-Lambert-Beer Law, the absorbance of light introduced by a sample is proportional to the chromophore concentration and the optical pathlength. Thus, increasing the optical pathlength of a sensor cell will increase the absorbance signal observed and therefore, potentially, its sensitivity. Compared to a conventional cell with an optical pathlength of 1 cm, a sensor cell with an optical pathlength of 20 cm would increase the measured absorbance 20 fold, thus, for example, a 0.001 AU signal obtained with a 1 cm cell would be measured to be 0.02 AU with such a measurement arrangement. However, with conventional technology, it is difficult to transmit a collimated probing light beam over such a distance without substantial light loss or the use of advanced and expensive collimating optics. To overcome this problem, waveguide principles can be employed, when developing sample cells with increased optical pathlength. Such a light guiding sensor cell can be formed when the analyte solution functions as a core of a waveguide, surrounded by a tubular material, the cladding, possessing a lower refractive index. In such an arrangement, light is guided and confined in the liquid core by total internal reflection at the core/cladding interface and optical fibres can be employed to transport light to and from the sample cell. Additionally, such sensor arrangements are particularly suitable to be combined with optical fibres for light transfer, forming a flexible sensor system.

A number of sensor cells with long optical pathlengths have been developed, and their experimental performance either in the area of communications or sensor technology has been published, as reviewed in the subsequent section. The principle of the guiding

effect may be used to divide them into a four different groups, being bare glass or fused silica tubes, glass or fused silica tubes with a reflective coating, tubes coated internally or externally with low refractive index polymers or finally plastic tubes with low refractive indices. The development of such sample cells is described briefly in the following sections.

5.2.1 Bare glass or fused silica tubes without reflective coatings

Early research on guiding light in fused silica tubes or so-called hollow waveguides has been published by Stone [1] in 1972 and others who investigated the potential usefulness of hollow quartz fibres filled with tetrachloroethylene or a mixture of tetrachloroethylene and carbon tetrachloride, both having a refractive index higher than that of fused silica, for long distance optical communications. Although never used in telecommunications, it was demonstrated that light could be transported in the liquid core of such a waveguide with transmission losses of around 20 dB km^{-1} in the near infrared part of the light spectrum. Fuwa *et al.* filled such a long capillary cell with carbon disulfide having a higher refractive index than the cell wall and formed the first waveguide of a length of 50 m to enhance the sensitivity in ordinary colorimetry [2] in 1984. A fibre-optic-coupled sample tube, consisting of glass a capillary tube with a length of 1 m and an inner diameter of 1.27 mm and an outer diameter of 1.77 mm was developed by Schwab *et al.* in 1987 [3]. This sample cell was developed to enhance the sensitivity in Raman spectroscopy and acted as a waveguide because it used the air/glass interface of the cell wall to confine the light in the waveguide. Early fluorescence detection involving the use of liquid core fibres, consisting of hollow fibres filled with carbon disulfide have been reported by Fujiwara *et al.* [4] in 1988. Tsunoda *et al.* described the use of liquid core waveguides in absorption techniques in 1989 [5]. Constructed from borosilicate-glass tubing, these waveguides relied on the effect of total internal reflection at the glass/air interface and were the first water-filled waveguides offering losses between 8 and 18 dB m^{-1} at 632.8 nm wavelength. In 1992, Wei *et al.* [6] modelled and described liquid core optical fibres (LCOF), using carbon disulfide having a higher refractive in-

dex than that of the LCOF wall, and thus creating an optical waveguide. The model was used to explain the deviations from the Beer-Lambert Law and the sensitivity enhancement of the cell at small concentrations in long absorption cells. Another theoretical and experimental study of the factors which affect the enhancement of sensitivity and detectability for flurometric sensing was published by Zhu *et al.* [7] in 1994. Benoit and Yappert published in 1996 a characterization of a simple Raman capillary/fibre optical sensor with reduced size and without focusing lenses or mirrors and filters with a 70-fold sensitivity and a 50-fold detectability enhancement [8].

5.2.2 Glass or fused silica tubes with reflective coatings

Early applications of liquid core fibres in analytical chemistry were reported on enhancing weak signals in Raman spectroscopy by confining the excitation radiation and collecting the Raman scattered light over longer interaction lengths [9, 10]. The usage of long capillary cells (LCC) to enhance the sensitivity in absorption spectroscopy was introduced by Lei *et al.* [11]. They studied the light guidance in LCCs and the effect of transmissibility when the outside of the LCC used was coated with reflective and non-reflective material (black coarse tape, aluminium foil). Using Pyrex glass as the material of the capillary, they found that the cell did not act as a waveguide because the refractive index of water in the core was smaller that the refractive index of the glass. However, Lei *et al.* [11] showed that the guidance of the light inside the capillary could be improved some 25-fold, when the outside was coated with a reflective material, such as aluminium or silver, when compared to black coarse tape, which it was assumed would completely absorb the light. Further work has included that of Dasgupta [12] who developed a multi-path arrangement by coating the inside of a helical cell with silver to extend the range of optical absorbance measurements. He proposed that this arrangement would vary its effective optical pathlength as a function of absorbance, resulting in a sensitivity enhancement at low analyte concentrations. An interesting approach was reported by Alaluf *et al.* who coated the inside of plastic hollow tubes with a metal layer

(Ag) and grew a thin dielectric overlayer of AgI by direct iodination, which could be employed as a filter in the mid-infrared region of the light spectrum [13].

5.2.3 Tubes coated internally or externally with low-refractive index polymers

Liquid core fibres or waveguides, based on low refractive coatings, such as Teflon AF, a clear amorphous fluoropolymer having a refractive index of 1.29-1.31, in the inside or outside of a glass or plastic tubing to form a waveguide with water as a core have been reported by Gilby and Carson [14] 1992, Dress and Franke [15, 16] in 1996 and 1997, and Hong and Burgress [17] in 1996. Dress and Franke reported light losses as low as 1.6 dB m^{-1} in a liquid core waveguide realized by coating the inner surface of cylindrical absorption cell with Teflon AF, it having a lower refractive than water and thus proved its applicability for water and aqueous solution analysis in the visible part of the light spectrum. Another possibility found was to coat the outside of a fused silica capillary with Teflon AF, not strictly forming a waveguide but with low light losses. This approach was reported by Liu [18, 19] in 1995, Munk [20] in 1997, and Altkorn *et al.* [21] in 1997. Altkorn reported light losses of approximately 1 dB m^{-1} in the visible region of the light spectrum using water filled fused silica tubing coated with a thin layer of Teflon AF 2400 having an inner diameter of 530 µm and an outer diameter of 630 µm.

5.2.4 Plastic tubes

The use of FEP-tubing as a sensor cell forming an optical waveguide was published in 1990 by Tsunoda *et al.* [22]. However, although the refractive index of FEP, poly(tetrafluoroethylene-co-hexafluoropropylene) is 1.35, its waveguide properties cannot be used directly for water analysis, with water having a refractive index of 1.33. Lui reported in 1995 on the usage of Teflon AF as a cell wall material, having a refractive index lower than that of water, forming a waveguide [18]. Light losses below 3 dB m^{-1} in the visible part of the light spectrum were reported by Altkorn *et al.* [23] in 1997 for Teflon AF 2400 capillaries filled with water. At nearly the same time, Waterbury *et al.*

described a sensor system for dissolved iron concentrations, based on *Teflon AF LCW* with a 4.47 m pathlength [24] and a colorimetric nitrate and nitrite sensor [25]. Song *et al.* described in 1998 an application and a detailed procedure to use such a waveguide in Raman spectroscopy to enhance the traditionally weak Raman signals up to 20-fold in aqueous solutions and up to 120-fold in organic solvents [26]. A gas sensor based on the permeability of Teflon AF material was published recently (1998) by Dasgupta *et al.*, using a Teflon AF-tube as a waveguide, filled with a colour indicator, working with response times lower than one second [27].

5.2.5 Summary of previous work and objective of this Chapter

A brief review about the development of sensor cells with long optical pathlengths was given in the introduction. Although there has been considerable research activity in this field, it has not been extended to the ultraviolet part of the light spectrum. Similar work in the ultraviolet, as for example described in Chapter 4, has not been performed due to the unavailability of solarization-resistant optical fibres (UVI-fibres). The emphasis of this Chapter is the investigation of the applicability of two fibre-optic-based sensor systems for deep UV applications ($\lambda \leq 250$ nm), with one being based on an aluminium coated-capillary cell and one being based on a liquid core waveguide with an inner coating of Teflon AF. The advantages of combining UV-improved fibre-optic technology with these sensor cells will be discussed and their applicability for ultraviolet spectroscopy based water analysis investigated.

5.3 Ultraviolet detection system based on an aluminium coated capillary cell

Fused silica capillaries with an aluminium coating, having an inner diameter, ID, of 0.6 mm and an outer diameter, OD, of 1 mm were prepared for the following experiments. The prime advantage of these capillaries as sample cells is their simple and robust design, the high reflectivity of aluminium in the ultraviolet and the resistance of

the fused silica to chemical interaction with many solvents. The light guidance in such a cell arrangement relies on partial internal reflectance at the solvent / fused silica interface and the fused silica / aluminium interface to allow UV-VIS light to propagate along the cell axis. The total intensity of the light transmitted through a long glass capillary cell containing, for example, water as a solvent with its lower refractive index than fused silica, is comprised of light rays taking many path through the capillary centre or through the walls [11]. To improve the light coupling at the input and to separate wall-propagated light from centre propagated light at the output of the cell, fibres with a core diameter of 400 μm were inserted in the capillary cell to increase the coupling efficiency.

5.3.1 Experimental set-up

The individual components of a fibre-optic-based sensor system, as discussed in Chapters 2 and 3, were optimized for use in the ultraviolet. The optical arrangement comprised a deuterium lamp, DL, a fibre coupling system, LS, arranged to compensate for the higher loss of UV in the fibre and absorption cell, an input and output fibre, FI, FO, both of length 2 m with a core diameter of 410 μm and a capillary-based absorption cell, CE, of length 100 mm. The output fibre, FO, was coupled to the optical fibre input of the spectrometer, FOS, with a standard SMA connector.
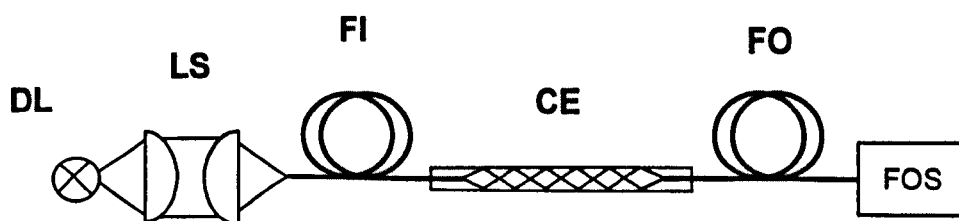
Fig. 5-1: Complete optical set-up of an optical fibre based sensor, comprising a deuterium lamp (DL), a lens system (LS), input and output fibres (FI, FO), a capillary based absorption cell (CE) and a fibre-optic spectrometer (FOS).

An integration time of 40 ms was found to be sufficient to obtain a full-range reference spectrum. Thus, although averaging each sample 50 times, a time of only two seconds was necessary to complete a measurement cycle. Fig. 5-1 shows the complete optical

arrangement of the sensor system; its performance will be described in the following sub-sections.

5.3.2 Intensity profile of the capillary in the visible

The light distribution in the absorption cell, CE, was observed with a CCD camera. Light from a helium neon (HeNe) laser was coupled into the centre of the capillary cell with an optical fibre having a core diameter of ≈ 410 µm and a numerical aperture, NA, of ≈ 0.22. Fig. 5-2 shows the nearfield intensity-distribution measured with a beam-profiler at the output of the capillary cell, either filled with air or water.
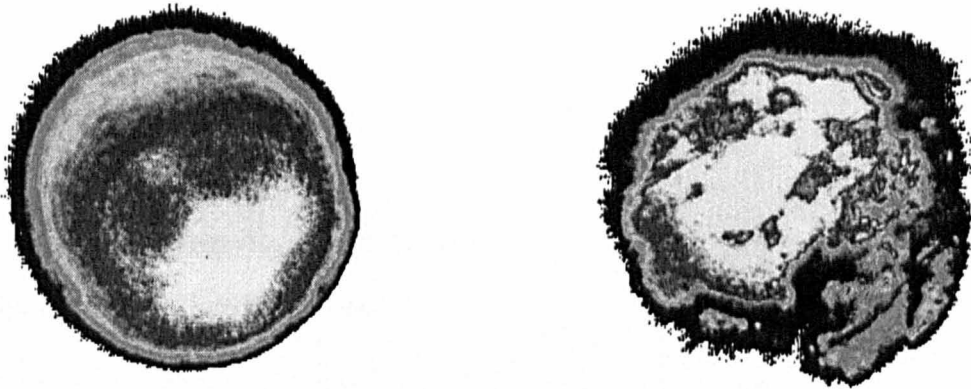
Fig. 5-2: Intensity-profiles at the endface of a capillary, filled with air (left) and water (right)

It was observed that light transportation only takes place in the air/water region. In contrast to descriptions given by Lei et al. [10], there was no light observed in the capillary wall.

5.3.3 Performance of aluminium coated sensor cells in the ultraviolet

A major interest in such a cell design was its internal losses in the UV-C region of the light spectrum, including the question of how much these cells would improve the guidance of light compared to the use of a free space arrangement. The spectral attenuation of the capillary cell, filled with de-ionized water, was measured between 195 nm and 400 nm wavelength by sliding the output fibre, FO, in steps of 1 cm through

CE. The light loss inside the absorption cell, CE, as a function of wavelength is shown in Fig. 5-3 for three different optical pathlengths of 2 , 5 and 10 cm.
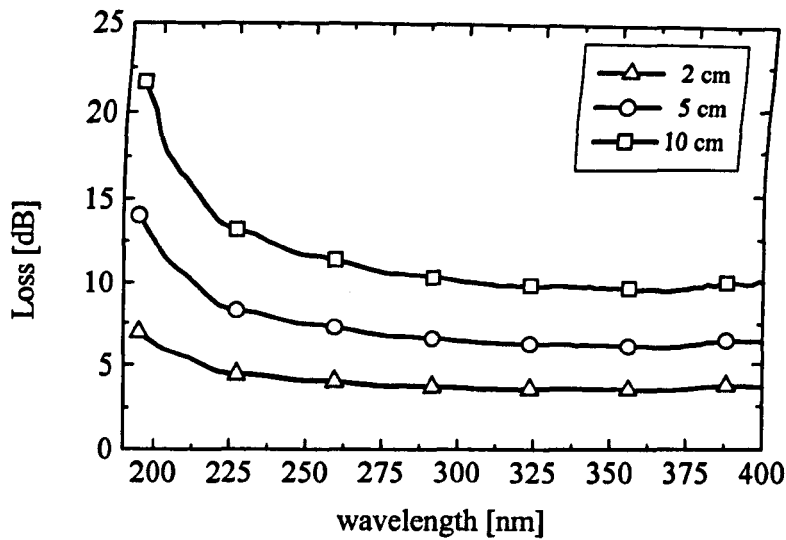
Fig. 5-3: Loss in capillary based absorption cells with 2 cm, 5 cm, and 10 cm length respectively, filled with de-ionized water.

It can be observed that light losses increase at wavelengths below 300 nm, this being caused by the increased losses at the water/cell interface and the absorption of water in that wavelength region (Section 4.3). For comparison, the geometric free-space loss, L, was estimated as an axial coupling loss between the input fibre, FI, and the output fibre, FO, of the same diameter, taking the wavelength-dependent absorption loss of UV light in water [28] into account. The result of this comparison is shown in Fig. 5-4, indicating clearly the advantage of this approach. After an initial coupling loss of approximately 1.5 dB, the capillary based absorption cells were shown to have a 1.7 dB cm⁻¹ light loss at 200 nm and a 0.8 dB cm⁻¹ light loss at 300 nm wavelength. This results in an optical pathlength of 10 cm yielding a light loss of approximately 10 dB at 300 nm, and 20 dB at 200 nm in the capillary cell, but giving a light loss of approximately 44 dB at 300 nm and 54 dB at 200 nm wavelength in a free space arrangement, as for example used with the reflectance cell in Chapter 4.
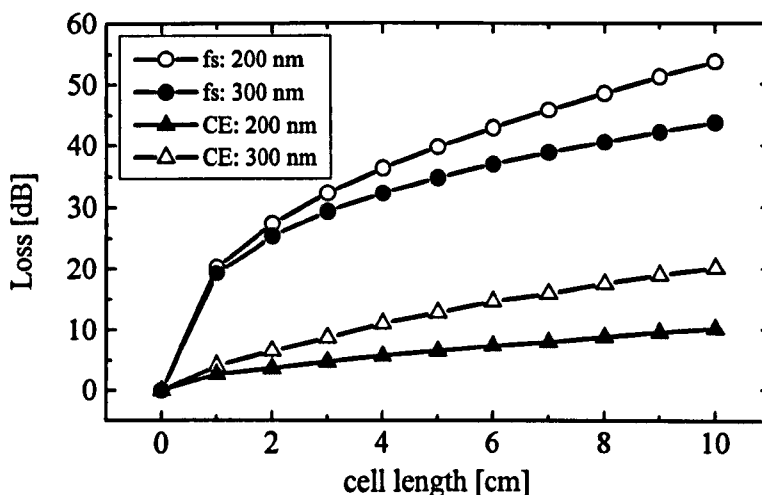
Fig. 5-4: Absorption loss inside a water-filled capillary (CE) and in a free space arrangement (fs) at 200 nm and 300 nm respectively as a function of cell-length.

At wavelengths between 300 nm and 730 nm, a constant loss 0.8 dB cm^{-1} light intensity could be observed. However, although the losses in the cells are high, an effective transmission of light between 195 nm and 400 nm wavelength is possible with these capillaries. Thus the fibre-optic-based sensor arrangement described may be applied in the following section to measure the concentration of residual chlorine in aqueous solution, to demonstrate its potential.

5.3.4 Chlorine sensing with the combined optical system

A number of sensor schemes for measuring residual chlorine have been designed and reported. For example, early work had tended to concentrate on developing chlorine-sensitive electrochemically-based electrode probes [29]. More recently, optical methods have also been investigated. An illustration of this is the use of chemiluminescence to determine very small chlorine concentrations, at the parts per billion (ppb) level, in a range of water samples [30]. In addition, colorimetric techniques have proved to be accurate and reliable for the determination of various species in water [31] and these have been applied to the measurement of chlorine concentrations in both natural and proc-

essed waters. Aoki and Munemori [32] have developed and reported an effective technique for the measurement of chlorine in the form of the hypochlorite ion (OCl⁻), which absorbs in the ultraviolet (UV) spectral region. Cl_2 monitoring based on the monochromatic measurement of the hypochlorite ion (OCl⁻) in the UV at 290 nm has been reported by Mouaziz et al [33, 34]. The species of particular interest, in this case the hypochlorite ion (OCl⁻), was removed by reduction to the Cl⁻ form by the addition of sodium sulphite. The optical part of this monochromatic residual chlorine monitor (RCM) consisted essentially of a phosphor-coated mercury discharge lamp with a main emission peak at 290 nm, an optical fibre coupled flow-through cell, a UV enhanced silicon diode detector with an interference filter centred around 290 nm and an appropriate reagent handling system. The main advantages of this monitor included a high dynamic range combined with high sensitivity, realized with a phase locked loop detection system and a simple but robust optical system. However, only a single wavelength could be observed and no information about the remaining part of the optical spectrum could readily be made available in this configuration. Reagents had to be used for both sample conditioning and cleaning to prevent fouling of the optics by calcification. Additionally, the performance of the RCM was shown to vary with a wide range of different water samples, as a result of which the system had to be calibrated for operation with a particular type of water before use.

The fibre-optic based polychromatic sensor system described above was applied to measure the concentration of residual chlorine in aqueous solution. A primary aim was to have available both more and specific data, resulting in a reduction in the interference effects from other species, with a greater independence of the type of source water. `Experimental results of the sensor system in measuring residual chlorine

Dependent on the temperature, and more important on the pH of the sample solution, dissolved chlorine (Cl_2), hypochlorous acid (HOCl) and the hypochlorite ion (OCl⁻) are produced when chlorine is added to water. Akoi *et al.* showed that at pH values lower than 3 most of the chlorine present is in the form of dissolved gas (Cl_2), at pH values

around 5 chlorine mainly exists in the form of HOCl and is converted to the OCl⁻ form if the pH is increased to 9 or higher [32, 34]. The presence of the various forms of chlorine in water as a function of pH is shown in Fig. 5-5.
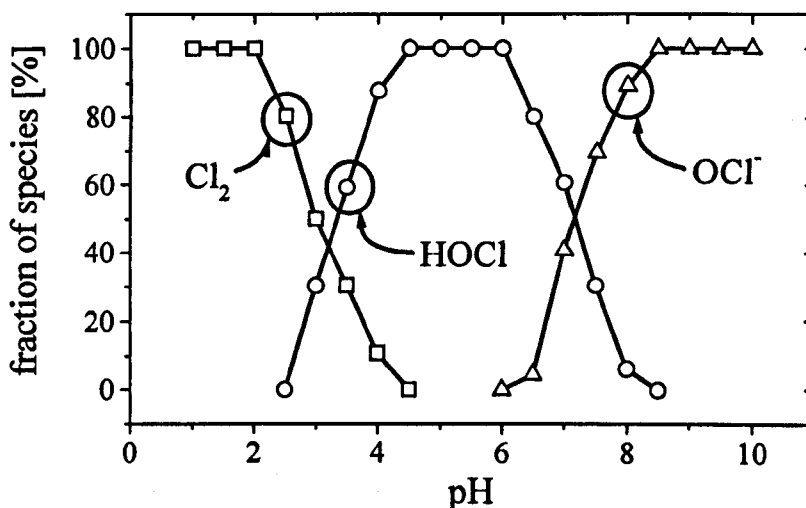
Fig. 5-5: Presence of Cl₂, HOCl and OCl⁻ as a function of pH in aqueous solution

Sodium hydroxide (NaOH) and hydrochloric acid (HCl) were used in experiments in this work to vary the pH of the sample solution between 2 and 10, enabling a study of the pH-dependence of the sensor system. Fig. 5-6 shows the absorption spectra of 5.7 mg l⁻¹ of free chlorine at a pH of 2 as Cl₂ with an absorption peak centred around 229 nm, at a pH of 5 as HOCl with an absorption peak centred around 233 nm and at a pH of 10 in the form of the OCl⁻ ion with an absorption peak centred around 290 nm wavelength in de-ionized water. The relative absorption of chlorine at 229 nm, 233 nm and 290 nm wavelength as a function of pH is shown in Fig. 5-7, indicating that the strongest absorption peak, that of the OCl⁻ ion, is situated around 290 nm. Calibration curves for free chlorine determination as dissolved chlorine (Cl₂), hypochlorous acid (HOCl) and in the form of the hypochlorite ion (OCl⁻) at a pH of 2, 5, 10 respectively were prepared and referenced with a commercial reagent kit relying on the colorimetric DPD (diethyl-p-phenyldiamine) method [35], as shown in Fig. 5-8 and Tab. 5-1.

200 225 250 275 300 325 350 375 400

wavelength [nm]
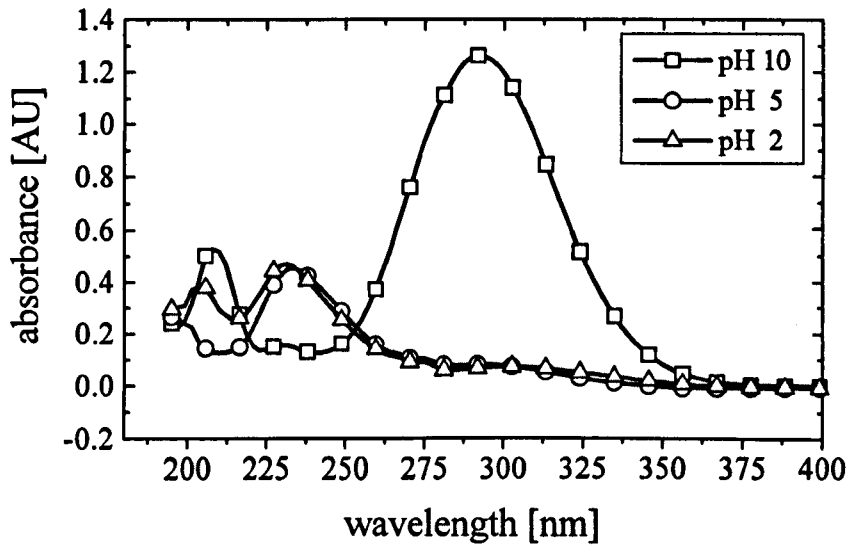
Fig. 5-6: Absorbance spectra of 5.76 mg l⁻¹ free chlorine as dissolved chlorine (Cl₂) at pH 2, as hypochlorous acid (HOCl), at pH 5, and in the form of the hypochlorite ion (OCl⁻), at pH 10.
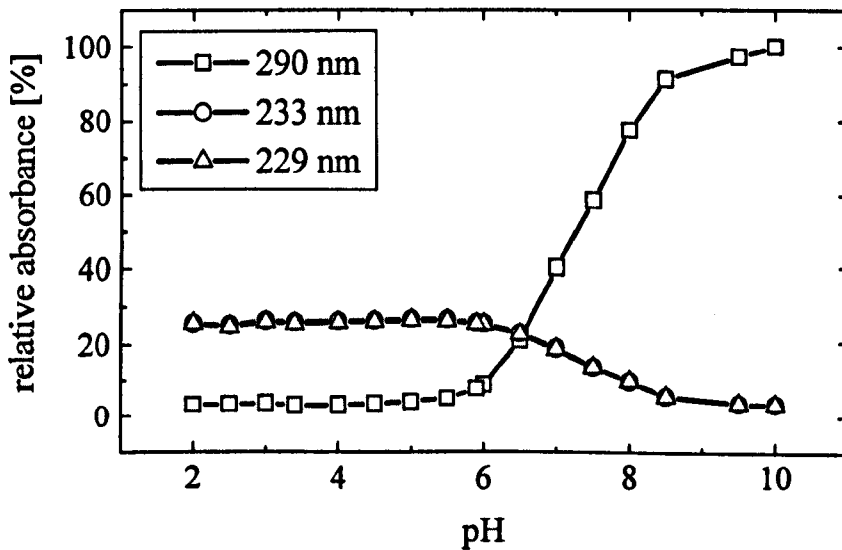
Fig. 5-7: Relative absorbance of the free chlorine species Cl₂ at 229 nm, HOCl at 233 nm and OCl⁻ at 290 nm as a function of pH.
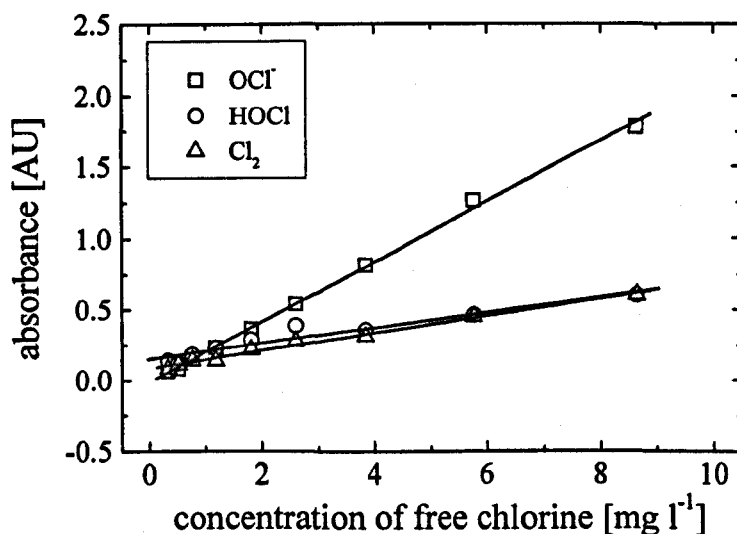
Fig. 5-8: Calibration curves for free chlorine determination as Cl_2 [pH 2, 229 nm], as HOCl [pH 5, 233 nm] and in the form of the OCl⁻ ion [pH 10, 290 nm].

Defining the detection limit for the analyte as twice its standard error, as a result a detection limit of free chlorine in de-ionized water of 0.2 mg l⁻¹, when determined in the form of the OCl⁻ ion, of 0.6 mg l⁻¹ when determined as HOCl and of 1.6 mg l⁻¹ when determined as Cl_2 could be achieved. For UV absorption measurements, the hypochlorite ion was found to be most suitable for measurement because the OCl⁻ ion has the strongest molar absorption coefficient and has its absorption peak centred around 290 nm compared to the overlapping peaks of dissolved Cl_2 at 229 nm and HOCl at 233 nm. Additionally the absorption measurement at 290 nm is far less affected by the presence of nitrite and nitrate ions with their large absorption peaks centred around 203 and 210 nm commonly present in natural water. There is a significant improvement in the sensitivity of this system compared to a laboratory-based instrument, such as a HP 8452 UV/VIS spectrometer with a standard 1 cm path length absorption cell, due to the better defined optical system.

Sample	DPD [mg l⁻¹]	Absorption [AU]	Found OCl⁻ [mg/l]	Error of found OCl⁻ [mg l⁻¹]
1	(o)	1,77	7,92	0,089
2	(o)	1,24	5,56	0,057
3	3.70 (o)	0,830	3,77	0,051
4	2.50 (o)	0,545	2,50	0,048
5	1.71	0,335	1,57	0,046
6	1.14	0,232	1,11	0,045
7	0.75	0,147	0,736	0,045
8	0.47	0,096	0,507	0,045
9	0.314	0,060	0,349	0,045
10	0,200	0,036	0,240	0,045

Tab. 5-1: Determination of chlorine concentration. Samples marked with (o) were measured outside the specified range of the DPD test.

5.3.5 Results and discussion

In this work the feasibility and benefits of constructing a fibre-optic based UV-VIS absorption spectrometer system, demonstrated in the measurement of free chlorine in the form of the hypochlorite ion at a pH of 10 in de-ionized water with a detection limit of 0.2 mg l⁻¹ an absorption cell of 430 mm length, has been shown, but in which its full potential has not been completely utilized. As the pH of the sample is varied, free chlorine can also be determined as hypochlorous acid with a detection limit of 0.6 mg l⁻¹ and as dissolved chlorine with a detection limit of 1.6 mg l⁻¹. The system is based on a simple and robust optical arrangement. In particular the monolithic design of the optical fibre based spectrometer simplifies the development of on-line instrumentation.

However, the limiting factor in the miniaturization of the optical components was found in the relatively high optical losses in the sensor cell. Additionally, the construction of a liquid handling system for the capillary-based absorption cell was found to be difficult because of its small inner diameter and the pressure needed to pump the sample through the absorption cell. The aim, at this stage, was to demonstrate the optimization of the optical system and to develop a sample cell with an increased optical pathlength of 43 cm to enable sampling of chemical species with low molar absorption

coefficients. However, when UVI fibres were included, polychromatic measurement were possible and provide the opportunity to use the spectral information available from measurements at other wavelengths to compensate e.g. for turbidity (500 -700 nm), nitrate (210 - 230 nm), organic matter (240 - 270 nm) and other UV absorbing species by applying multicomponent and neural network data analysis techniques, as for example described in the work of Benjathapanun *et al.* [36]. Such a system has the potential for a more generic application, e.g. in the monitoring of several UV-absorbing species simultaneously.

Finally, the relatively high loss of 1.7 dB cm^{-1} and 0.8 dB cm^{-1} at 200 nm and 300 nm respectively are limiting the maximum pathlength of the capillary cell to approximately 50 cm, due to the sensitivity of the spectrometer module. In the following section, a so-called liquid core waveguide is introduced, featuring (after input and output coupling losses) a stable transportation of light, nearly independent of the optical pathlength of the sensor cell, with the main source of loss being the attenuation of water, used as the waveguide core.

5.4 Ultraviolet sensor system based on a liquid core waveguide (LCW)

A compact optical sensor system with a high transparency in the deep ultraviolet (UV) region (λ>190 nm), designed for water quality analysis, is discussed in the following sections. This system is configured using, as described above, a deuterium lamp, UVI fibres, a spectrometer module and a Teflon AF coated liquid core waveguide (LCW) capillary cell. To raise the sensitivity of the sensor system, the absorption pathlength has been increased significantly using the lightguiding properties of the LCW consisting of a cylindrical glass tube with a Teflon AF 2400 inner coating of about 50 μm thickness. Due to the lower refractive index of Teflon AF in comparison to water, the LCW works as a waveguide. The arrangement and especially the sample cell exhibit low spectral loss in the range between wavelength of 200 nm to 400 nm and can be used to detect small impurity concentrations in water. The optical losses of the sensor system

are discussed and its performance in the ultraviolet was evaluated by measuring several pollutant concentrations in water.

5.4.1 Light guiding in the liquid-core waveguide (LCW)

A liquid-core waveguide (LCW) was used as the main optical component of the sensor system. The cross section of the LCW is illustrated in Fig. 5-9. It consists of a cylindrical glass tube (inner diameter = 3 mm) with a TEFLON AF 2400 [37, 38, 39] inner coating of about 50 μm thickness. The Teflon AF family (chemical name: fluorinated (ethylenic-cyclo oxyaliphatic substituted ethylenic) coploymer) is marketed as two main products, Teflon AF 2400 and Teflon AF 1600. Teflon AF is an amorphous material with the lowest commercially available index of refraction, as low as 1.29 and 1.32 for λ= 632.8 nm of Teflon AF 2400 and AF 1600 respectively. It features a light transmission from the deep ultraviolet to the near or middle infrared part of the spectrum. As the refractive index of water is higher (1.33 at 632.8 nm) than that of Teflon AF, a true waveguide can be constructed, having water as the core and Teflon AF as the cladding material. The practical realization of this waveguide consists of cylindrical glass tube with an inner diameter of 3 mm and an outer diameter of 6 mm. The inner surface is coated with a thin layer of Teflon AF 2400 of a thickness of 50 μm. Light is coupled into and out of the LCW with the type of UVI fibres characterized and discussed earlier. In the experiments carried out with the LCW, UVI fibres with a core diameter of 600 μm and a cladding diameter of 660 μm are used. The fibre length of each fibre was 4 m, a significant length for use in remote sensing applications and resulting from the high degree of transparency of the fibre at wavelengths below 230 nm. These fibres are centred in the LCW and placed parallel to the glass tube axis. To achieve a laminar flow in the core, the liquid of interest enters outside the optical path between both ends of the coupling fibres. The distance between both fibres in the LCW, representing the optical pathlength, is Z_{LCW}= 203 mm.
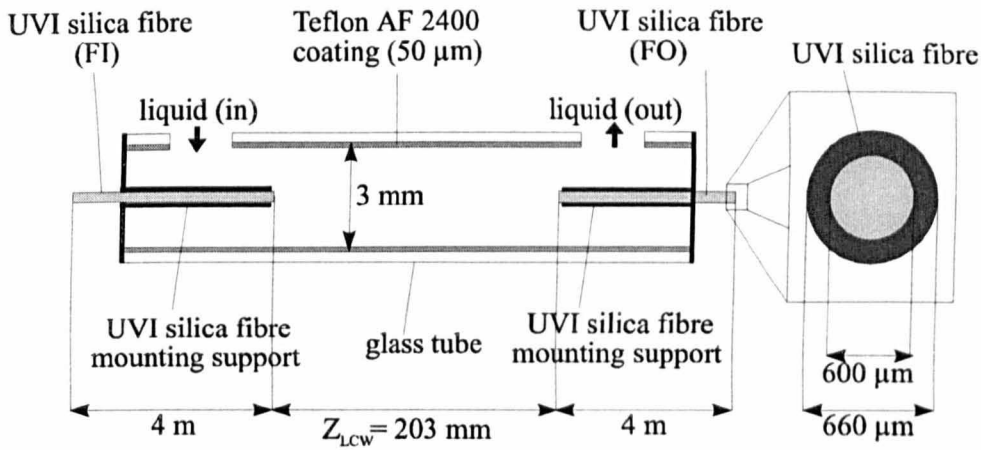
Fig. 5-9: Cross section of the cylindrical liquid-core waveguide (LCW). The sketch illustrates all characteristic geometrical dimensions of the LCW system and especially the UV-silica fibre dimensions that are used in the experiments.

The light guiding properties and sensitivity improvement when using this special kind of LCW for pollution detection in aqueous liquids in the visible spectral range had been demonstrated earlier by Dress and Franke [15, 16]. In this section, the characteristics of the system in the UV- spectral range from 200 nm to 350 nm are investigated. As a first characterization of the sensor system, theoretical calculations describing the light guiding properties of the LCW system have been performed. The Teflon AF coated tube may be regarded as being filled with pure water as the core of the LCW. Fig. 5-10 illustrates the losses of the LCW system for different lengths, Z_{LCW}, this being the direct distance between both fibre front faces in the Teflon AF coated glass tube. The theoretical LCW considerations were based on the ray picture model which was discussed in previous work [15, 16] and validated for the visible spectral range [16]. Light losses in the LCW are calculated for three different wavelengths: one in the visible at $\lambda = 632.8$ nm and at two wavelengths in the UV region at $\lambda = 200$ nm and $\lambda = 300$ nm, where the analytical experiments are performed. Due to the presence of material dispersion, the values for the complex refractive index, $n+jk$, of all the relevant media are a function of wavelength, λ, and are considered within the calculations.
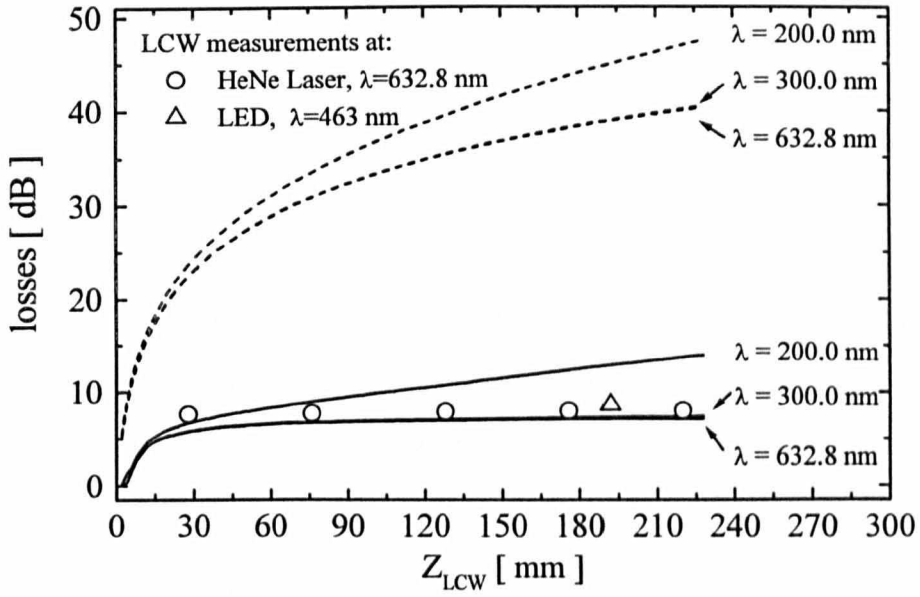
Fig. 5-10: Loss values of the LCW system for several distances Z_{LCW}; the theoretical calculations based on a ray picture model (LCW-losses, solid lines) and a geometry model (free space losses, dotted lines)

TEFLON AF 2400	632.8	1.290	$3.22 \cdot 10^{-6}$
	300.0	1.307	$8.31 \cdot 10^{-6}$
	200.0	1.329	$1.22 \cdot 10^{-4}$
UV-silica fiber core	632.8	1.457	$1.27 \cdot 10^{-10}$
	300.0	1.488	$2.93 \cdot 10^{-10}$
	200.0	1.551	$4.03 \cdot 10^{-9}$
UV-silica fiber cladding	632.8	1.440	$< 1.00 \cdot 10^{-9}$
	300.0	1.470	$< 3.00 \cdot 10^{-9}$
	200.0	1.530	$< 5.00 \cdot 10^{-8}$

Tab. 5-2: Values for the complex refractive indices of all relevant media, which are used within the theoretical loss calculations for different distances, Z_{LCW}, and geometries.

The values used in the simulations, listed in Tab. 5-2, are taken from the work of Fleming *et al.* [40] and Querry *et al.* [41]. Additionally, absorption measurements of thin Teflon AF 2400 films at $\lambda = 200$ nm and $\lambda = 300$ nm were performed. The real parts of the complex refractive index of TEFLON AF® 2400 at $\lambda = 200$ nm and $\lambda = 300$ nm respectively may be calculated using the Sellmeier dispersion equation, using known data in the optical range [42]. All loss values are compared to those of the free space geometry situation, which is defined by two UVI fibres which are positioned opposite each other at a distance Z_{LCW} in water. The free space calculations are based on a model described in the work of Belz *et al.* [43]. Using such a comparison, the improvement in using the LCW geometry over conventional absorption cells becomes evident.

The results calculated for 632.8 nm and 300 nm are almost identical (Fig. 5-10, solid line). However, compared to the free space arrangement (when filled with pure water) a gain of about 33 dB for a distance between the input and output fibre of $Z_{LCW}= 203$ mm could be achieved. This gain is seen to increase with distance because the slope of the free space curve is higher than that associated with the LCW, with the latter approaching the guiding losses for large distances. In a previous publication, a guiding loss of 0.02 dB cm⁻¹ has been determined experimentally for a wavelength of 632.8 nm [16]. A detailed analysis of this, the lower graph (632.8 nm, solid line) in Fig. 5-10 yields a loss of 0.03 dB cm⁻¹ for high Z_{LCW} and thus an additional length of 1 m would only increase the losses by 3 dB. The theoretical loss curves of Fig. 5-10 clearly indicate that the major source of losses in the case of the LCW are coupling losses, obvious from the shape of the LCW loss curves. For an absorption length of about 60 mm, the losses have already reached a value of about 6 dB, mainly representing the in- and out-coupling processes, whereas for distances larger than 60 mm, the loss curve mainly represents the result of the guiding process. In case of the free space geometry ($\lambda = 632.8$ nm, dashed curve, Fig. 5-10) the coupling losses are extended over the full range of lengths considered, Z_{LCW}. The reduced light guiding losses of the LCW geometry, compared to those of the free space geometry with increasing distance, represent an important advantage for the measurement of low concentrations in absorption

spectroscopy. A large optical pathlength, showing reasonable losses, is a crucial requirement for this technique. At 632.8 nm, the critical angle for total internal reflection between water and Teflon is 75.4°. At a wavelength which is much shorter, such as at $\lambda = 300$ nm, this angle is shifted to 72.4° and therefore the numerical aperture of the LCW slightly increases. However, these improved guiding characteristics do not significantly affect the amount of light coupling, because the fibre and the LCW apertures had already been optimized for a wavelength of 632.8 nm. A slight decrease of losses for both geometries can be observed for a wavelength of 300 nm due to the lower imaginary part of the refractive index of water in this spectral range (Tab. 5-2).

The spectral properties of water cause a decrease in the guiding losses of the LCW, which can be determined from the lower graph (Fig. 5, solid line for $\lambda = 300$ nm) to be 0.021 dB cm^{-1}. Moving to an even shorter wavelength of 200 nm, the imaginary parts of the refractive indices of water and Teflon AF increase by almost two orders of magnitude (Table 1). In the case of the LCW, the shape of the calculated loss curve is seen to change and the difference in the behaviour for short and long distances is less pronounced. For short values of Z_{LCW}, the major loss contribution is still caused by coupling losses. However, for $Z_{LCW} > 60$ mm, there is a significant increase in the losses, showing a slope of 0.32 dB cm^{-1}. These increased loss values are obviously due to the increased absorption losses in water and losses in reflectivity at the interface between water and Teflon AF. The increased absorption in water at 200 nm also affects the loss curve in the free space geometry, these being for $Z_{LCW} = 203$ mm a value of 46.2 dB and for the LCW, 13.2 dB respectively, so the gain due to the LCW geometry of 33 dB remains unchanged when comparing the results at different wavelengths. Fig. 5-10 also includes loss-measurements for different distances Z_{LCW} at $\lambda = 632.8$ nm and one value at $\lambda = 463$ nm. The experimental loss-values are larger than the theoretical ones. This difference of about 1 dB can be explained by the simplifications made within the theoretical model [15, 16]. A linear regression of the experimental results (filled circles, $\lambda = 632.8$ nm) yields a guiding loss of 0.02 dB cm^{-1} and a coupling loss of 7.7 dB. Thus, a

fibre-optic sensor-system with a high light guidance efficiency has been developed. Its applicability for water analysis will be evaluated by measuring nitrate and residual chlorine concentrations in water, as reported in the subsequent sections.

5.4.2 Performance of the liquid core waveguide in the ultraviolet

The deep UV region is of particular interest in water quality analysis. Earlier, the improvement achieved by use of ultraviolet improved (UVI) fibres was discussed and with these fibres better and more stable guidance of light, in the deep UV region, from a deuterium lamp to an optical cell and from the optical cell to a detector is possible. The concept of the liquid core guide (LCW), having water as its optical core, allows the confinement of the optical energy to the optical cell. The improvement of optical losses in comparison to a conventional "free space" optical cell (Fig. 5-10) was demonstrated. An optimum wavelength in the vicinity of 300 nm was found for the LCW, due to the excellent transparency of water in this spectral region (Chapter 4). However for the deep UV ($\lambda < 230$ nm) the imaginary part of the refractive index of water increases, which directly affects the guiding losses of the LCW. Nevertheless even at $\lambda = 200$ nm among the different possible alternatives, the LCW remains the most advantageous to use in an optical measurement system. Fig. 5-11 illustrates the experimental arrangement used in an investigation of measurements on several water samples.
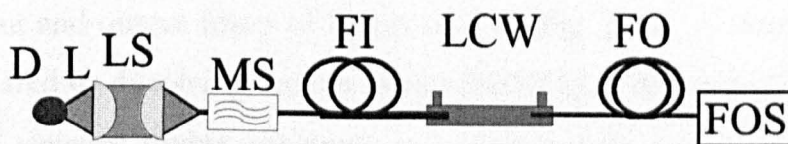

Fig. 5-11: Sketch of the experimental arrangement used for the analytical measurements, comprising a deuterium lamp, DL, a lens coupling system, LS, a mode scrambler, MS, input and output fibre, FI and FO, a liquid core waveguide, LCW, and a fibre-optic spectrometer, FOS.

The LCW is connected at one side to a light source system through a UVI silica fibre, FI, it comprising a deuterium lamp, DL, a lens system, LS and a modescambler, MS. On the other side the LCW is connected to a fibre-optic spectrometer, FOS, through a similar fibre connection and then to personal computer to detect and store the transmitted electronic spectral data.

5.4.3 Determination of nitrate in aqueous solutions

Selective and simple methods for the determination of nitrate in water are increasingly required to serve the rising interest that has been shown in monitoring the quality of drinking water, since high concentrations of nitrate in water are indicative of poor water quality. Methods to determine the concentration of nitrate in water have been extensively discussed in Chapter 4. They range from nitrate selective electrodes and colorimetric methods to direct UV absorption spectroscopy. Due to the increased absorption of water in the deep UV ($\leq$ 250 nm) the losses of any optical cell filled with H_2O will increase in this wavelength region (Chapter 4). However the LCW system remains the most favorable one to use, as discussed in Section 5.4.1, and in combination with the UVI fibers described in Chapter 2, this allowing far more sensitive nitrate measurements to be performed than were previously possible with fiber-based optical systems. Nitrate concentrations were determined to exemplify the optical limits of detection of the sensor system with an LCW having an optical pathlength of Z_{LCW}= 203 mm and using input and output fibers of length of 4 m (Fig. 5-11). A nitrate ion standard solution, prepared by dissolving sodium nitrate ($NaNO_3$) in de-ionized water, was used for preparing aqueous nitrate solutions, at concentrations ranging from 6 μg l^{-1} to 408 μg l^{-1}. The measured spectra (190 nm $< \lambda <$ 270 nm) are shown in Fig. 5-12 for NO_3^- concentrations between 0.01 mg l^{-1} and 0.8 mg l^{-1}. A slight shift of the absorption maximum at 203 nm, caused by stray light effects in the spectrometer module could be observed. To show the improvement in sensitivity and the effect of the SNR improvement on the limit of detection, the calibration curves at different wavelengths ranging from 200 nm to 220 nm were determined, as shown in Fig. 5-13.
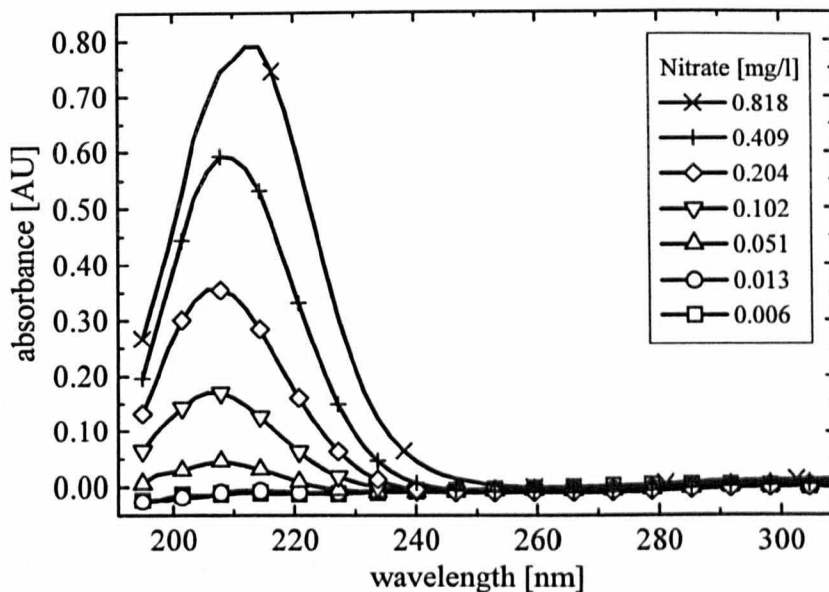
Fig. 5-12: Absorption measurements from 190 nm to 300 nm for several nitrate concentrations in water (Θ = 17.5 °C, Z_{LCW}= 203 mm)
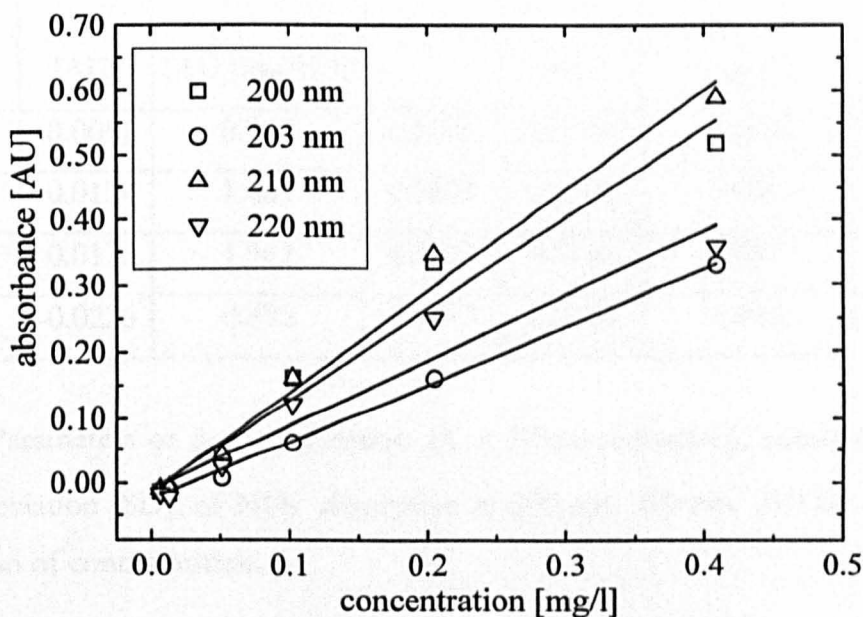
Fig. 5-13: Nitrate (NO_3) calibration curves at 200 nm, 203 nm, 210 nm and 220 nm wavelength in the nitrate concentration range from 0 to 0.4 mg l^{-1} (Θ = 17.5 °C, Z_{LCW} = 203 mm).

The performance of this sensor system can be expressed in terms of a linear regression, where the slope defines its sensitivity, and the standard deviation its limit of detection. Calibration curves were calculated for concentrations ranging from 0 to 0.4 mg l^{-1} NO$_3^-$, as the absorption measurement at 0.8 mg l^{-1} was already found to exceed the range of the sensor system. Table 2 shows the intercept, A, and slope, B, as well as the correlation coefficient, R, and the standard deviation, SD, of the linear regression at wavelength of 200 nm, 203 nm, 210 nm and 220 nm. The highest sensitivity, represented by the slope (B= 1.56 l mg^{-1}) of the linear regression is found for 210 nm wavelength, close to the maximum of absorption (Fig. 5-12). The values for the intercept, A, shown in Tab. 5-3, deviate from the expected case of A= 0 approximately within the experimental error. However all four linear regressions, shown in Fig. 5-13, represent a good fit to the experimental data, as shown by the correlation coefficient, R, and the standard deviation, SD.

wavelength	A	B	R	SD	$\Delta c = \dfrac{SD}{B}$	c$_{Limit}$
[nm]	[AU]	[AU (mg/l)$^{-1}$]		[AU]	[mg l^{-1}]	[mg l^{-1}]
200	-0.0051	0.979	0.9795	0.0338	0.035	0.070
203	-0.0124	1.401	0.9869	0.0385	0.027	0.054
210	-0.0173	1.561	0.9949	0.0266	0.017	0.034
220	-0.0226	0.878	0.9973	0.0108	0.012	0.024

Tab. 5-3: Parameters of linear regression (A + B*concentration), correlation (R), and standard deviation (SD), of NO$_3^-$ absorption at 200 nm, 203 nm, 210 nm and 220 nm as a function of concentration.

From the standard deviation of the fit, SD, the error in the concentration, Δc, can be calculated to be Δc=SD B^{-1}. Thus, defining the detection limit of the sensor again as twice the standard deviation of the measurement, a detection limit of 24 µg l^{-1} could be

achieved at a wavelength of 220 nm, predominantly used in direct UV absorption spectroscopy for the detection of nitrate, because of the significantly improved SNR. Compared to the reflectance cell described in Chapter 4, with its limits of detection of 0.50 mg l^{-1}, 0.40 mg l^{-1}, 0.32 mg l^{-1}, 1.06 mg l^{-1} obtained at 200 nm, 203 nm, 210 nm and 220 nm, a seven-fold, seven-fold, ten-fold and forty-four-fold improvement in the detection limit could be achieved respectively.

5.4.4 Determination of residual chlorine in aqueous solutions

Several sensor schemes to measure the concentration of free chlorine in natural and processed water samples have been developed over recent years; some of these have been reviewed in Section 5.3.4. However, all the absorption cells used suffered from the fact that they did not have a waveguide structure and that their basic optical attenuation was high. In this section, the advantage of replacing the largest source of light loss, the absorption cell, with a liquid core waveguide (LCW) and utilizing its significant reduction of light power losses in the optical system, as described earlier, is discussed. Due to the high optical transparency of the LCW, a short integration of 30 ms could be chosen. Thus averaging each sample 10 times, a measurement cycle could be completed in 0.3 s.

As discussed earlier, free chlorine can be found in water as a function of pH, mainly in three different forms. At pH values < 3, chlorine exists in water as dissolved chlorine (Cl_2), between pH values of 3 and 9 as hypochlorous acid (HOCl) and if the pH of the solution is higher that 9, chlorine exists in the form of the hypochlorite ion (OCl$^-$). OCl$^-$ was found to be most suitable for UV absorption measurements for several reasons. The OCl$^-$ ion has the strongest absorption coefficient and its corresponding absorption peak is centered around 290 nm, compared to the absorption peaks of HOCl and Cl_2, which are centered around wavelengths of 233 nm and 229 nm. Therefore the OCl$^-$ ion is far less affected by the broad and strong absorption peaks of nitrate and nitrite ions with their absorption peaks centered around 203 nm and 210 nm wavelengths, and commonly present in natural waters as discussed in section 5.3.4. Sodium hydroxide

(NaOH) was used to increase the pH of the sample solutions used to achieve pH values higher than 10. The concentration of OCl⁻ was then obtained by measuring the decrease in the transmission of UV light at the 290 nm wavelength.
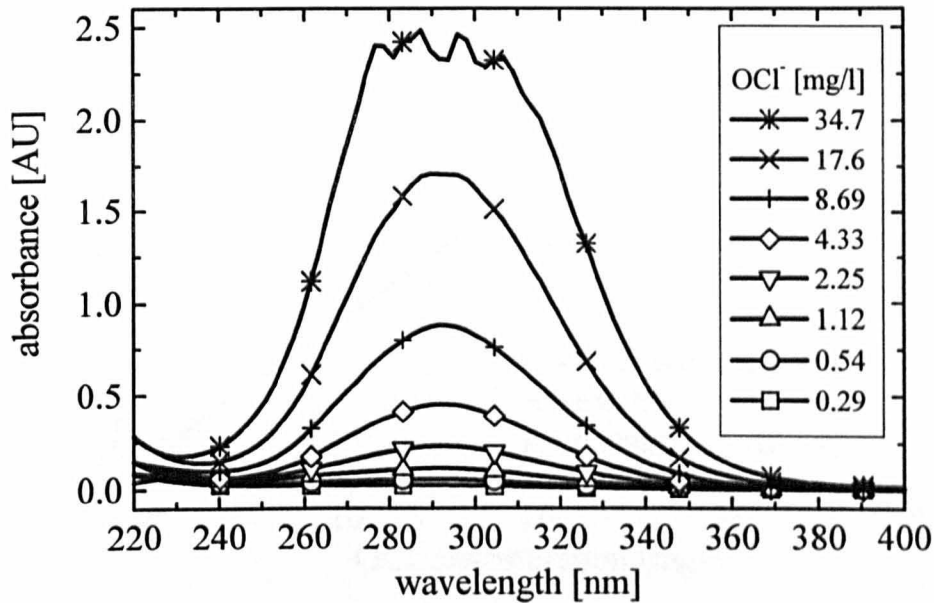
Fig. 5-14: Absorption measurements from 220 nm up to 400 nm of OCl⁻ at several concentrations smaller than 35 mg l⁻¹ (pH = 10.2, Θ = 17.5 °C, Z_{LCW}= 203 mm)

A commercial reagent kit relying on the colorimetric DPD (diethyl-p-phenyldiamine) method [35] was used to provide reference measurements to calibrate the sensor system. Fig. 5-14 shows the absorption peak of the OCl⁻ ion, centered around 290 nm, between wavelength of 196 nm and 400 nm and caused by OCl⁻ concentrations ranging from 0.29 mg l⁻¹ to 34.7 mg l⁻¹ at pH values larger than 10. The absorption peak at 290 nm is clearly detectable for OCl⁻ concentrations as low as 0.28 mg l⁻¹. In Fig. 5-14, the maximum absorption at 290 nm is plotted as a function of sample concentration. Up to a value of 17.6 mg l⁻¹, the measured absorption maxima follow a straight line, as indicated. The slope of this linear regression (here 0.0985 l mg⁻¹) is proportional to the optical pathlength, Z_{LCW}. Therefore the sensitivity of the system may be adjusted by varying the length of the LCW. According to Fig. 5-14, the spectrum for 34.7 mg l⁻¹ OCl⁻ is already beyond the range of a system configured for maximum sensitivity to low

concentrations. Measuring in this concentration range (>30 mg l⁻¹) a shorter LCW would be required. Therefore this value was not considered for the linear regression shown in Fig. 5-15.
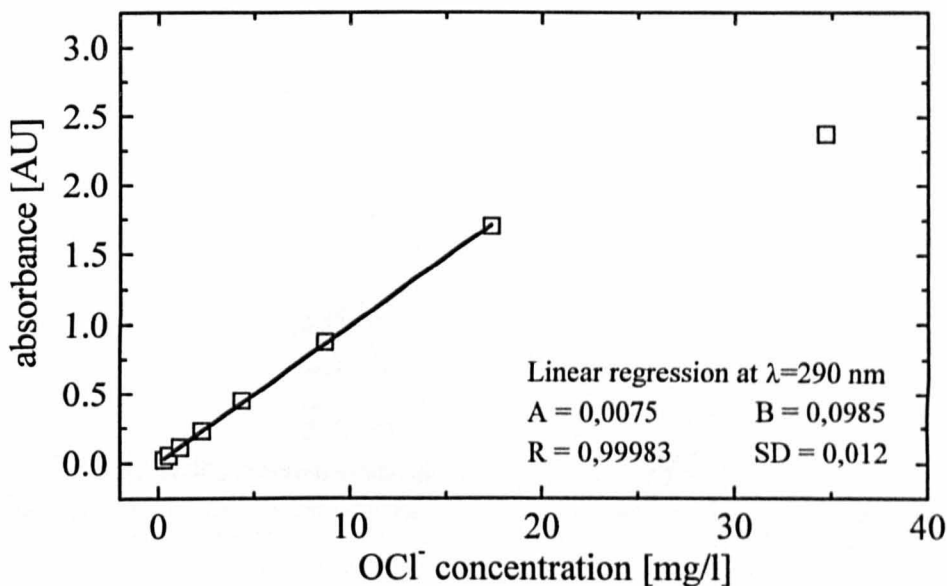
Fig. 5-15: OCl⁻ calibration curve for the absorption values at 290 nm from Fig. 7 (pH = 10.2, Θ = 17.5 °C, Z_{LCW}= 203 mm)

In the spectral range around 300 nm, according to Fig. 5-10, the guided losses are low mainly due to the excellent transparency of water, which would allow large values of Z_{LCW} to be used. A detection limit, $\Delta c = SD\ B^{-1}$, of 0.24 mg l⁻¹ could be achieved with this optical setup. Taking the low integration time, and therefore high optical through-put of the LCW into account, this detection limit could easily be improved by increasing the optical pathlength in the LCW.

5.4.5 Determination of acetylsalicylic acid in aqueous solutions

Acetylsalicylic acid ($C_9H_8O_4$), commonly known as Aspirin, is colourless, crystalline and slightly soluble in water. The substance is commonly used as a relief for mild forms of pain, including headache and joint and muscle pain [44]. The reagent has been selected

---

as an illustration of the system performance because of its wide use and its broad and strong absorption peaks below 250 nm wavelength in water. A standard acetylsalicylic acid solution was prepared by dissolving an appropriate amount in de-ionized water and mixing it for a period of 24 hours in an ultrasonic bath at room temperature. Sample solutions ranging from 0.2 mg l^{-1} to 2 mg l^{-1} were then prepared. The absorption spectra of C$_9$H$_8$O$_4$ was measured between 195 nm and 400 nm wavelength with varying concentrations, as shown in Fig. 5-16.
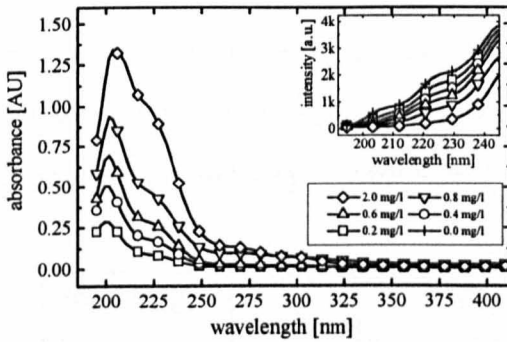
Fig. 5-16: Absorption spectra of Aspirin with concentrations ranging from 0.2 mg l^{-1} to 2.0 mg l^{-1} as a function of wavelength.
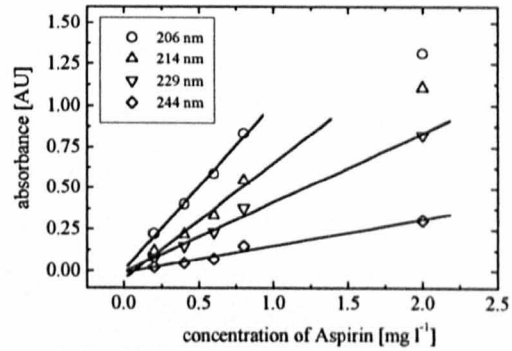
Fig. 5-17: Calibration curves of Aspirin (206 nm, 214 nm, 229 nm and 244 nm).

The inserted figure in Fig. 5-16 shows the intensity spectra of the measurements in the most interesting wavelength region below 240 nm, indicating that measurements around 200 nm with the LCW, having an optical pathlength of 177 mm and the input and output fibres of 3 m lengths are possible. A shift of the absorbance maximum is observed at high values, limiting the range of the sensor system. Calibration curves have been calculated for 206 nm, 214 nm, 229 nm and 244 nm wavelengths to investigate the improvement in sensitivity and range with improving signal to noise ratio (SNR) of the experimental setup, as shown in Fig. 5-17.

Up to a concentration of 0.8 mg l^{-1}, the measured absorption spectra follow a straight line, as indicated in Fig. 5-17, for all wavelengths. The absorption values measured at

206 nm and 214 nm wavelength for a concentration of 2 mg l⁻¹ are already beyond the range of the system at these wavelengths, as shown in Fig. 5-16, and therefore not considered for the linear regression shown in Fig. 5-17 and Tab. 5-4. Only the calibration curves created from 229 nm and 244 nm wavelength data include the 2 mg l⁻¹ concentration, showing the improved dynamic range at these wavelengths. Tab. 5-4 shows the intercept, A, the slope, B, as well as the correlation factor, R, and the standard deviation of the calibration line fit at wavelength of 206 nm, 214 nm, 229 nm and 244 nm. The intercept of the calibration curves for wavelengths of 214 nm, 229 nm and 244 nm were found to differ from 0 only within the experimental error. A detection limit of 50 µg l⁻¹, 120 µg l⁻¹, 140 µg l⁻¹ and 260 µg l⁻¹ could be obtained at 206 nm, 214 nm, 229 nm and 244 nm respectively with a reasonable range.

wavelength	$\underline{A}$	$\underline{B}$	$\underline{R}$	$\underline{SD}$	$\Delta c = \dfrac{SD}{B}$	c_{Limit}
[nm]	[AU]	[AU (mg/l) ⁻¹]		[AU]	[mg l⁻¹]	[mg l⁻¹]
206	0.007	1.007	0.997	0.025	0.025	0.05
214	-0.044	0.698	0.983	0.041	0.059	0.12
229	-0.004	0.419	0.996	0.030	0.072	0.14
244	-0.009	0.160	0.988	0.021	0.131	0.26

Tab. 5-4: Parameters of linear regression (A + B*concentration), correlation (R), and standard deviation (SD), error of concentration, Δc, and limit of detection, c_{Limit}, of acetylsalicylic acid absorption at 206 nm, 214 nm, 229 nm and 244 nm wavelength.

5.5 Summary and Discussion

By combining the aluminium coated capillary cell or the LCW with UVI-fibres for optimum UV transparency (Chapter 2), the UV fibre coupling system described in Chapter 2 and the spectrometer described in Chapter 3, a powerful tool for UV- spectroscopy-based sensing has been developed. Reference signals (nominally 0 mg l⁻¹) taken before and after the concentration measurements correlated within the standard devia-

tion of the signal, indicating a stable transportation of UV-light in the sensor system throughout the experiments performed. The physical limit of light losses which could reached in such a sensor cell is given by the attenuation of pure water itself (Chapter 4) and was calculated to be 0.3 dB cm^{-1} at 200 nm and 0.008 dB cm^{-1} at 300 nm wavelength. With the aluminium coated capillary cell, light losses of approximately 1.7 dB cm^{-1} at 200 nm and 0.8 dB cm 300 nm wavelength respectively have been obtained experimentally. However, the simulations of the LCW, confirmed in the visible, showed that light losses as low as 0.32 dB cm^{-1} at 200 nm and 0.021 dB cm^{-1} at 300 nm could be achieved. Although these simulations have not been confirmed experimentally, the advantage of the LCW compared to the aluminium coated capillary cell could be seen by their improved performance at wavelengths below 250 nm in the determination of nitrate ion concentrations, of the two sensor systems evaluated, the LCW is from the optical point of view the most favourite absorbance cell system for UV applications. However, the fused silica capillary cell with an outer coating of aluminium has its advantages, such as being much more chemically inert compared to the delicate internal coating of Teflon AF in the LCW.

Thus, two fibre-optic-based sensor systems with highly improved sensitivity in the ultraviolet part of the spectrum have been developed. Defining the detection limit as twice the standard deviation of the calibration curve, a detection limit of residual chlorine in the form of the hypochlorite ion of 0.2 mg l^{-1} could be observed with an aluminium coated capillary cell having an optical pathlength of 43 cm. Using a LCW with an optical pathlength of 20.3 cm, a detection limit of 0.07 mg l^{-1}, 0.05 mg l^{-1}, 0.03 mg l^{-1} and 0.024 mg l^{-1} of NO_3^- ions could be detected at 200 nm, 203 nm, 210 nm and 220 nm respectively, exemplifying its applicability as a UV-spectroscopy tool for remote sensor analysis. Additionally, the same sensor system could be used for residual chlorine detection, having a detection limit of 0.24 mg l^{-1} of OCl$^-$ ions at 290 nm wavelength.

Finally the sensor arrangement was used to determine acetylsalicylic acid concentrations in aqueous solutions with a detection limit of 50 µg l^{-1}, 120 µg l^{-1}, 140 µg l^{-1} and

260 µg l^{-1} at 206 nm, 214 nm, 229 nm and 244 nm wavelength. Measurements in different concentration ranges would require to match the sensor cells increasing or decreasing their optical pathlength in both cases.

5.6 References

1 J. Stone, "Optical Transmission of Liquid-core Quartz Fibers", Appl. Phys. Letters Vol. 20, No. 7, (1972), 239-240.

2 K. Fuwa, W. Lei, K. Fujiawara, "Colorimetry with a Total-Reflection Long Capillary Cell", Anal. Chem., (1984), Vol. 56, 1640-1644.

3 S. D. Schwab, R. L. McCreery, "Remote, Long-Pathlength Cell for High-Sensitivity Raman Spectroscopy", Applied Spectroscopy, (1987), Vol. 41, No. 1, 126-130.

4 K. Fujiwara, J. B. Simeonsson, B. W. Smith, J. D. Winefordner, "Waveguide Capillary Flow Cell for Fluorometry", Anal. Chem., (1988), Vol. 60, 1065-1068.

5 K. I. Tsunoda, A. Nomura, J. Yamada, S. Nishi, "The Possibility of Signal Enhancement in Liquid Absorption Spectrometry with a Long Capillary Cell Utilizing Successive Total Reflection at the Outer Cell Surface", Applied Spectroscopy, (1989), Vol. 43, No. 1, 49-55.

6 W. Wei, H. Qushe, W. Tao, F. Minzhao, L. Yuanmin and R. Gouxia, "Absorbance Study of Liquid-Core Optical Fibers in Spectrophotometry", Anal. Chem., (1992), Vol. 64, 22-25.

7 Z. Y. Zhu, M. C. Yappert, "Sensitivity Enhancement in Capillary/Fiber-Optic Fluorometric Sensors", Anal. Chem, (1994), Vol. 66, No. 5, 761-764.

8 V. Benoit, M. C. Yappert, "Characterization of a Simple Raman Capillary/Fiber Optical Sensor", Anal. Chem., (1996), Vol. 68, No. 13, 2255-2258.

9 E. P. Ippen, "Lower-power quasi-cw Raman oscillator", Appl. Phys. Lett., (1970), Vol. 16, 303-305.

10 G. E. Walrafen, J. Stones, "Intensification of spontaneous Raman spectra by using liquid core optical fibers", Applied Spectroscopy, (1972), Vol. 26, 585-589.

11 W. Lei, K. Fujiwara and K. Fuwa, "Determination of Phosphorus in Natural Waters by Long-Capillary-Cell Absorption Spectrometry", Anal. Chem., (1983), Vol. 55, 951-955.

12 P.K. Dasgupta, "Multipath Cells for Extending Dynamic Range of Optical Absorbance Measurements", Anal. Chem., (1984), Vol. 56, 1401-1303

13 M. Alaluf, J. Dror, R. Dahan, N. Croitoru, "Plastic hollow fibers as a selective infrared radiation transmitting medium", J. Appl. Phys., (1992), Vol. 72, No. 9, 3878-3883.

14 A. C. Gilby, W. W. Carson, "Photometric apparatus with a flow cell coated with an amorphous fluropolymer", US Patent 5,184,192 (2 Februar 1993).

15 P. Dress, H. Franke: "A cylindrical liquid-core waveguide", Appl. Phys. B, (1996), Vol. 63, No. 1, pp. 12-19.

16 P. Dress, H. Franke, "Increasing the accuracy of liquid analysis and pH-value control using a liquid-core waveguide", Rev. Sci. Inst., (1997), Vol. 68, No. 5, 2167-2171.

17 K. Hong, L. Burgress, "Liquid core waveguides for chemical sensing", in Chemical, Biochemical, and Environmental Fiber Sensors VI (1994), R. A. Lieberman, ed., Proc. SPIE 2293, 71-79.

18 S. Y Liu, US Patent 5,416,879, May 16, 1995.

19 S. Y Liu, US Patent 5,444,807, August 22, 1995.

20 M. N. Munk, U.S. Patent 5,608,517, March 4, 1997.

21 R. Altkorn, I. Koev, A. Gottlieb, "Waveguide capillary cell for low-refractive-index liquids", Applied Spectroscopy, (1997), Vol. 51, 1554.

22 K. I. Tsunoda, A. Nomura, J. Yamada, S. Nishi, "The use of Poly(tetrafluoroethylene-co-hexafluoropropylene) Tubing as a Waveguide Capillary Cell for Liquid Absorption Spectrometry", Applied Spectroscopy, (1990), Vol. 44, No. 1, 163-165.

23 R. Altkorn, I. Koev, R. P. Van Duyne, M. Litorja, "Low-loss liquid-core optical fiber for low-refractive-index liquids: fabrication, characterization, and application in Raman spectroscopy", Applied Optics, (1997), Vol. 36, No. 34, 8992-8998.

24 R. D. Waterbury, W. S. Yao, R. H. Byrne, "Long pathlength absorbance spectroscopy: trace analysis of Fe(II) using a 4.5 m liquid core waveguide", Analytica Chimica Acta, (1997), Vol. 357, No. 1-2, 99-102.

25 W. S. Yao, R. H. Bryne, R. D. Waterbury, "Determination of nanomolar concentrations of nitrite and nitrate in natural waters using long path length absorbance spectroscopy", Environmental Science & Technology, (1998), Vol. 32, No. 17, 2646-2649.

26 L. Song, S. Y. Liu, V. Zhelyaskov, M. A. El-Sayed, "Application of Liquid Waveguide to Raman Spectroscopy in Aqueous Solution", Applied Spectroscopy, (1998), Vol. 52, No. 10, 1364-1367.

27 P. K. Dasgupta, Z. Genfa, S. K. Poruthoor, S. Caldwell, S. Dong, S. Y. Liu, "High Sensitivity Gas Sensors Based on Gas Permeable Liquid Core Waveguide and Long-Path Absorbance Detection", Analytical Chemistry, (1998), Vol. 70, No. 22, 4661-4669.

28 E.D. Palik: Handbook of Optical Constants of Solids II, Academic Press, San Diego, (1991), 1059-1077.

29 L. P. Rigdon, G.J. Moody and L.W. Frazer, "Determination of residual chlorine in water with computer automation and a residual-chlorine electrode", Anal. Chem., (1978), Vol. 50 465-468.

30 D. F. Marino and J.D. Ingle, Jr., "Determination of chlorine in water by luminol chemiluminescence", Anal. Chem., (1981), Vol. 53, 455-458.

31 Standard Methods for the Examination of Water and Waste-water, American Public Health Association, Washington, DC, 14th edn., (1975), 304-349.

32 T. Aoki and M. Munemori, "Continuos flow determination of free chlorine in water", Anal. Chem., (1983), Vol. 55, 209-212.

33 R. Briggs, K. T. V. Grattan, Z. Mouaziz and T. Elvidge, "On-line monitoring of residual chlorine", in Advances in Pollution Control Instrumentation, Control and Automation of Water and Wastewater Treatment and Transport Systems, Pergamon Press, Oxford, (1990), 39-49.

34 Z. Mouaziz, R. Briggs, I. Hamilton and K. T. V. Grattan, "Design and implementation of a fibre-optic-based residual chlorine monitor", Sensors and Actuators B, (1993), Vol. 11, 431-440.

35 LCK 310/343 Chlorine/Ozone/Chlorine dioxide test, Dr. Lange (UK), Chamberly (1996).

36 N. Benjathapanun, W.J.O. Boyle, K.T.V. Grattan, "Binary Encoded 2nd Differential Spectrometry using UV-Vis Spectra Data and Neural Networks in the Estimation of Species Type and Concentration", IEE Proceedings A, Science, Measurement & Technology, accepted for publication 1996.

37 DU PONT Specialty Polymers Division, "product information on TEFLON AF 1600 / 2400", Wilmington DE, (1990).

38 P.R. Resnik: "The preparation and properties of a new family of amorphous flouro-polymers: TEFLON AF", Polymer preprints, (1990), Vol. 31, No. 1, 312-313.

39 J.H. Lowry, J.S. Mendlowitz, N.S. Subbramanian, "Optical characteristics of Teflon AF fluoroplastic materials", Opt. Eng. Vol. 31, No. 9, (1992), pp. 1982-1985.

40 J.W. Fleming, D.L. Wood, "Refractive index dispersion and related properties in fluorine doped silica", Appl. Opt., (1983), Vol. 22, No. 19, 3102- 3104.

41 M.R. Querry, D.M. Wieliczka, D.J. Segelstein, "Water (H_2O)", Handbook of optical constants of solids II, Academic Press, (1991), 1059-1077.

42 J.H. Lowry, J.S. Mendlowitz, N.S. Subbramanian, "Optical characteristics of Teflon AF fluoroplastic materials", Opt. Eng., (1992), Vol. 31, No. 9, 1982-1985.

43 M. Belz, W. J. O. Boyle, K. -F. Klein, K.T.V. Grattan, "Smart sensor approach for a fiber-optic based residual chlorine monitor", Paper presented at Europt(r)ode III, Zürich, (April 1996), Book of Abstracts, 194, published in Sensors and Actuators B, (1997), Vol. 39-123, 380-385.

44 D.M. Considine, G.D. Considine, "Van Nostrand Reinhold encyclopedia of chemistry", fourth edition, New York, (1984), 4-5.

6. Conclusions and future work

6.1 Summary of the work carried out and significance of the results

A growing need in the scientific and industrial world has been found for the development of simple, robust and inexpensive optical sensor systems for water quality and process monitoring. In order to fulfil this need, a polychromatic fibre-optic-based sensor system has been developed to perform highly sensitive UV-absorption measurements in the deep UV region of the optical spectrum, previously much less accessible with fibre-optic equipment. Including fibre-optics in such a sensor system has provided flexibility in the design and offered the possibility of remote sensing, decreasing health hazards and interference that can affect either the user or the measurement. The intention of this work was to investigate the performance of the individual components of a fibre-optic-based UV sensor system for potential field applications and to combine newly available technology, such as ultraviolet transmission improved fibres and recently available monolithic fibre based spectrometer systems.

The work was based on the use of hydrogen-gas-doped optical fibres showing a significant improvement in the transmission of ultraviolet light at wavelengths below 230 nm. After a "warming up" time of 30 minutes, an equilibrium of generation and regeneration of E'centres during UV-exposure was found. The induced attenuation of the main UV-absorption band around 214 nm is less than 0.4 dB m^{-1} and therefore this is nearly two orders of magnitude smaller, under the same test-conditions, than that when compared to the use of standard fibre. Lifetimes of approximately 15 month and 21 month for UVI-fibres with a core diameter of 500 µm or 600 µm respectively can be expected at room temperature, rendering these fibres suitable for the UV-sensor applications envisaged in this work. To improve the signal to noise ratio (SNR) and to decrease the effect of stray light, limiting the range of the polychromatic detector system, the principle of wavelength selective fibre coupling with fused silica lenses was described.

Two inexpensive fibre-optic based spectrometer modules have been investigated for potential use in field applications, as an integral part of a polychromatic UV-sensor system based on fibre optics. The influence of temperature variations on the dark output and the wavelength stability has been studied. Varying the ambient temperature of the spectrometer modules showed a significant effect on the dark output, which should be monitored under working conditions. With this kind of spectrometer, the main source of noise was found within the spectrometers themselves. An averaged noise level of 2.7 ± 0.6 a.u. was found for FOS-I within the temperature range of 5 °C to 42 °C and the use of integration times varying between 13 ms and 585 ms. FOS-II was found to have lower averaged noise level varying from 1.0 ± 0.2 a.u. to 2.0 ± 0.5 a.u. at temperatures ranging from 6.0 °C to 43.6 °C, indicating a temperature dependence on the averaged noise level. A wavelength, drift induced by temperature variations, typically found in field applications, was investigated with a specially developed calibration algorithm. A drift of approximately 0.006 nm K^{-1} for FOS-I and approximately 0.17 nm K^{-1} for FOS-II could be observed. However, using the 656.1 deuterium peak for on-line correction, FOS-II could be stabilized to a wavelength accuracy of 0.7 nm within the temperature range. Finally, the sensitivity of the detector arrays of FOS-I and FOS-II was investigated in the ultraviolet at wavelengths between 200 nm and 300 nm, when connected to a typical sensor arrangement. Especially below 250 nm wavelength, FOS-I showed a clear advantage compared to FOS-II. However, the work described in this Chapter showed that the spectrometers investigated could be used as polychromatic detectors in fibre-optic-based UV-sensors.

A fibre-optic-nitrate sensor, based on a reflectance cell and optimized for the deep ultraviolet part of the light spectrum has been developed. Ultraviolet improved fibres (UVI fibres) of length 4 metres have been used to enable a transfer of UV light to and from the sensor cell. The sensor system was found to be stable after a "warming up" period of 30 minutes. Four calibration curves, calculated at 199 nm, 203 nm 210 nm and 220 nm wavelengths, resulted in detection limits of 0.50 mg l⁻¹, 0.40 mg l⁻¹,

0.32 mg l^{-1} and 1.06 mg l^{-1} NO$_3^-$ respectively, proving the feasibility of fibre-optic sensor systems at wavelength below 250 nm.

However, only short optical pathlength and therefore low sensitivities were possible with the reflectance cell used in the nitrate sensor. To increase the optical pathlength and therefore the sensitivity of the sensor arrangement, the use of aluminium coated capillary cells, and more important, the use of a liquid core waveguide based on a inner coating of Teflon AF was investigated. With the aluminium coated capillary cell, light losses of approximately 1.7 dB cm^{-1} at 200 nm and 0.8 dB cm^{-1} 300 nm respectively have been obtained experimentally. Using an aluminium coated capillary cell with an optical pathlength of 43 cm, a chlorine sensing system with detection limits of residual chlorine in the form of the hypochlorite ion of 0.2 mg l^{-1} could be achieved at a wavelength of 290 nm and a pH greater than 10. As the pH of the sample is varied, free chlorine could also be determined as hypochlorous acid with a detection limit of 0.6 mg l^{-1} at 233 nm and as dissolved chlorine with a detection limit of 1.6 mg l^{-1} at 229 nm. However, the simulations of the performance of the LCW, confirmed in the visible, showed that light losses as low as 0.32 dB cm^{-1}. at 200 nm and 0.021 dB cm^{-1} at 300 nm, close to the physical limit of light losses given by the attenuation of water itself, could be achieved. Although these simulations have not been confirmed experimentally, the advantage of the LCW compared to the aluminium coated capillary cell could be seen by its improved performance at wavelengths below 250 nm in the determination of nitrate ions. With the LCW, a detection limit of 0.07 mg l^{-1}, 0.05 mg l^{-1}, 0.03 mg l^{-1} and 0.024 mg l^{-1} of NO$_3^-$ ions could be achieved at 200 nm, 203 nm, 210 nm and 220 nm respectively, exemplifying its applicability as a UV-spectroscopy tool for remote sensor applications and process control.

6.2 Future work

It has been shown that fibre-optic-based sensor systems can be applied to several absorption spectroscopy applications in the 200 nm to 250 nm wavelength region.

However, during the limited time available no long term field trials such as over a period of several weeks have been performed. Some most interesting effects to investigate in future work of this kind would be the short- and long-term behaviour of the hydrogen treated silica fibres, in a field environment, at varying temperatures. Additionally, the durability of the sensor cells and especially of the LCW in long term experiments would need to be determined, and the effect on them of biofouling, as well as non-destructive cleaning techniques investigated should be determined.

Further, it may be useful to find a replacement for the deuterium light source with its limited lifetime of approximately 1000 hours and high power consumption. Obviously, for example, xenon discharge lamps could be applied. However, especially for UV-analysis, their high intensity output in the visible and in the near infrared would need to be filtered out with for example in-fibre Bragg gratings or other special optics to be coupled into the sensor system, to reduce the high magnitudes of stray light effects commonly found when using this kind of light source.

Although a polychromatic sensor system has been developed, only single wavelengths have been used for detecting chemical species. Consequently, there is a significant potential to increase the measurement accuracy by applying multi-wavelength detection techniques or further, using principle component analysis (PCA) and artificial neural networks to classify and determine mixtures of several chemical species present in a water sample.

New techniques for water monitoring may be created, due to the fact that UV-laser light can be transported through these UV-improved fibres. Tunable lasers in the deep

UV-region around the 220 nm wavelength region, more powerful in output than the deuterium-lamp, may be used with fibre-optics and the long path absorption cells to monitor lower levels of impurities. On the other hand, existing and powerful methods can be transferred into this new region around the 200 nm wavelength, as for example, *in-situ* ultraviolet resonance Raman spectroscopy, or ultraviolet fluorescence spectroscopy.

In conclusion, the work described in this thesis demonstrates quite clearly the applicability and stability of optical fibre based UV-sensors to monitor molecular species in aqueous solutions.

7. List of Publications

1. K-F. Klein, H. Rode, M. Belz, W.J.O. Boyle, K.T.V. Grattan, "Water quality measurement using fiber optics at wavelengths below 230 nm", Proceedings of the Society of Photo-optical Instrumentation Engineers (SPIE), (1996), Vol.2836, Ch.43, 186-194.

2. M. Belz, W. J. O. Boyle, K. -F. Klein, K.T.V. Grattan: ""Smart sensor approach for a fiber-optic based residual chlorine monitor", Paper presented at Europt(r)ode III, Zürich, (April 1996), Book of Abstracts, 194, published in Sensors and Actuators B, (1997), Vol. 39-123, 380-385.

3. K.-F. Klein, P. Schließmann, E. Smolka, G. Hillrichs, M. Belz, W.J.O. Boyle, K.T.V. Grattan, "UV-stabilized silica based fiber for applications around 200 nm wavelength", Paper presented at Europt(r)ode III, Zürich, (April 1996), Book of Abstracts, 160, published in Sensors and Actuators B, (1997), Vol. 39-123, 305-309.

4. M. Belz, W.J.O. Boyle, K.-F. Klein and K.T.V. Grattan: "Water Quality Measurement using fibre optics at wavelength below 250 nm", in: J. Halttunen (ed.), Proceedings of the XIV IMEKO World Congress (Tampere 1-6. June 1997), Finnish Automation Support, Helsinki, (1997), paper 352, Vol. XA, 151-155.

5. M. Belz, P. Dress, K.-F. Klein, W.J.O. Boyle, H. Franke and K.T.V. Grattan, "Liquid Core Waveguide with Fiber Optic coupling for Remote Pollution Monitoring in the deep Ultraviolet", Poster presented at 7'th IAWQ Workshop on Instrumentation, Control and Automation and Wastewater Treatment and Transport Systems, Brighton (UK), July 1997, published in Water Science and Technology, (1998), Vol. 37, No. 12, 279-284.

6. M. Belz, P. Lacki, A. Nowakowski, W.J.O. Boyle and K.T.V. Grattan: "Remote Nitrate Sensing with Fibre Optics at 203 nm", Paper presented at EUROSENSORS XI,

The 11th European Conference on Solid State Transducers, Warsaw, Poland, (September 1997), 1571-1574.

7. P. Dress, H. Franke, M. Belz, K.T.V. Grattan, K.-F. Klein, "Water-core-fiber optic chemical sensor for pollution monitoring in the deep UV", Paper presented at 12th International Conference on Optical Fiber Sensors, Willamsburg, Virginia, USA, (October 1997), 282-285.

8. P. Dress, M. Belz, K.-F. Klein, K.T.V. Grattan, H. Franke, "Water-core-waveguide for pollution measurements in the deep ultra-violet", Applied Optics, (1998), Vol.37, No.21, 4991-4997.

9. K.-F. Klein, M. Belz, P. Dress, B. Schelle, W.J.O. Boyle, K.T.V. Grattan and H. Franke, "Ultrasensitive detection system for fiber-optic-based ultraviolet spectroscopy", Paper presented at Photonics West (BiOS'98), (January 1998), Proceedings of Micro- and Nanofabricated Structures and Devices for Biomedical Environmental Applications, SPIE, Vol. 3258, paper 3258-11, 75-81.

10. P. Dress, M. Belz, K.-F. Klein, K.T.V. Grattan, H. Franke, "Physical analysis of teflon coated capillary waveguides", Sensors and Actuators B, (1998), Vol. 51, 278-284.

11. J. Bourilkov, M. Belz, W.J.O. Boyle, K.T.V. Grattan, "Electrical pH control in aqueous solutions", Proceedings of the Society of Photo-optical Instrumentation Engineers (SPIE), (1998), Vol. 3538, Ch. 35, 268-277.